PRELIMINARY DESIGN FOR A REVERSE BRAYTON CYCLE CRYOGENIC COOLER

Phase I Final Report

Contract #NAS5-31281

Period of Performance: September 1990 - December 1992

Walter Swift
Creare Inc.

CREARE INC.
HANOVER, NH 03755

TN-508
December 10, 1993

TABLE OF CONTENTS

REPORT DOCUMENTATION PAGE

Form Approved
OMB No. 0704-0188

1. AGENCY USE ONLY *(Leave blank)*	2. REPORT DATE	3. REPORT TYPE AND DATES COVERED
	December 1993	Contractor Report

4. TITLE AND SUBTITLE

Preliminary Design for a Reverse Brayton Cycle Cryogenic Cooler

5. FUNDING NUMBERS

NAS5-31281

6. AUTHOR(S)

Walter L. Swift

7. PERFORMING ORGANIZATION NAME(S) AND ADDRESS(ES)

Creare, Inc.
P.O. Box 71
Etna Road
Hanover, NH 03755

8. PERFORMING ORGANIZATION REPORT NUMBER

9. SPONSORING/MONITORING AGENCY NAME(S) AND ADDRESS(ES)

National Aeronautics and Space Administration
Washington, D.C. 20546–0001

10. SPONSORING/MONITORING AGENCY REPORT NUMBER

CR-189341

11. SUPPLEMENTARY NOTES

12a. DISTRIBUTION/AVAILABILITY STATEMENT

Unclassified–Unlimited
Subject Category 31

12b. DISTRIBUTION CODE

13. ABSTRACT *(Maximum 200 words)*

A long life, single stage, reverse Brayton cycle cryogenic cooler is being developed for applications in space. The system is designed to provide 5 W of cooling at a temperature of 65 Kelvin with a total cycle input power of less than 200 watts. Key features of the approach include high speed, miniature turbomachines, an all metal, high performance, compact heat exchanger and a simple, high frequency, three phase motor drive.

In Phase I, a preliminary design of the system was performed. Analyses and trade studies were used to establish the thermodynamic performance of the system and the performance specifications for individual components. Key mechanical features for components were defined and assembly layouts for the components and the system were prepared. Critical materials and processes were identified. Component and brassboard system level tests were conducted at cryogenic temperatures. The system met the cooling requirement of 5 W at 65 K. The system was also operated over a range of cooling loads from 0.5 W @ 37 K to 10 W at 65 K. Input power to the system was higher than target values. The heat exchanger and inverter met or exceeded their respective performance targets. The compresssor/motor assembly was marginally below its performance target. The turboexpander met its aerodynamic efficiency target, but overall performance was below target because of excessive heat leak. The heat leak will be reduced to an acceptable value in the engineering model.

The results of Phase I indicate that the 200 watt input power requirement can be met with state-of-the-art technology in a system which has very flexible integration requirements and negligible vibration levels. Subsequent work will focus on further optimization of component performance and the design and demonstration of the Engineering Model.

14. SUBJECT TERMS

cryocooler, Reverse-Brayton Cycle, gas bearings,
turboexpander, compressor

15. NUMBER OF PAGES

76

16. PRICE CODE

17. SECURITY CLASSIFICATION OF REPORT	18. SECURITY CLASSIFICATION OF THIS PAGE	19. SECURITY CLASSIFICATION OF ABSTRACT	20. LIMITATION OF ABSTRACT
Unclassified	Unclassified	Unclassified	Unlimited

NASA National Aeronautics and Space Administration

Report Documentation Page

1. Report No.	2. Government Accession No.	3. Recipient's Catalog No.

4. Title and Subtitle

PRELIMINARY DESIGN FOR A REVERSE BRAYTON CYCLE CRYOGENIC COOLER

5. Report Date

DECEMBER 10, 1993

6. Performing Organization Code

7. Author(s)

WALTER L. SWIFT

8. Performing Organization Report No.

TN-508

10. Work Unit No.

9. Performing Organization Name and Address

Creare, Inc.
P.O. Box 71 Etna Road
Hanover, NH 03755

11. Contract or Grant No.

NAS5-31281

13. Type of Report and Period Covered

PHASE I FINAL REPORT

12. Sponsoring Agency Name and Address

NASA Goddard Space Flight Center
Code 713.1
Greenbelt Road
Greenbelt, MD 20771

14. Sponsoring Agency Code

15. Supplementary Notes

16. Abstract

A long life, single stage, reverse Brayton cycle cryogenic cooler is being developed for applications in space. The system is designed to provide 5 W of cooling at a temperature of 65 Kelvin with a total cycle input power of less than 200 watts. Key features of the approach include high speed, miniature turbomachines, an all metal, high performance, compact heat exchanger and a simple, high frequency, three phase motor drive.

In Phase I, a preliminary design of the system was performed. Analyses and trade studies were used to establish the thermodynamic performance of the system and the performance specifications for individual components. Key mechanical features for components were defined and assembly layouts for the components and the system were prepared. Critical materials and processes were identified. Component and brassboard system level tests were conducted at cryogenic temperatures. The system met the cooling requirement of 5 W at 65 K. The system was also operated over a range of cooling loads from 0.5 W @ 37 K to 10 W at 65 K. Input power to the system was higher than target values. The heat exchanger and inverter met or exceeded their respective performance targets. The compressor/motor assembly was marginally below its performance target. The turboexpander met its aerodynamic efficiency target, but overall performance was below target because of excessive heat leak. The heat leak will be reduced to an acceptable value in the engineering model.

The results of Phase I indicate that the 200 watt input power requirement can be met with state of the art technology in a system which has very flexible integration requirements and negligible vibration levels. Subsequent work will focus on further optimization of component performance and the design and demonstration of the Engineering Model.

17. Key Words (Suggested by Author(s))	18. Distribution Statement
CRYOCOOLER, REVERSE-BRAYTON CYCLE, GAS BEARINGS, TURBOEXPANDER, COMPRESSOR	

19. Security Classif. (of this report)	20. Security Classif. (of this page)	21. No. of pages	22. Price
UNCLASSIFIED	UNCLASSIFIED	76	

NASA FORM 1626 OCT 86

The key technical results achieved during Phase I include the following:

- The brassboard system operated successfully and reliably to temperatures well below the design point, demonstrating a cooling capacity of slightly more than 0.5 W at 37 K, and a range of capacities from 4 W to 10 W at 65 K.
- The performance tests demonstrated that design targets can be met with only modest changes to the individual component designs.
- Several series of cooldown and moderate duration steady state tests at cryogenic temperatures demonstrated the robustness of the system.
- The system tests provided excellent data for detailed characterization of each of the components.

The tests and analyses performed during Phase I provided key information confirming that the overall objectives of the program can be met. The design and fabrication of the Engineering Model hardware is currently proceeding with the expectation that system performance tests on the Engineering Model will be completed by early 1994. Following performance tests at Creare, the Engineering Model is to be delivered to Phillips Laboratory for extended life tests with the goal of monitoring system behavior for a period of five years..

PROJECT SUMMARY

The objective of this program is to develop and test a Reverse Brayton Cycle Cryogenic Cooler for use in space. The cryocooler will be designed to meet the following requirements:

- 5 years continuous operation on orbit with 0.95 reliability, an operating goal of 10 years,
- compatibility with launch and abort landing environments for the Shuttle Transport System,
- 5 watts of cooling at 65 K, and
- high thermodynamic efficiency (electrical input power < 200 W DC).

The technical approach is to combine miniature turbomachines and a high performance, all metal heat exchanger in a reverse Brayton cycle configuration to meet the goals listed above. Specifically, the design of the reverse-Brayton Cryocooler relies on the following high performance components:

- a miniature turboexpander with gas bearings,
- a miniature centrifugal compressor with gas bearings,
- an all-metal, high performance heat exchanger, and
- an innovative motor controller.

The program consists of four phases: Phase I - Preliminary Design, Phase II - Engineering Model Fabrication and Test, Phase III - Endurance Test of the Engineering Model, and Phase IV - Prototype Cooler Fabrication and Test.

The technical objective of Phase I has been to establish the preliminary design of the cryocooler and Ground Support Equipment (GSE) and demonstrate critical component performance. Tests of a closed loop system incorporating brassboard level components were conducted in Phase I. System and component performance data were obtained at over a range of temperatures and loads down to 37 K. System and component modeling was performed to assess the effects of design modifications at the component level and to predict overall system performance. The test results were used to verify component and system models. These results were also used to establish the designs of Engineering Model hardware.

LIST OF FIGURES

TABLES.

1. INTRODUCTION

This report presents the results of Phase I of a program to develop a Closed Cycle Cryogenic Cooler. Phase I was performed during the period September 1990 - December 1992. The technical effort during this time focused on preliminary design of the cryocooler, modeling and analysis of the system, and critical component testing to support the design and analysis efforts. The work was performed by Creare under contract #NAS5-31281 to NASA/GSFC. Funding was provided by SDIO, with Program Management through Phillips Laboratory.

The initial scope of work for Phase I focused on a six month Preliminary Design effort supported by limited testing at the component level. This effort was expanded and extended in scope to provide for system level tests of brassboard hardware at cryogenic temperatures extending down to 40 K. This report presents the results of the Phase I work including performance analyses for the system, a description of the Engineering Model design, and system level test results for a wide range of test conditions, including two separate turboexpanders.

1.1 Background

There is a critical need for mechanical cryogenic coolers that can reliably provide refrigeration to sensors and associated equipment in space over extended periods of time. Temperatures can vary from about 100 K down to below 10 K, with loads varying from tens of watts to tens of milliwatts, depending on the application. In some cases, there are requirements to provide cooling at several temperatures, either to accommodate external loads, or to provide cooling for colder stage refrigerators. Within the broad spectrum of requirements, there are some common attributes for all mechanical coolers that are desirable for space applications:

- high reliability,
- long life,
- high thermodynamic efficiency,
- very low vibration,
- flexibility in packaging and integration,
- low weight, and
- simplicity and robustness.

A significant amount of effort has been invested in the development of mechanical cryocoolers that will meet various temperature and load requirements while exhibiting as many of the desirable features listed above as is possible. Among the candidate systems currently being pursued, the turbomachine-based reverse Brayton cryocooler (TRBC) offers the promise of meeting each of these requirements for a broad range of temperatures and loads.

The basic elements of the TRBC include a centrifugal compressor, a turbine, and a counterflow heat exchanger. Depending on temperatures and loads, one or more of each of these basic components may be required within the cycle. The components are connected within a steady flow, fluid loop. The system is highly modular, allowing for heat absorption and rejection

at locations that are relatively remote from the components. Because of this distributed system configuration, packaging and integration is very flexible.

Because cooling loads for most space applications are relatively low (typically less than 10 W), the turbomachines are very small. Shaft speeds are high, requiring the use of gas or electromagnetic bearings. If self acting gas bearings are used, electronics and controls are reduced, simplifying the system and enhancing reliability as a result. The combination of small size, high speed and precision gas bearings results in machines that operate with virtually no detectable vibration, eliminating the need for vibration compensation devices. These desirable features come at some cost. The cost is in thermodynamic performance and system mass. In order to increase thermodynamic performance (reduce input power) and reduce mass, advances in precision fabrication techniques are required.

For the past fifteen years, Creare has been working actively to reduce the size and increase the performance of the basic components of the TRBC, the turbomachines and the heat exchanger. This work has been supported by internal research funds, the Air Force (Phillips Laboratory and Wright Laboratory), SDIO and NASA/GSFC. Much of the early component development work was funded through the Small Business Innovation Research program. Technical activities focused on developing advanced fabrication methods, principally in the area of electric discharge machining. These advanced methods were then used to produce key system components with high precision in small sizes. Turbine rotors with aerodynamic blading at a diameter of 2 mm, solid compressor impellers with aerodynamic swept back blades at a diameter of 15 mm, and perforated plates for heat exchangers with thousands of precision perforations on the order of 0.1 mm in size are now possible. The result of these advances is that the thermodynamic performance of the basic components of the TRBC have been significantly improved. This has extended the practical use of this type system to lower refrigeration capacities. In other words, these advances have made the reverse Brayton cryocooler competitive with other approaches at low cooling capacities from the standpoint of input power and system mass.

This program is focused on a specific set of operating requirements in order to demonstrate and confirm the status of the technology in the form of an operating system. The hardware is being built to supply 5 W of cooling at 65 K, with a limit on input power of 200 W. An eventual goal of 150 W input power for these conditions is desired. However, the system, because of its modular architecture, lends itself to the use of other components to meet slightly different operating requirements (different loads and temperatures), or to incorporate new technology that will improve the overall system performance, weight or reliability. As a result, portions of the current program focus on the how the cycle can meet other operating conditions.

1.2 Phase I Technical Objectives and Workscope

The overall objective of Phase I was to establish convincing data through analysis and tests that the system specifications could eventually meet in a prototype cooler. In Phase I, existing (brassboard) hardware was tested individually and in a closed loop system configuration. Modeling and analyses at the component level were performed to predict system level

performance. The test results were used to corroborate and correct the models and to guide the design of the Engineering Model hardware. In the next Phase of work, the Engineering Model system is expected to meet performance requirements during tests and demonstrate long life behavior during extended endurance testing.

At the start of Phase I, the basic components that make up a single stage reverse Brayton cooler already existed. These four basic components included:

- an inverter that converts DC input power to three phase AC power at variable frequency to drive the motor and compressor,
- a compressor that consists of a drive motor and centrifugal compressor to pressurize and circulate the flow through the cycle,
- a counterflow heat exchanger, that precools the high pressure gas flowing to the cold end of the cooler, and
- a turboexpander that provides the net refrigeration for the cycle.

Each of these components had been developed and demonstrated at some level. In general, the important operational features of each had been verified by testing. In Phase I, each was carried to the next level of maturation. Important improvements in performance or in mechanical robustness were implemented and evaluated by test.

Inverter. The brassboard inverter had been developed under an SBIR program [1]. It had been successfully tested by driving a dummy load (resistor and inductor circuit) that simulated the electrical characteristics of the induction motor used in the compressor. It met or exceeded expected performance levels during those tests. During Phase I, this inverter was first used to drive an early generation version of the compressor with pressurized gas bearings, then used to demonstrate startup capability and normal control capability of later generation compressors that incorporated self acting gas bearings and modified aerodynamics. During Phase I, it was used as the workhorse driver for all compressor development and for all cryogenic system level tests. Important operational and performance data were gathered in Phase I that allowed for optimizing the relationship between voltage, current, frequency and slip during operation with the induction motor.

Compressor. The compressor had also been developed under an SBIR program [2]. The original assembly consisted of a low efficiency, drilled hole impeller on a solid shaft that was supported by pressurized journal bearings and a magnetic thrust bearing. This assembly had been used to develop the three phase, solid rotor induction motor up to speeds that would be required. During Phase I, fabrication methods for the solid shaft were improved, a self acting gas bearing system, including the thrust bearing was successfully integrated, and the impeller and diffuser aerodynamics were significantly improved. A major part of this improvement involved the fabrication of a solid impeller incorporating aerodynamic swept-back blades. Operational and

performance data were obtained during benchtop open loop testing and during system level cryogenic tests.

Heat Exchanger. The all metal, slotted plate heat exchanger was built and tested during Phase I. The design had evolved from an SBIR contract during which key modeling and fabrication methods development were performed [3]. A reduced scale test article had also been fabricated and tested during the SBIR program to verify that the models were accurate. In Phase I, a full scale test article was built and tested at cryogenic temperatures. The device slightly exceeded expected performance levels in both thermal effectiveness and in pressure losses. The model was upgraded to more accurately reflect the actual behavior of the device.

Turboexpander. The turboexpander design dates from several prior independent and related machines. The brassboard test article existed from a prior SBIR project in which it had been tested at cryogenic temperatures to characterize its performance [2]. During Phase I, the machine was physically modified to increase its speed and improve efficiency. It was also tested over a range temperatures that extended the performance data for the machine. Finally, the temperature of the warm end of the machine was varied to corroborate thermal modeling of the assembly that is important in determining parasitic heat leak. A second, low capacity turboexpander was also tested in the closed loop system. This machine existed from a prior development program. It had been designed for operation in helium at 4.2 K. The machine was not optimized for this system at these temperatures, but it provided valuable data for a low capacity cooling system (of the order of 1 or 2 watts, between 65 K and 40 K). The data base obtained from the tests on both machines provided important guidance on optimization of the designs for higher performance.

In addition to the data obtained and improvements made at the component level, the test programs supplied useful experience at the system level. System preparation, gas cleaning techniques, data acquisition and reduction methods and overall system operation and control methods were developed and improved. This early experience with brassboard hardware provided valuable information that can be reflected in the design and test of the Engineering Model.

1.3 Scope of this Report

As noted above, Phase I focused on characterizing the system, developing components to assure that system requirements could be met, and developing a preliminary design of the Engineering Model that incorporates the information from the analyses and tests. This report also focuses on these three broad topics.

The first portion of the report describes the system: the design point requirements, the system hardware configuration, and thermodynamic description. Overall performance of the cycle is related to the individual requirements of the components. Descriptions of the components are provided.

The middle portion of the report discusses development carried out in Phase I on the components. This includes analyses and several series of tests.

The final sections of the report describe the preliminary design of the Engineering Model. Differences between Engineering Model and the brassboard components are discussed.

2. SYSTEM DESCRIPTION AND ANALYSIS

This section describes operational requirements of the cryocooler and the overall design of the system. The thermodynamic cycle and hardware configuration are presented. The modeling that is used to predict component and overall system performance is discussed. Predictions of cycle performance over a range of temperatures and loads are presented. Descriptions of the components and how their features are incorporated in the system model are also given.

2.1 Cycle Design Point

The cryocooler is designed to provide 5 W of refrigeration at a temperature of 65 K. The nominal heat rejection temperature for the system is 280 K, and electric input power is to be less than 200 W. In addition to meeting life and reliability goals, the most important design drivers are system power and mass. Each is to be reduced to the extent possible. More detailed specifications and operational requirements are summarized in Table 2.1. These have been extracted from the specifications [4].

Table 2.1 Design Point and System Specifications, Summarized

Performance	
Refrigeration Load	5 W
Load Temperature	65 K
Input Power	<200 W
Heat Rejection Temperature	225 K - 275 K + 30°C gradient
Weight	To be Minimized
Cooldown	< 24 hr. from ambient
Reliability	0.95 for 10 yr, 50,000 hr. operation
Mission	33,000 hr Non-Operative
	50,000 hr. Operating

2.2 System Description

The cryocooler is based on the reverse Brayton cycle. Miniature, high speed turbomachines provide for pressurization of the gas at the warm end of the cycle and expansion at the cold end. A counterflow heat exchanger provides for exchange of heat between the high pressure and low pressure gas streams as they flow through the system. The driving strategy for

the system design is to use features which have the highest potential for robustness and reliability - configured to achieve the highest practical level of performance.

Figure 2.1 is a schematic of the system and Figure 2.2 illustrates the thermodynamic cycle. A centrifugal compressor pressurizes gas (neon) which flows through an aftercooler to reject heat of compression to a thermal bus. The gas then continues through a counterflow heat exchanger where it is cooled by the return flow. The gas expands through a radial flow turbine which produces useful refrigeration. The gas absorbs heat from the load, then returns through the low pressure side of the heat exchanger, cooling the high pressure stream. The flow is continuous, and all temperatures and pressures are relatively steady state when at the normal operating conditions.

Power to the system is supplied as unregulated DC power at 28 V, +/- 7 V. This power is first converted to controlled 28 VDC +/- 0.2 V to match the input requirements of the inverter. In the inverter, the regulated 28 VDC power is converted to three phase high frequency power to drive the induction motor in the compressor. Losses from the voltage regulator and the inverter are rejected as heat by a conduction path to the heat rejection interface.

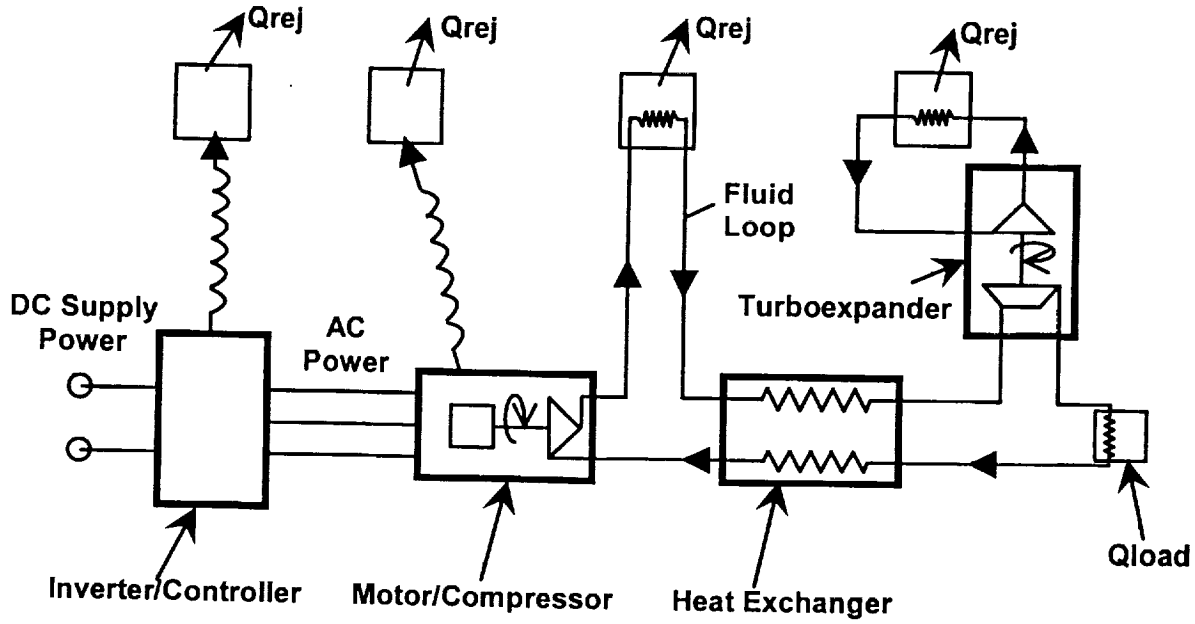

Figure 2.1. Schematic Of Reverse Brayton Cryogenic Cooler

The motor and compressor are contained in an integral assembly. The heat of compression and heat due to motor losses can be transmitted to the heat rejection interface by a combination of conduction through the housing and convection through an aftercooler. The original specification for the system called for rejection of all heat to an undefined fluid loop. The current design uses a combination of convection and conduction to accomplish this.

Heat must also be rejected from the turboexpander. The expansion of the gas through the turbine produces shaft power that is absorbed and dissipated by a brake wheel in the warm end of the turboexpander assembly. The brake circulates warm neon through a separate, but connected fluid loop. The gas in the brake circuit is heated by the brake and then cooled by rejecting heat to a suitable heat rejection site. The current design is based on this heat rejection occurring at the temperature of the interface with the fluid loop. However, there are advantages to rejecting this heat at a separate, isolated radiator at lower temperatures. If the brake heat can be rejected at a lower temperature, less heat is conducted from the warm end of the turboexpander assembly into the cold end. This parasitic heat leak is a relatively important cycle penalty.

Start and stop operation of the system has not yet been totally defined. In testing to date, the compressor has been started virtually instantaneously by presetting the inverter frequency to about 3000 Hz (corresponding to 3000 revs/second), then throwing the power switch. The frequency is then increased to the desired operating condition (which has varied during tests from about 6500 rps to 7500 rps). Shutdown of the system simply requires that the power be switched off. Both machines coast down to a stop without incident. More complex start and stop procedures may evolve as testing and system integration issues become defined for the Engineering Model.

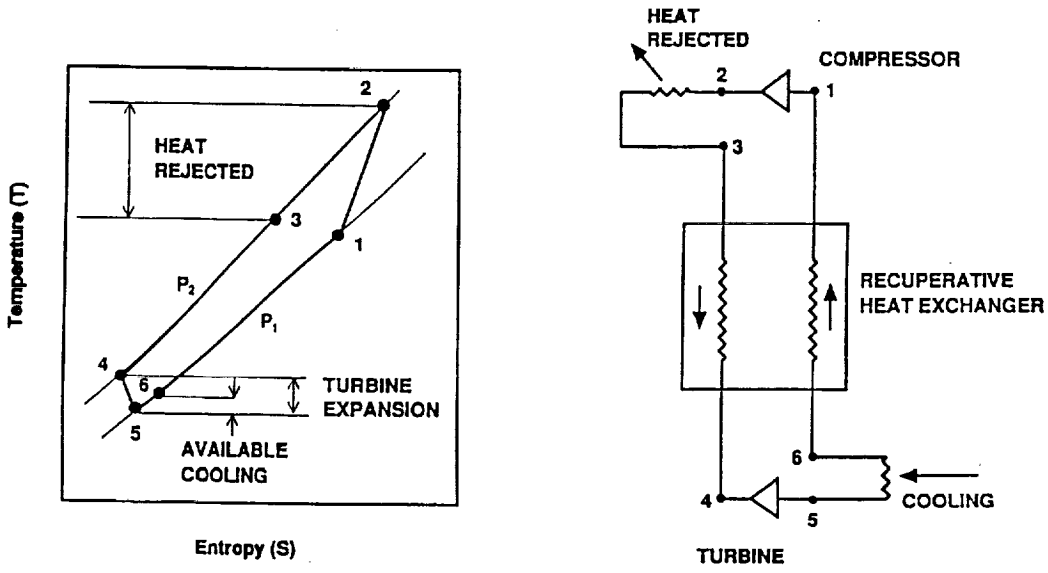

Figure 2.2. Thermodynamic Cycle For Reverse Brayton Cryocooler

Because of the thermal mass and high effectiveness of the heat exchanger, rapid and precise control of the load temperature by adjusting either the compressor or turbine speed is impractical. The system is basically designed to run open loop at a fixed frequency that could be adjusted on command signal to provide for speed changes to the system operation. Rapid and precise control of the load temperature will be better accomplished by means of either a thermal stabilizing mass and/or a small incrementally adjustable heater. Details for these components have not yet been defined.

2.3 Thermodynamic Analysis

A thermodynamic model of the cycle was developed to provide predictions of performance as a function of important operating variables. Details of the model are presented in a separate document [5], but important features are discussed in this section. Results from system predictions are presented in the next section. Since the original formulation of the model discussed in [5], several variations and improvements have been incorporated to provide additional detail or to correct simplifications or assumptions that were initially used. The model will continue to evolve in the direction of increased accuracy, mainly in the form of improved component modeling resulting from test data. The generic cycle model is formulated in a Lotus 123 spreadsheet. Supplementary system analyses were also performed using a Creare-proprietary optimization code in which performance characteristics are related to geometric details of the components. These analyses were used to refine individual component designs in order to optimize the overall system performance.

The cycle model consists of a methodology for calculating (among other things) cooling load and input power to the cycle for operating conditions selectable by the user. The model makes use of component performance characterization variables, such as efficiency, thermal effectiveness, pressure loss coefficients, and standard thermodynamic relations for compression and expansion to yield results. The component performance variables are obtained from a combination of proprietary models, non-proprietary empirical data and standard methods of analysis. This section discusses the equations used in the analysis. A discussion of the values used for performance variables is provided in the descriptions of the components.

The original formulation of the model was intended for predicting cooler performance for the following conditions:

- cooling loads from 0 to 10 W
- load temperatures from 55 K to 90 K,
- heat rejection temperature from 260 K to 325 K.

The model has been subsequently modified in two ways. The range of load temperatures has been extended to 35 K. And a second version of the model has been formulated in which a load versus temperature curve for fixed input power can be predicted [6]. This incorporates off design performance of the turbine and heat exchanger as the load temperature varies from the design value of 65 K.

A diagram illustrating the features relevant to the system model is shown in Figure 2.3. Input and output nodes for individual components are identified in the figure. The numbers at the nodes are referred to later in the list of equations used in the model.

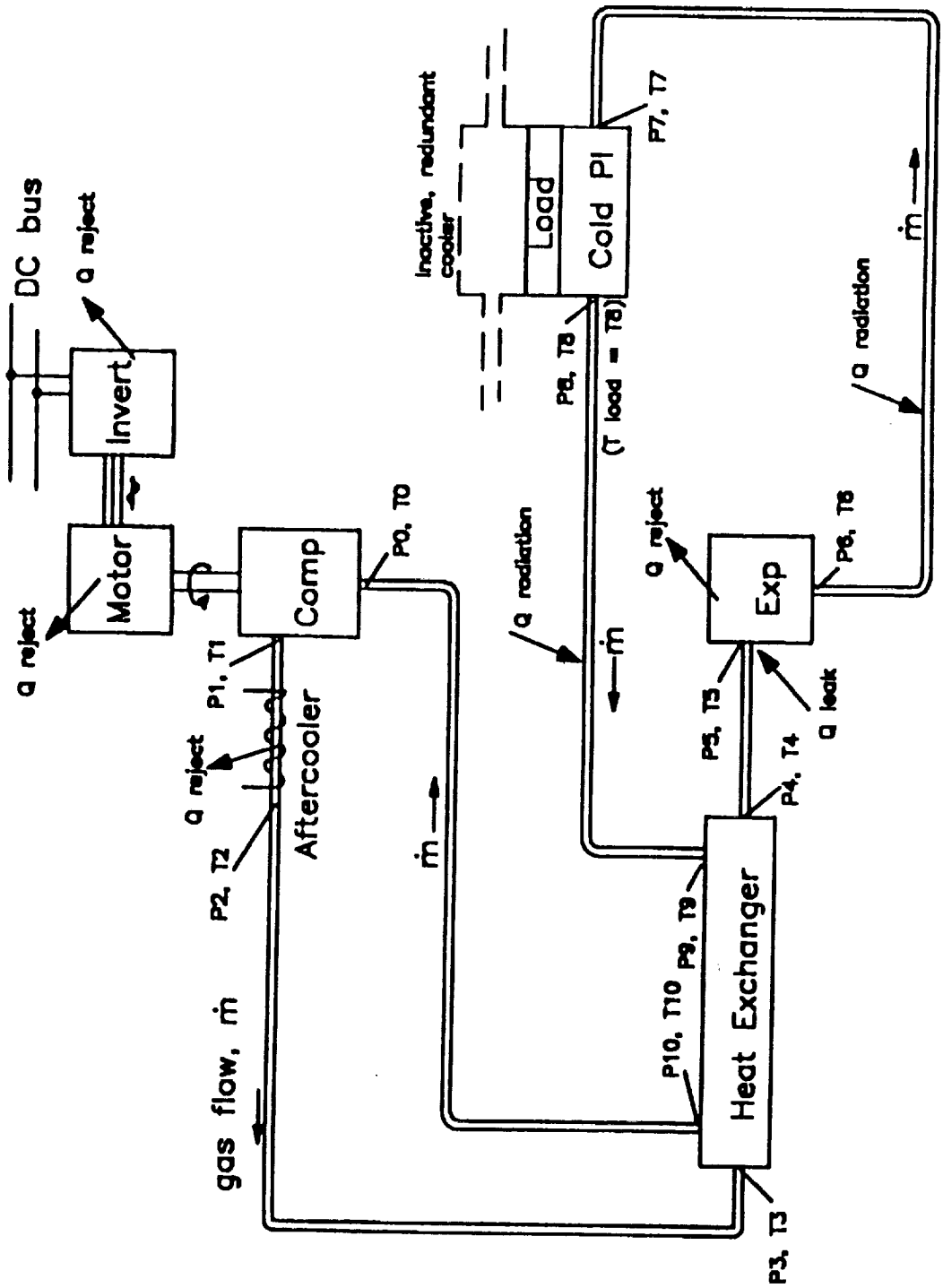

Figure 2.3. Cryogenic Cooler Thermodynamic Model Diagram

In addition to the primary heat load interfaces for the cryocooler, the load and the heat rejection interface, there are several subsidiary parasitic heat loads that are considered by the model. Radiation to the cold end of the cycle is accommodated in three ways. Radiation to the heat exchanger, is included within the thermal effectiveness for that component. Radiation to the cold end tubing is determined by off-line calculations, and input as heat loads. Radiation to the cold end of the turboexpander is accommodated within the total heat leak in that component. The total parasitic heat leak from the warm end of the turboexpander to the cold end is calculated by detailed thermal models of that component, and characterized by a first order equation depending on the brake temperature and the cold end temperature in the machine. The model also accommodates the heat load from a separate, non-operating cryocooler interfacing at the load. This parasitic heat load is calculated off-line and input as a numerical value. The external thermal bus to which all cycle heat is rejected is assumed to be at a constant temperature Trej.

The thermodynamic cycle model calculates overall cooler performance from conventional models of the individual components. For the inverter, motor, compressor and turboexpander, the conversion of input power to useful power is characterized as an efficiency:

$$\eta = (\text{net output power}) / (\text{input power})$$

For the aftercooler and heat exchanger, the component performance parameter is the thermal effectiveness:

$$\varepsilon = (\text{heat transferred}) / (\text{maximum possible heat transfer})$$

Parasitic effects such as pressure losses are accommodated by separate calculation.

The general structure of the model and method of solution is outlined in Figure 2.4. The study case variables are selected by the user for a steady state operating point. Model inputs to the calculation include gas properties, component dimensions, performance factors such as efficiency and effectiveness values, and parasitic effects. The model then calculates cycle temperatures, pressures, refrigeration capacity and input power. The model also produces various other results that are useful for correlating with data or offline modeling and analyses. The gas properties in the model are real gas properties from [7]. However, for the purpose of illustrating some of the equations, ideal gas relationships are substituted in this report.

Figure 2.5 summarizes the functional calculations used by the model. Each of the blocks in the figure is a schematic representation of the main elements of the overall calculation.

1) For the compressor, starting with mass flow rate, pressure, and temperature at the inlet, the model uses compressor speed, compressor diameter, compressor efficiency, motor efficiency, inverter efficiency, and aftercooler effectiveness to calculate electric input power and pressure and temperature at the aftercooler exit.

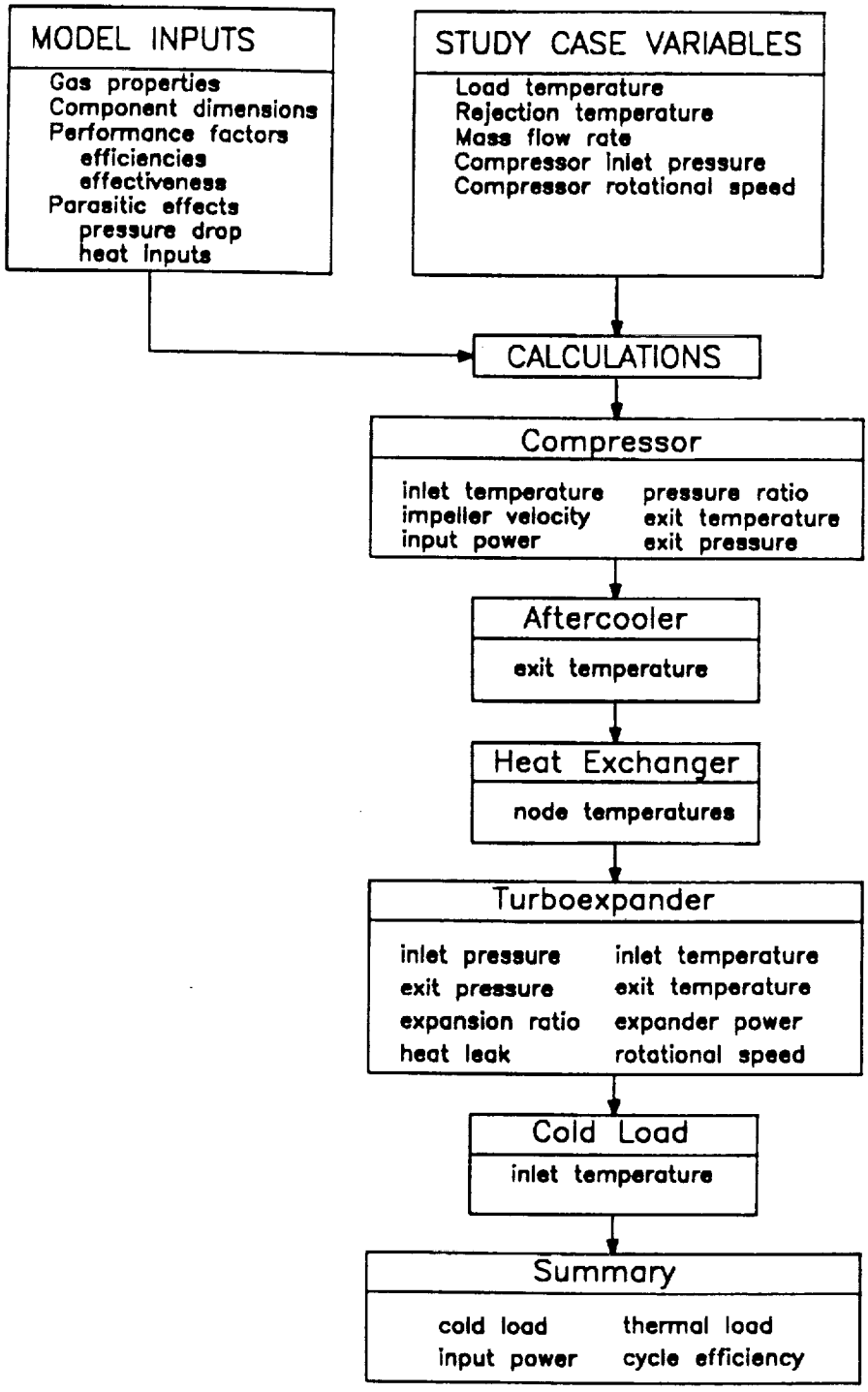

Figure 2.4. Thermodynamic Cycle Model Flow Chart

2) In the counterflow heat exchanger, temperatures at the inlet and exit ports for the high and low pressure streams are related by a functional relationship between thermal effectiveness and mass flow rate. Another functional relationship between pressure loss and flow rate is used to calculate the pressure loss in each stream.

3) In the turboexpander, an adiabatic efficiency relates exit temperature to inlet temperature and pressure ratio. Internal heat leak is applied as an equivalent increase of the temperature of the gas at the inlet to the turbine.

4) At the load, parasitic radiation, the heat load from the redundant cooler and the actual net useful refrigeration from the cycle are applied. The cold load temperature is assumed to be the temperature of the gas exiting from the cold plate - where refrigeration is supplied to the load.

5) Pressure losses in the tubing at the warm and cold ends have been estimated assuming two 1 meter lengths of tubing at the cold end and two 1 meter lengths at the warm end. These pressure losses are roughly 10 % of the pressure losses in the heat exchanger and have therefore been lumped into the heat exchanger pressure loss calculation.

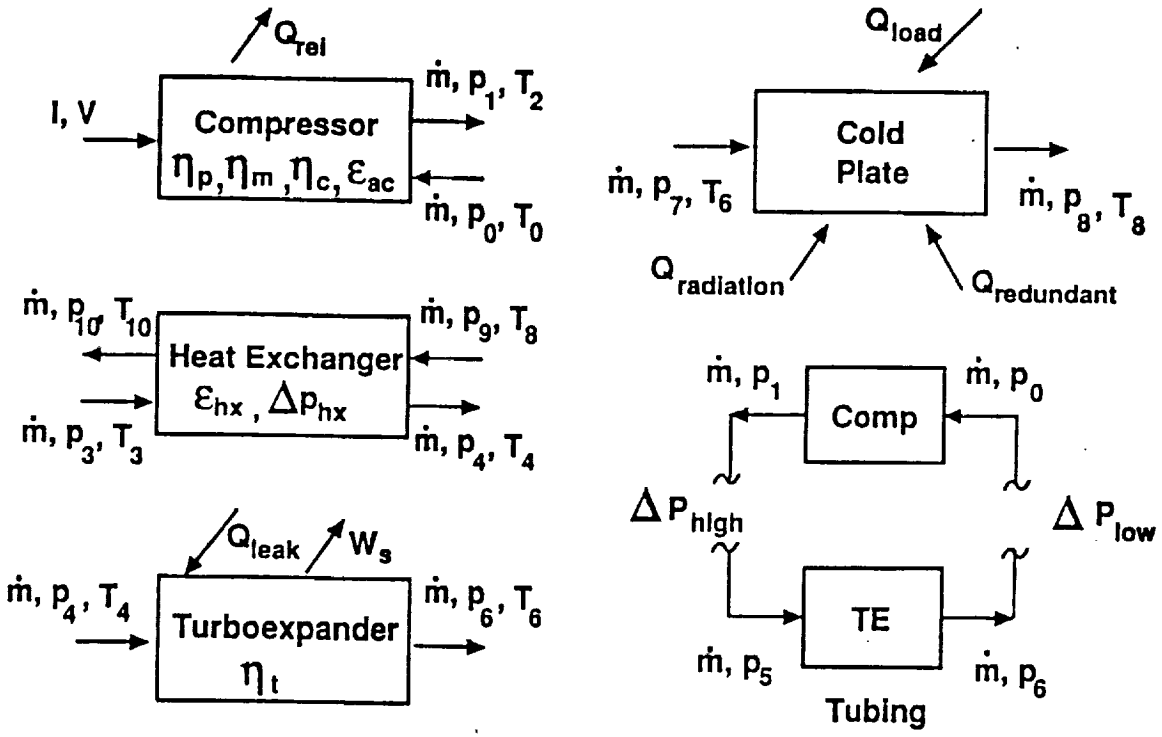

Figure 2.5. Summary of Component Block Models

2.4 Performance Predictions

Performance predictions for the cycle were carried out for several basic operating conditions. The model results presented in this section are tabulated below.

Model Study	Description
1	Design Point Operation
2	Steady Input Power (200W) Variable Load
3	Reduced Capacity System (40 K Case)

The first study was used to define the system parameters required to meet the design operating conditions. These parameters include system conditions such as flow rate, temperatures and pressures, and component characteristics such as efficiencies, operating speeds, and internal component sizes. In the second study, design performance characteristics of the Engineering Model hardware were extended to off design conditions to simulate the behavior of the system over a range of temperatures. The output from this study was predicted load and temperature for the Engineering Model if operated at a steady input power of 200 W over a range of load temperatures. The third study was used to evaluate the performance that could be achieved with hardware that was smaller (or the same) in a system designed for 2 W at 40 K.

2.4.1 Design Point Predictions

The design point operating conditions were predicted using expected performance values for the Engineering Model hardware. Important assumptions and system parameters are summarized in Table 2.1.

The results of the model predictions are shown schematically in Figure 2.6. The figure shows predicted temperatures and pressures at several locations within the system. Cooling load, parasitic loads and input power at these conditions are also summarized in the figure. The results from the design point prediction were used to finalize the expected performance points for the components. I.e., the model establishes compressor and turbine speeds, flow rates and pressure rise that will be required to meet the design operating conditions.

2.4.2 Variable Load Predictions

The basic features of the design point model were retained and expanded so that off design performance characteristics of the components could be used to establish off design performance of the cycle. For example, calculations were performed assuming that the compressor input power (hence, the compressor speed) is constant and the cold end load is reduced from 5 W to 0 W. Under these conditions, the cold end temperature will decrease as the load is reduced. This will reduce the temperature at the inlet to the turboexpander and therefore reduce the enthalpy drop through the turbine (for the same pressure ratio). The net result is a reduction in turbine speed and hence, a change in the flow rate through the turbine. As the

Table 2.2. Thermal Model Input Values For Design Point Prediction		
Gas Properties	Specific Heat Capacity, J/g-K	1.035
	Gas Constant, J/g-K	0.412
	Specific Heat Ratio	1.667
Geometry	Compressor Impeller Diameter, cm	1.524
	Turbine Rotor Diameter, cm	0.318
Parasitic Effects	Pressure Loss, high side - dP/P	0.01
	Pressure Loss, low side - dP/P	0.01
	Radiation Heat Load (W)	0.15
	Redundant Cooler Load (W)	0.17
Design Variables	Power Conditioner Efficiency	0.90
	Motor Efficiency	0.51
	Compressor Efficiency	0.70
	Combined Power Train Efficiency	0.32
	Aftercooler Effectiveness	0.95
	Recuperator Effectiveness	0.993

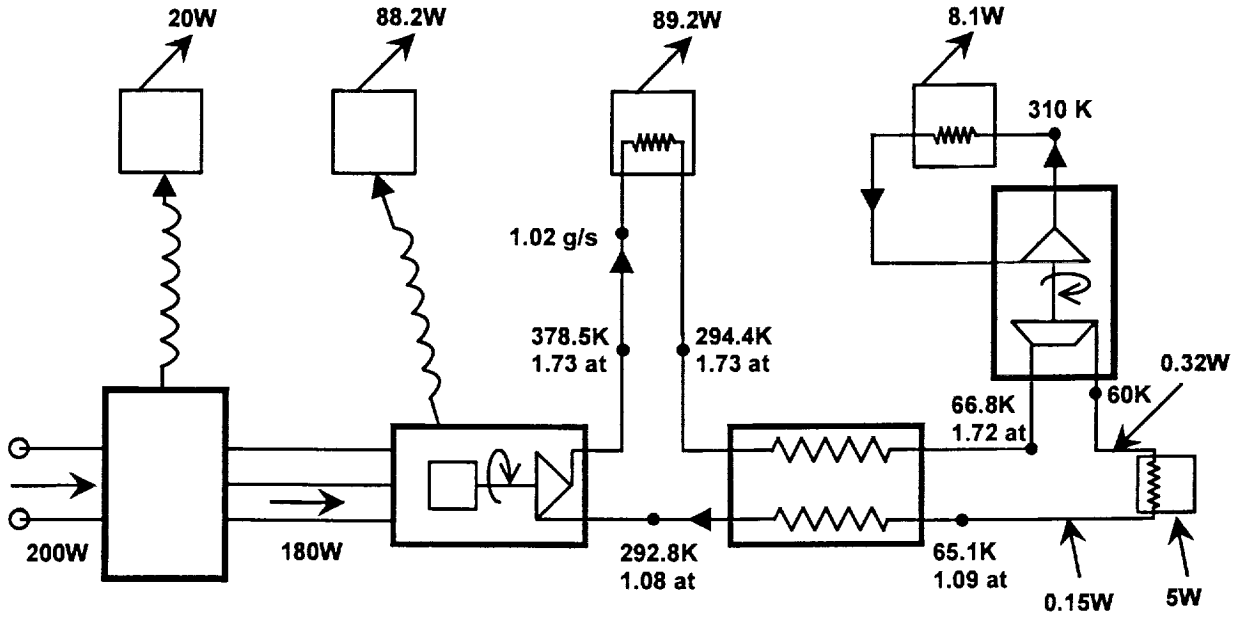

Figure 2.6. Predicted Design Point Operating Characteristics - Engineering Model

conditions at the turbine change, the turbine will tend to operate at a reduced efficiency. The flow rate through the heat exchanger will also change, accompanied by a slight decrease in the thermal effectiveness of this component. The total effect of these changes is that the system efficiency will decrease (relative to Carnot efficiency) as the low temperature end of the cycle moves away from 65K.

The turbine, compressor and heat exchanger performance relationships were characterized in curve fits through data for each component in the form of suitable dimensionless parameters (e.g. flow coefficient, head coefficient and efficiency for the two turbomachines, and effectiveness and flow rate for the recuperator). A FORTRAN version of the model was developed and integrated with an optimizing computer code that allows for the necessary iteration to solve for system conditions with variable component characteristics [6]. The model was then used to predict system input power as a function of load and temperature assuming that the input power and compressor speed remained constant.

The results of these calculations are shown in Figure 2.7. The curve in the figure relates the expected cycle net refrigeration capacity as a function of load temperature. The thermal rejection temperature for the system is the nominal design point value of 280 K. The input power for this prediction is 195 W from the electric bus. The predictions show that the cycle should be able to achieve a no-load temperature of about 35 K.

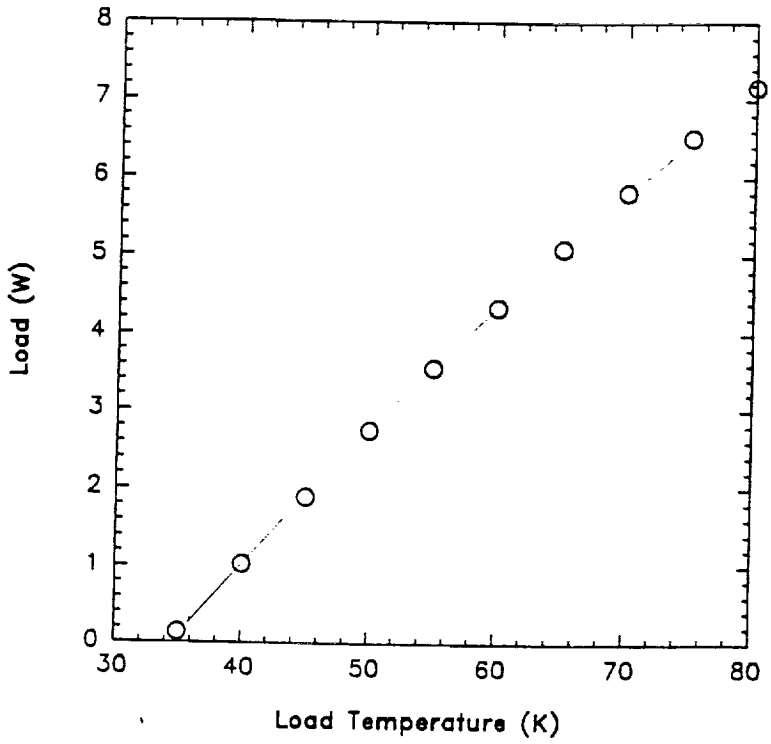

Figure 2.7. Cycle Performance

2.4.3 40 K Modeling

Studies were performed for three additional design points [8]. Two generic system models (Baseline and Advanced) were used to predict cycle performance and system mass for each of the design conditions. For the Baseline studies, the components for the Engineering Model were scaled to different sizes and speeds to reflect the designs that would be used to meet each design point condition without incorporating technology advances that may be available. For studies

using the Advanced system, some modifications to the design of individual components were incorporated to reflect the effects or realistic changes to the designs that could be incorporated.

The three design points and predicted system power and mass are summarized in Table 2.3. The values listed in the Table provide upper and lower bounds for input power and cryocooler mass for each of the design operating conditions. The following paragraphs summarize the assumptions used for each of the systems.

Table 2.3. Single Stage Reverse Brayton Cryocooler Performance and Mass			
Load Temperature(s)	35 K	35 K	35/65 K
Cooling Capacity	0.25 W	2.75 W	0.25/2.5 W
Parasitic Load	0.2 W	0.2 W	0.2 W
Baseline System			
Electric Input Power	200 W	386 W	337 W
Cryocooler Mass	15.5 kg	15.5 kg	18.7 kg
Advanced System			
Electric Input Power	160 W	260 W	230 W
Cryocooler Mass	11 kg	11 kg	12.5 kg

The performance of each of the Engineering Model components was used as a basis for the predictions listed above. For the Baseline studies, the tuboexpander and compressor sizes and design speeds were varied to provide optimum efficiency at the flow rates, pressures and temperatures dictated by the individual cycle optimizations. The slotted plate heat exchanger was used as the basis for the recuperator, without changes in size. I.e., the performance of the heat exchanger varied with flow rates and pressures. The inverter performance was characterized by a fixed efficiency for all cases. The mass of the inverter was scaled with electric power levels.

For the Advanced cycle, two changes were considered. First, a light weight heat exchanger replaced the slotted plate design as the recuperator. The effect of this modification on the predictions is to reduce system mass for equivalent performance levels. The second change was to allow for the use of an advanced turbine design with lower internal heat leak. The turbine could be either a turboexpander with the brake at 230 K or a turboalternator with the generator at about 100 K. Either of these devices would produce the equivalent result, a net gain in turbine efficiency, thereby reducing the cycle input power.

2.5 Component Descriptions

This section summarizes important physical and functional features for each of the main components in the cycle. Section 3 discusses additional details about developments that took place during Phase I to upgrade the hardware from their status prior to the beginning of this effort. Section 6 describes further modifications that will be implemented in the Engineering Model Hardware.

Power Conversion

The compressor is driven by a three phase induction motor. Power to the motor must be converted from unregulated DC voltage at the bus to controlled three phase AC power with a nearly sinusoidal waveform. Figure 2.8 is a schematic illustrating the electric power flow to the system. The power conversion package consists of a voltage pre-regulator and a transformer-coupled inverter. The pre-regulator has been functionally defined, but the hardware implementation has not yet been established. The pre-regulator must convert about 200 W of DC input power (28 V +/- 7 V) to 28 V +/- 0.2 V. The inverter portion of the package has been

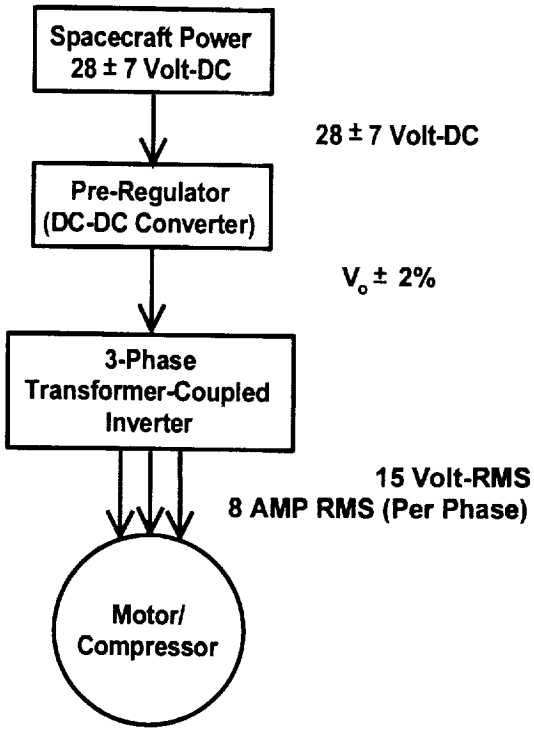

Figure 2.8. Schematic Diagram of Input Power Conversion

designed, fabricated and demonstrated. It converts the regulated DC power to variable frequency, three phase AC. A key feature of the inverter is the achievement of very low harmonic content with relatively simple electronics. Because current levels are high in the motor, the quality in approximating sinusoidal three phase current from the inverter is important in reducing overall electrical losses.

Figure 2.9 shows the basic circuit features of the inverter. The inverter consists of six transformer coils connected in series in a ring. The primary windings in the coils are sequentially energized from the DC supply by six pairs of MOSFET transistor switches that supply chopped voltage signals. The secondary windings provide a three phase Y - connected AC output to the motor. The timing pattern for the switches on the primary side is set by logic signals that trigger

the IR2110 bridge drivers that switch the MOSFETS on and off. The logic signals are generated by cascaded D-type flip flop elements that are triggered by clock signals from a timing chip.

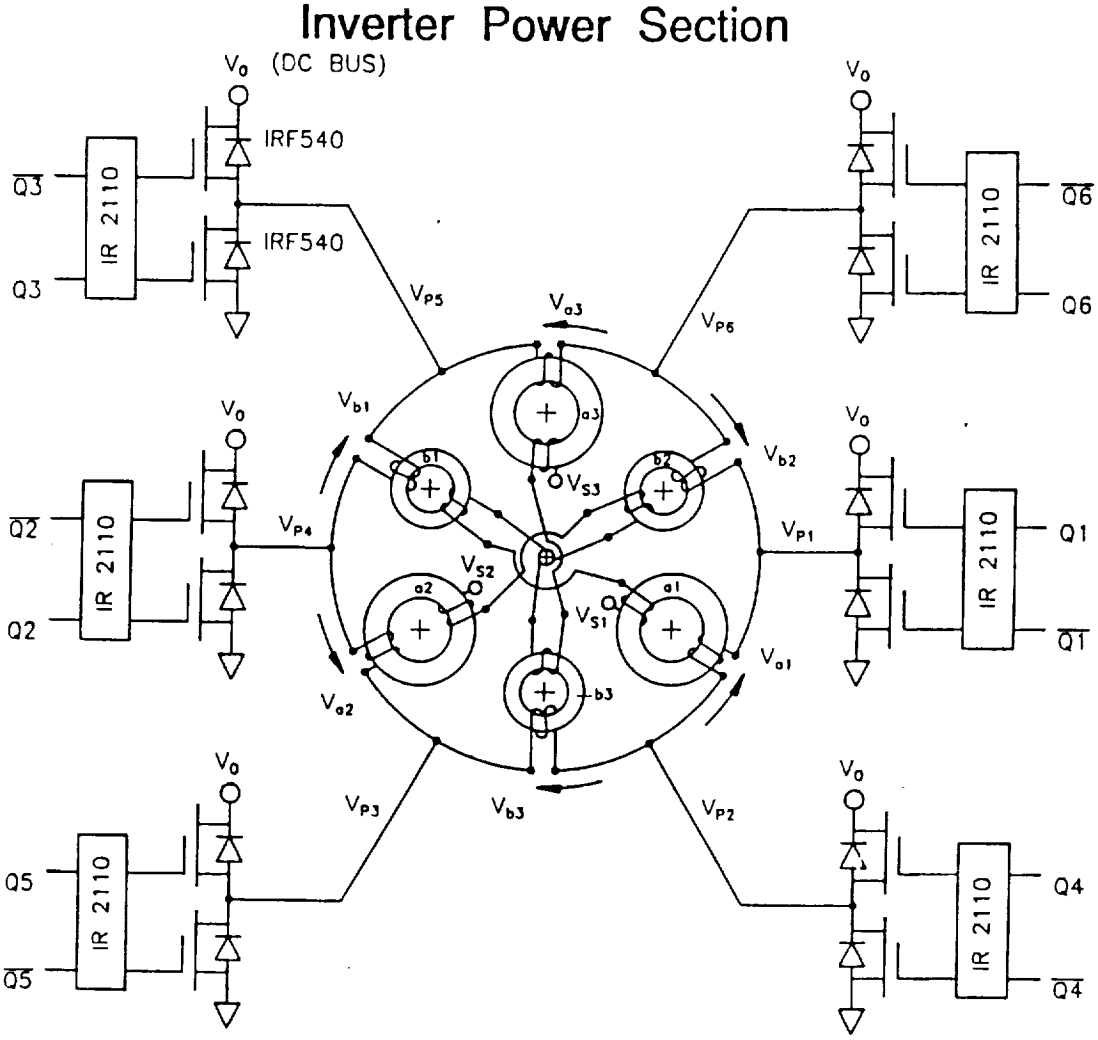

Figure 2.9. Simplified Circuit Diagram of Inverter

Each of the primary voltage (Vp) waveforms is a square wave with a period of 12 clock periods. The inverter output is constructed from these waveforms and therefore has the same period. The inverter output frequency is thus one-twelfth the clock frequency. It is set through a potentiometer adjustment of the timing chip. Figure 2.10 illustrates typical wave forms generated by the inverter.

For fixed transformer winding ratios, there are basically only two controllable variables that influence the output voltage waveform. These are the DC input voltage and the clock frequency. The operation of the motor/compressor during testing has been controlled by

manually adjusting frequency and supply voltage. In this way, characteristics for the motor/compressor and the inverter circuitry could be evaluated as functions of frequency, slip and supply voltage. During operation of the system in a space environment, the circuitry would be modified to maintain a fixed ratio between supply voltage and frequency near an optimum efficiency. The start sequence would also be programmed to meet power and cooldown timing requirements for the cycle.

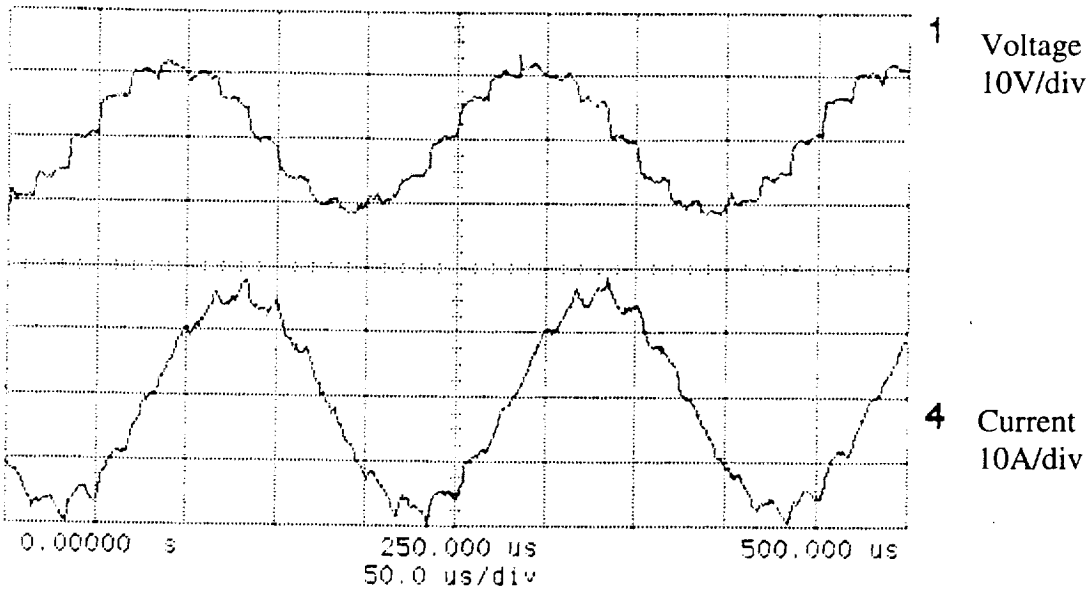

Figure 2.10. Inverter Output Waveforms

The performance of the power conversion system is characterized as the efficiency of the regulator and the efficiency of the inverter. The efficiency of the inverter has been measured in testing. At optimum conditions corresponding to an input power of 390W, the peak measured efficiency was 0.95. We expect a comparable level of performance on the Engineering Model at 200W input. We've assumed that the regulation portion of the power conditioning can be built with at least as high an efficiency as the inverter portion, i.e., the regulator efficiency will also be 0.95. The overall efficiency of the motor controller is the product of the two components, 0.90. The heat due to losses from the power conversion system will be conductively transmitted to a cold mounting plate.

Motor/Compressor

The motor/compressor converts input three phase AC power to useful fluid power in the form of a continuous flow of gas at a suitable pressure ratio.

The compressor is a single stage centrifugal machine with an impeller approximately 15.24 mm (0.6") diameter. The impeller is attached to a solid rotor shaft of 6.35 mm (0.25") diameter that is an integral part of the three phase, brushless induction motor. The motor is

compact, and the size and design speed of the machine are intended to achieve the highest possible overall efficiency for the assembly. The shaft is supported on tilt pad, self acting gas journal bearings. Axial loads are carried by a spiral groove gas thrust bearing acting on opposing external surfaces of the impeller.

The performance of the machine is characterized as an overall efficiency, the ratio of useful fluid power to input electric power. The useful fluid power is given by the product of flow rate and isentropic enthalpy rise of the fluid as it is compressed. The electric input power is the time integrated AC power input to the motor. The major losses in the assembly consist of electrical losses in the motor, windage and drag losses in the bearings, and at the clearance seals, leakage losses around the impeller and aerodynamic losses in the impeller and diffuser. In addition to the heat of compression of the gas, each of these losses contributes to additional heat generation. Since the machine is small, and constructed as an integral assembly, measurement of the individual losses is impractical. The performance of the machine is determined by tests that yield overall efficiency, and calculations to estimate relative contribution of internal components. From the standpoint of overall cycle performance, it is the overall efficiency that is important. From the standpoint of design optimization of the machine, it is the supporting analysis that provides guidance in design and optimization of the machine.

In the brassboard test hardware, the motor/compressor is cooled by water circulating through the housing. The original design basis for the system incorporated a fluid loop for cycle heat rejection. However, the design of the Engineering Model will include means for conducting a major portion of the heat from the assembly conductively to a cold base plate. A portion of the heat due to compression will be rejected to a similar cold plate through an aftercooler.

Recuperative Heat Exchanger

The counterflow heat exchanger provides for efficient precooling of the high pressure gas flowing from the compressor to the turbine inlet. Important features of the design combine low pressure losses, high transverse heat transfer between the gas paths and low axial heat transfer from the warm end of the assembly to the cold end. A further important characteristic is that no organics are present in the assembly eliminating the potential for contaminants from outgassing.

The heat exchanger consists of two annular thin wall stainless steel tubes in which 300 pairs of copper disks and matching annular copper rings are axially positioned. The disks and rings each have two annular rows of slots accurately machined by an automated electric discharge machining process. Warm gas passing through the slots in the disks give up heat that is conductively transferred to the outer matching ring through the wall of the stainless tube. The overall configuration is designed specifically for very high thermal effectiveness with low pressure losses.

In the brassboard test article, the disks and rings are separate components, soldered to the tube walls. Axial positioning is done by means of "dimpling" the tube walls during the assembly process, and visually aligning each disk/ring pair as they are inserted. In the Engineering Model, the disk/ring pairs are replaced by solid disks. The disks are separated by stainless thin wall

spacers that provide structural support and a pressure boundary between the two counterflowing gas streams. The assembly is vacuum brazed with headers for the tube connections at each end.

The performance of the heat exchanger is defined in terms of a thermal effectiveness, the ratio of heat transferred between the two streams to the maximum amount possible, and pressure losses in each of the high and low pressure streams. Axial conduction and radiation from external surfaces are included in the definition of thermal effectiveness.

Turboexpander

Useful refrigeration for the cycle is produced by expansion of the gas as it flows through the turboexpander. This refrigeration is used to cool the load and absorb heat from other parasitic heat losses at the cold end. The shaft work that is produced from the expansion is absorbed by a brake on the same shaft. The brake circulates gas through a dissipative circuit where the work is rejected as heat.

There are two important characteristics that affect the performance of the turbine, the adiabatic efficiency and the heat leak. The adiabatic efficiency reflects the aerodynamic performance of the turbine. The heat leak is determined by the operating temperatures of the brake circuit and the turbine. If the turbine were 100 % efficient, the refrigeration produced in the turbine would equal that of a pure isentropic expansion. The net refrigeration from the machine would be reduced by the heat leak from the brake to the turbine. In the present machine, the adiabatic efficiency at design point is about 0.78. The effect of heat leak is to reduce the net efficiency of the turbine to about 50%.

The parasitic heat leak within the turboexpander assembly is a substantial portion of the overall loss at the cold end. Figure 2.11 shows the heat leak in watts as a function of cold and warm end temperatures for two turboexpander designs. The first (Fig. 2.11a) gives the heat leak for the baseline machine that was tested during Phase I. Figure 2.11b gives the heat leak for the Engineering Model Design. The difference between the two machines is in the wall thickness of the support tube between the warm and cold ends of the machine. For the tested turbine, this thickness was 0.254 mm (0.010"). In the Engineering Model, the wall thickness is reduced to 0.152 mm (0.006").

A reduction in warm end temperature can have a substantial effect on cycle performance. Using Figure 2.11b as a guide, if the brake temperature is reduced from 300k to 240k, the heat leak is reduced by about 0.7 W. This corresponds to a reduction in input power to the cycle of about 20 W. Such a change should be relatively straightforward to implement. Since the brake is a circulator, it is capable of pumping fluid to a separate cold plate or radiator for rejection. The total heat to be rejected is of the order of 8 W. The most important consideration in reducing brake temperature concerns the reliable operation of the bearings. For this design, the journal bearings are of the self acting type, in which the shaft is supported on a film of gas between the shaft surface and tilting pads. Clearances in this type bearing are very small, in order to reduce clearance and leakage losses at the turbine rotor. In separate tests, this type bearing has been successfully run at speeds to 10,000 revs per second at temperatures as low as 180 K.

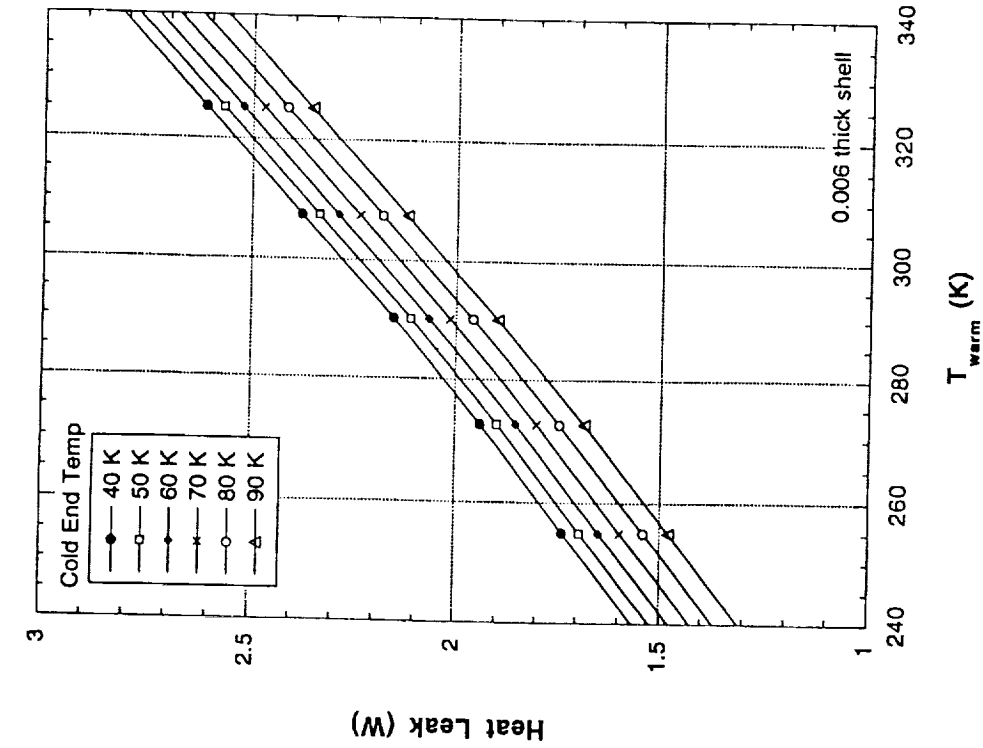

(b) 0.152 mm (0.006") wall thickness

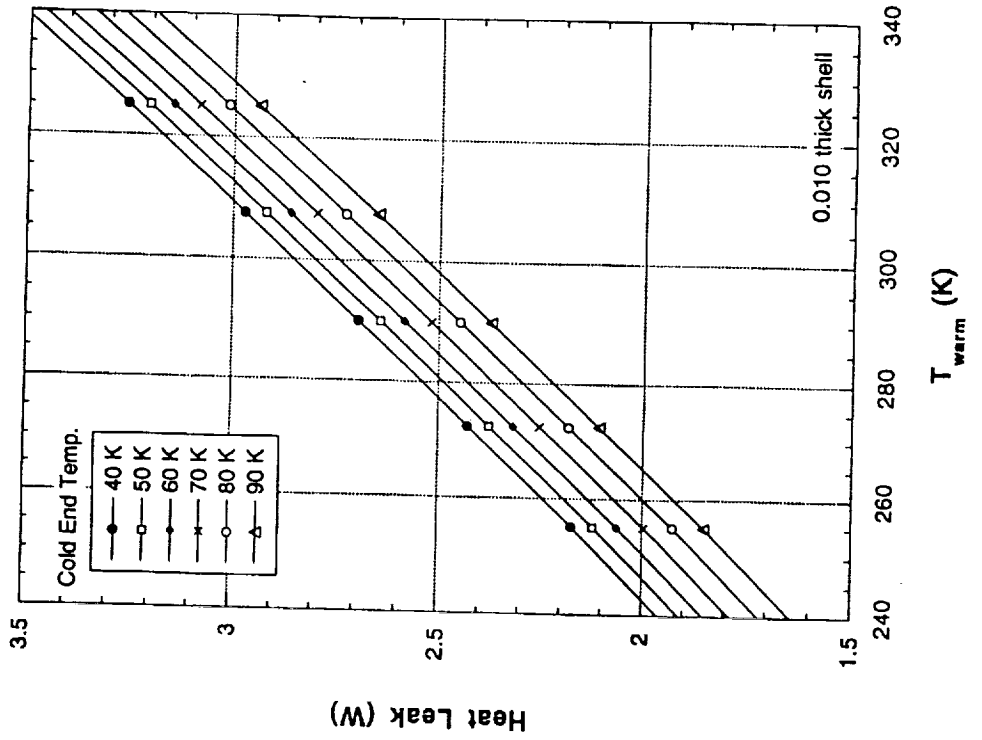

(a) 0.254 mm (0.010") wall thickness shell

Figure 2.11. Turboexpander Heat Leak

3. CRITICAL COMPONENT DEVELOPMENT

A major part of Phase I activities focused on developing the components in the cycle to a level suitable for use in the Engineering Model. These efforts are broadly divided into two categories:

1) analyses and tests to support the thermodynamic performance goals of the cycle, and

2) developments to demonstrate critical mechanical features to be used in components.

The first category includes tests on each of the four components. Some were performed at the component level, but most of the tests were carried out with components assembled in a closed cycle at cryogenic temperatures. The developments include aerodynamic improvements to the compressor and turboexpander, and determination of the optimum voltage-frequency relationship for the motor and inverter. The mechanical developments included work on the bearing systems for the compressor and fabrication methods for the compressor and the heat exchanger. This section contains three parts. The first describes the development activities associated with each component. The second section describes test facilities and procedures used to perform the tests. The third section provides information about instruments and data acquisition.

3.1 Component Testing

Inverter

The inverter used for all tests to date was developed through a NASA/GSFC funded project under the SBIR program. Figure 3.1 is a photograph of the inverter. During its initial development, a breadboard assembly was built and tested with an early version of the compressor. There were no additional development modifications required to this device during Phase I of this program. It was used routinely to drive the motor/compressor during bearing development and aerodynamic development tests. It was also used during all closed loop system tests. During Phase I it accumulated approximately 1000 hours of use over a broad range of conditions. Its performance with the motor was well characterized during tests to optimize the relationships between voltage frequency and slip speed. Although the design point input power for the system is 200W or less, the inverter has been operated to power levels in excess of 400W. These power levels were used to help speed the cooldown of the system and to achieve the 10W cooling power during the tests in December The only modification required to date has been the replacement of the potentiometer used to set frequency.

Motor/Compressor

Developments for the motor/compressor assembly include improvements to the bearing system and improvements in aerodynamic performance of the compressor. Bearing developments were conducted in bench top tests without the requirements for closed loop

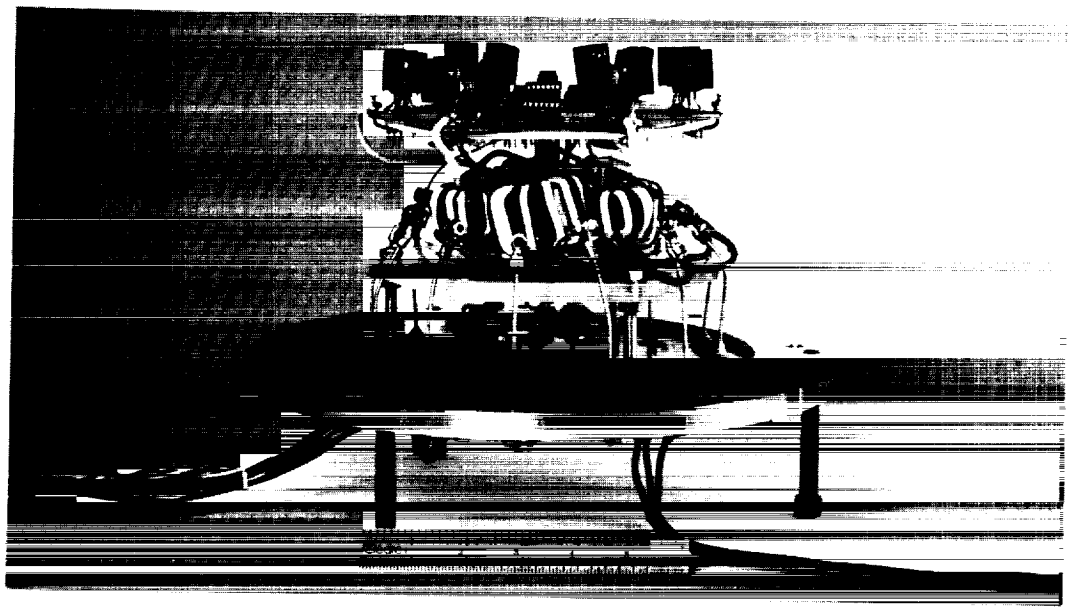

Figure 3.1. Three Phase Inverter Test Article

operation. Aerodynamic improvements involved the fabrication of new impellers and diffusers. Performance tests were conducted to support the aerodynamic developments. These tests consisted of compressor tests in an isolated closed loop and system level tests with the entire cryocooler in operation.

The original motor/compressor assembly incorporated pressurized gas bearings to provide radial support for the shaft and a passive permanent magnet thrust bearing to carry axial loads. This assembly had been useful in providing robust support for the shaft during the developments of the motor prior to the start of this effort. The bearing system had to be modified for use in space, because there is no external source of pressurized gas to activate the journal bearings. Self acting tilt pad gas bearings replaced the pressurized journal bearings. The magnetic thrust bearing was also replaced by a spiral groove self acting gas bearing in order to improve the reliability of start stop operation and to provide additional thrust carrying capacity. Figure 3.2 is a photograph showing a tilt pad journal bearing, the spiral groove thrust face for the impeller, and an impeller and shaft. Figure 3.3 is a photograph of the compressor assembly.

The bearing developments consisted of a series of spin tests with tilt pad bearings in which the clearances and tilt angle of the pads were varied until the desired stability and start up behavior was obtained. The initial settings can be predicted approximately by analysis. Final adjustments are performed using trial and error approaches with suitable instrumentation to observe and monitor shaft stability. The final settings for the tilt pad bearings are a compromise between high capacity (very close clearances) and low drag (relatively large clearances).

Tests to integrate the spiral groove thrust bearing were straightforward. The bearings were designed to meet the new impeller geometry (see following paragraphs). Mechanical spin tests were performed to verify that the bearings provided the necessary thrust capacity. No adjustments are required.

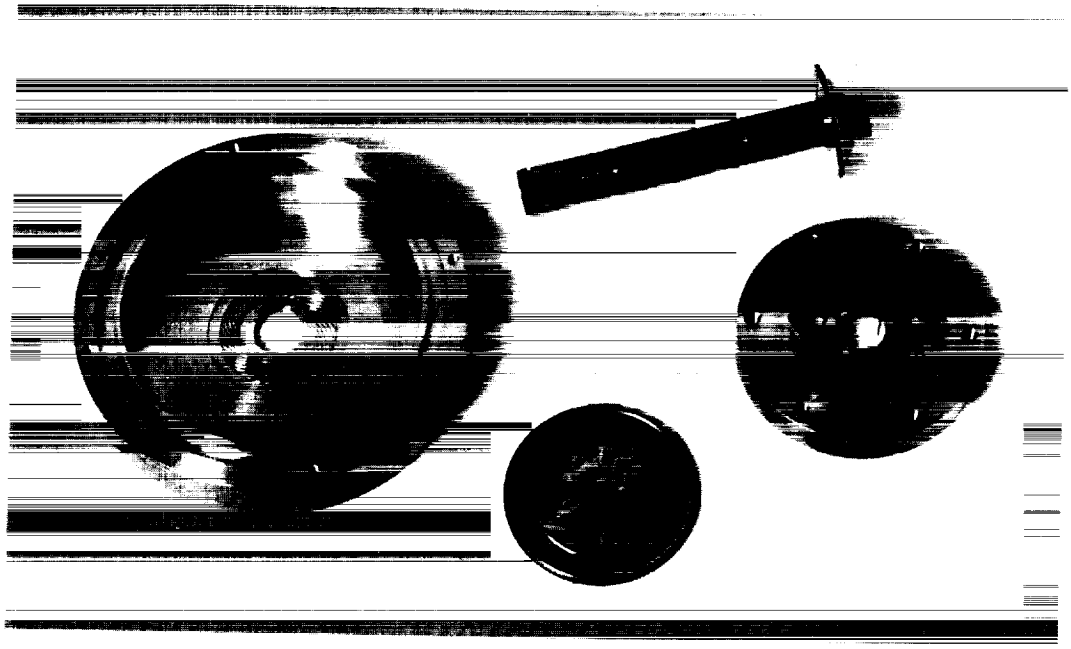

Figure 3.2. Compressor Impeller and Shaft (top), Tilt Pad Bearing (right) and Spiral Groove Thrust Face (left)

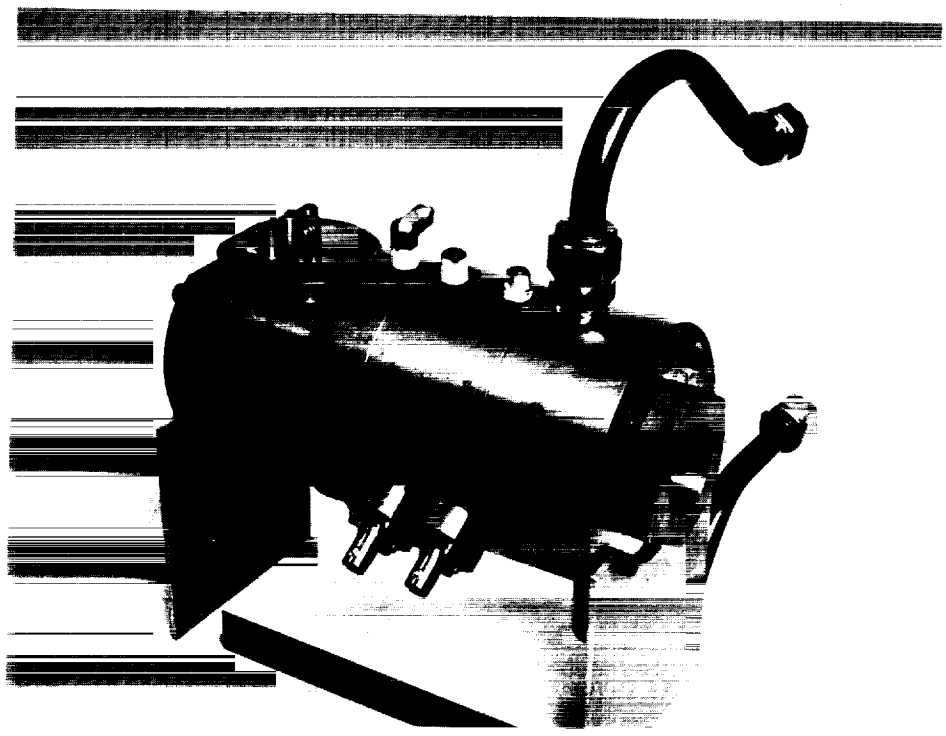

Figure 3.3. The Brassboard Compressor Assembly

Improvements to the aerodynamic performance of the compressor were made by redesigning the compressor impeller, and developing a diffuser. The initial assembly incorporated a drilled hole impeller. The drilled hole impeller was simple to fabricate and produced desired pressure and flow characteristics. However, the efficiency was poor, resulting in excessive input power. A replacement impeller with contoured flow channels was designed to improve the efficiency. A key feature of the new impeller is that it is machined from a solid piece of titanium alloy. This eliminates a need for brazing a two piece assembly, simplifying the balancing of the component and increasing the structural integrity. A plunged wire, electric discharge machining process is used to produce the required flow channels. Figure 3.4 shows the new and original impellers. A portion of the shroud on the new design on the right has been removed to show the internal flow passages.

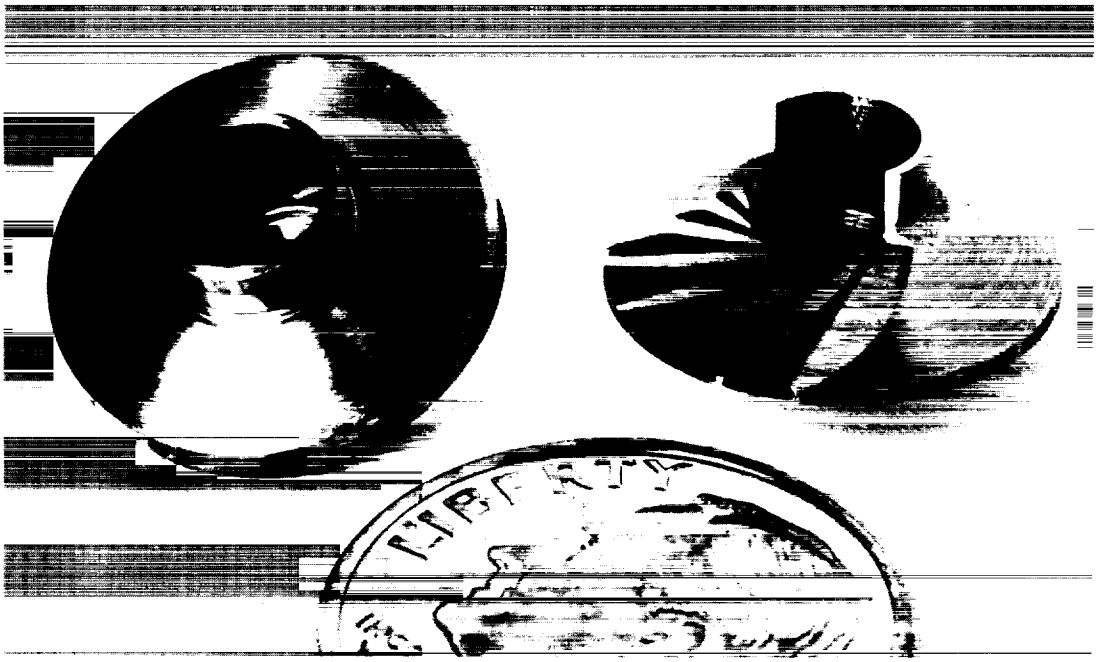

Figure 3.4. Original Drilled Hole Impeller (l) and Bladed Impeller (r)

In addition to the impeller development, several diffuser configurations were evaluated through testing with the impeller. Tests consisted of operating the compressor at several speeds, pressure ratios and flow rates for each geometry configuration. Tests were performed in neon and in air. Temperatures, flow rates, pressures and input power to the inverter were recorded. A series of performance curves were produced, from which final design geometries will be selected for use in the Engineering Model.

Heat Exchanger

Development of the counterflow heat exchanger focused on verifying that predictive modeling of performance was accurate and establishing new fabrication methods so that the

assembly could be brazed. The first objective was met by testing at cryogenic temperatures during tests of the entire cryocooler system. The second objective was met through design and subcomponent braze experiments.

The test article used in the brassboard assembly consisted of copper plates and stainless tubes that are soldered together using soft solder. Figure 3.5 is a photograph of a disk/ring pair showing the two annular rows of slots in each. Each slot is approximately 0.13 mm (0.005") wide x 3.5 mm (0.14") long. There are approximately 1000 slots in each annular row. This approach had the advantage that the assembly process was fairly straightforward. The disadvantages were that the assembly was not sufficiently strong to withstand launch vibration loads, and it was difficult to assure that all contaminants (primarily from the flux) could be removed. This prompted a redesign for the Engineering Model hardware that would rely on vacuum brazing. Thus, contaminants could be baked out at high temperature, and the assembly would have the required strength. The new design incorporates stainless steel spacers between copper plates replacing the stainless steel tubes and disk/ring pairs.

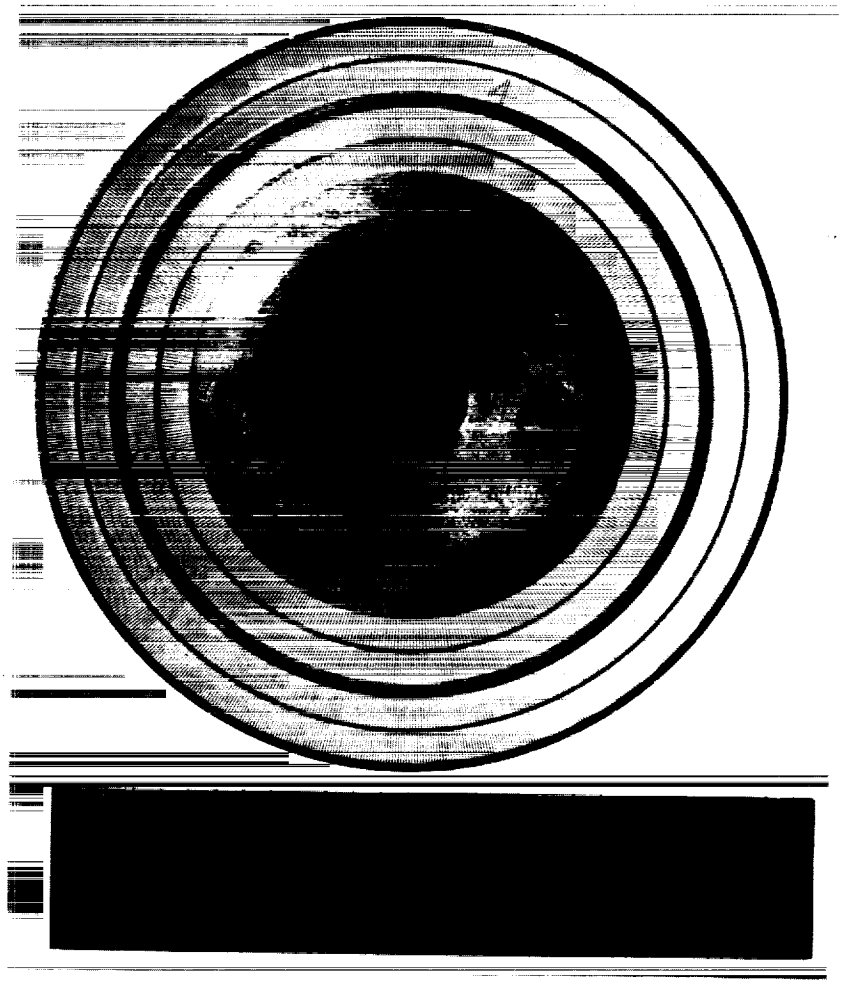

Figure 3.5. Disk/Ring Pair For Brassboard Heat Exchanger

Several series of braze trials were performed on plate and spacer subassemblies. Generally, the trials were conducted to assess cleaning and preparation methods, braze materials, temperatures and the effects of changes in geometry on the integrity of the brazed joints. Braze integrity was assessed by tear tests and helium leakage testing. These efforts were successful in finalizing a suitable configuration and fabrication methodology.

Tests to verify the predictive model of the heat exchanger were performed with the full cryocooler system operating at various conditions. The heat exchanger assembly was installed in the brassboard loop with the turboexpander and compressor. Measurements of flow rate, temperatures and pressures at the inlet and exit ports provided all the information necessary to accurately characterize the performance of the device. Test data were recorded for a range of flows and temperatures down to 35 K.

Turboexpander

Tests were performed with two turboexpanders. The brassboard turboexpander had been designed for roughly 8 W capacity at 65 K (thus providing about 5 W to the load and 3 W to accommodate heat exchanger ineffectiveness). This machine was tested with two brake diameters and over a range of brake temperatures. A second, smaller turboexpander with a capacity of about 5 W was tested at lower flow rates to assess the cycle at different loads. Both turboexpanders were tested at temperatures from about 300 K down to about 35 K Detailed performance data were obtained for temperatures between 70 K and 35 K.. All tests were conducted in the closed loop cycle. Fluid lines at the warm and cold end of each of the turboexpanders were readily adaptable to the flanged tube connections in the facility. Figure 3.6 is a photo showing the turboexpander housings and the two turbine shafts. The machine on the left has a 2.38 mm diameter turbine rotor, the one on the right is the 3.18 mm diameter rotor. The fittings on the housings are for warm and cold end tube connections.

These tests were primarily aimed at obtaining more to be used to verify aerodynamic modeling of the turbines and to provide corroborative data about heat leak within the turboexpander assemblies. The data were then used to upgrade the performance models for the turbines and for the cycle.

Closed Loop Brassboard System Tests

In addition to meeting the objectives stated above at the component level, the closed loop system tests provided practical operating experience with the system. The system includes instrumentation and controls that allow for detailed characterization of each of the components and controls so that pressures, flow rate and temperatures could be varied widely. The tests were performed with the complementary goals of documenting individual component performance and assessing the relative impact of variations in individual component performance on the overall behavior of the system. The next section describes the facility, instrumentation and controls.

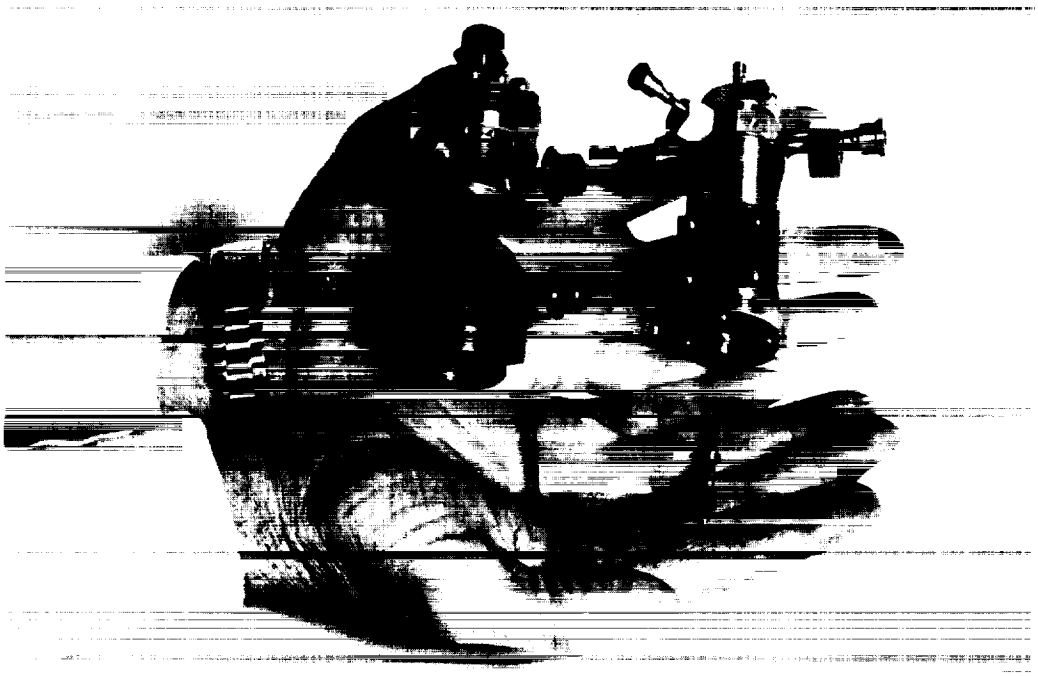

Figure 3.6. Turboexpander Housings and Two Turbine Shafts

3.2 Facility Description

Three series of tests were performed with the brassboard facility. The first series, performed June 9-12, 1992, provided data on the steady state operation of the inverter, compressor, heat exchanger and the 3.18 mm (0.125") diameter turboexpander with a 5.59 mm (0.22") diameter brake over a range of temperatures and inlet pressures. The second series, conducted in September 1992, provided performance data for the 2.38 mm turbine. The third series took place in December 1992. The 3.18 mm turboexpander was again tested, with a reduced diameter brake wheel and at higher system loads. The facility's primary components and configuration was the same for all of the tests. However, several modifications were implemented between the first and second series of tests. The most important of these changes was to include a provision for assisting the cooldown of the system with liquid nitrogen or helium, due to the decreased capacity of the 2.38 mm turbine compared to the 3.18 mm turbine. These changes affected only the cooldown rate, not the performance of the cooler at steady state conditions.

Test Facility

Figure 3.7 is a schematic showing the primary systems in the brassboard test facility. These systems include the power control system, the compressor, turboexpander, counterflow heat exchanger, gas management, and instrumentation and data acquisition subsystems. The working fluid in the system is neon. In addition to these components, a vacuum system

maintained the integrity of the vacuum vessel in which the heat exchanger and turboexpander were installed. Figure 3.8 is a more detailed flow diagram of the facility and support systems.

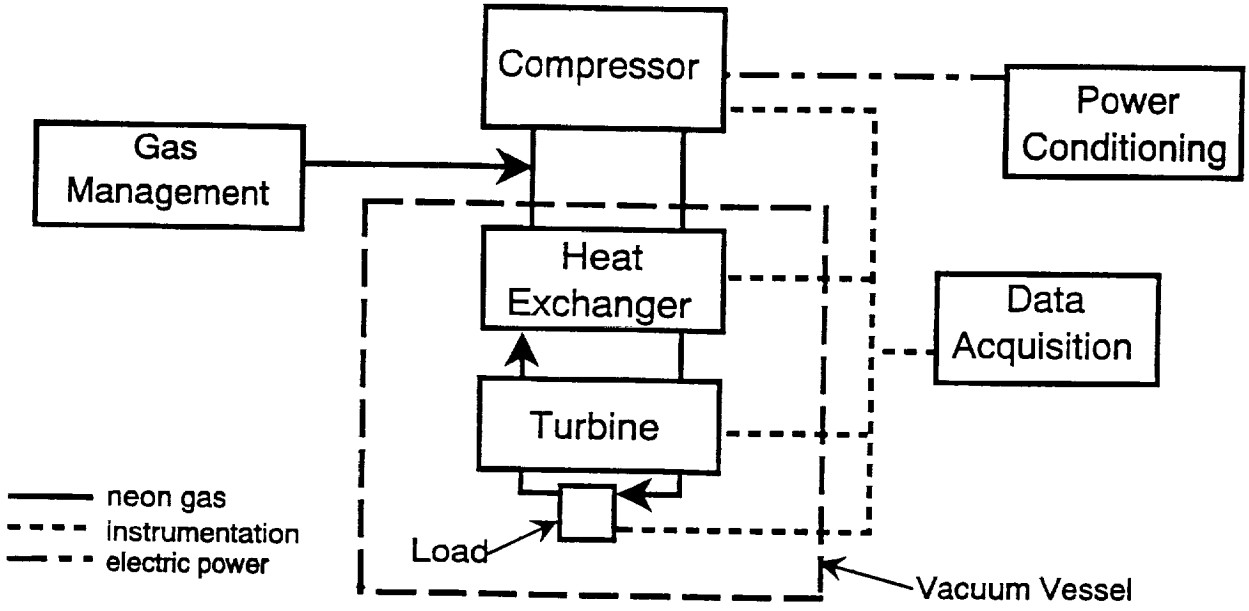

Figure 3.7. Generalized Test Facility Schematic

Power Conditioning

The power conditioning consists of the equipment necessary to convert 110 volt 60 Hz electricity to a form which could be used to drive the compressor. A DC power supply converted wall electricity to regulated DC power to drive the inverter. A Sorensen model DCR 40-25B2, rated to 25 amps, 40 volts was used for most tests. A Hewlett-Packard model 6269B rated at 50 amps, 40 volts was substituted for a short interval to allow for repairs to the Sorenson. The choice of power supply has no effect on results of the tests.

The other component in the power conditioning system is the rotating field inverter. The inverter converts the direct current to a three phase signal which is used to drive the compressor. As configured for the brassboard testing, the frequency and voltage were set independently.

Gas Management

The gas management system allows for purge and fill of the cryocooler and test loop, decontamination of the gas, isolation of sections of the facility for replacement of components, pressure control during testing and the bypassing of flow during cooldown or during subsystem testing. In general this system incorporated valves and extra flow loops that are required for all operations except steady state testing at design point.

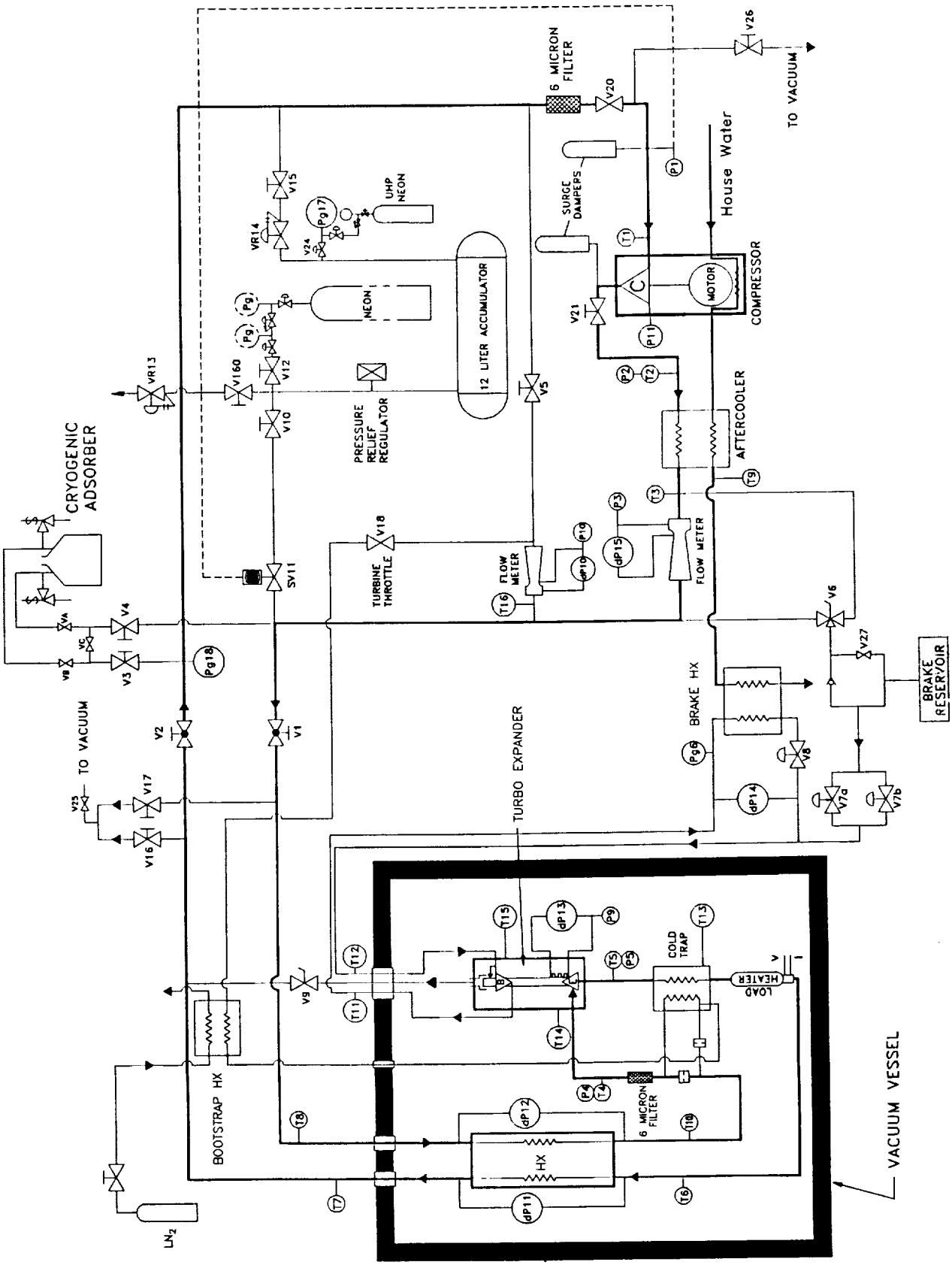

Figure 3.8. Detailed Facility Schematic

The system is initially supplied with neon from a gas cylinder. A three gallon accumulator tank is included in the circuit to provide a volume for use in regulating the system pressure. When the system pressure is high, gas from the compressor outlet is pumped into the accumulator. When system pressure is low, gas from the accumulator is bled back to the low pressure side of the flow circuit. The pressure control system was used to maintain relatively constant system pressure during cooldown and warm up of the system. The management system also provided make up gas to the system to compensate for a small but continuous leakage of neon out of the system. The leakage occurred in the warm portion of the flow circuit exposed to ambient. The tubing in the vacuum vessel was sealed to high vacuum levels.

Provisions were made with a compressor bypass circuit to permit control of flow to the turbine independent of the compressor flow rate. At the design point, the 3.18 mm turbine and the compressor have matching flow rates. For off design operation, and for tests with the 2.38 mm turbine, the turbine requires less than the full compressor flow. A portion of the compressor flow can be diverted through the bypass circuit by means of a manually operated valve.

The working fluid in the system is neon. Two grades of neon were used during brassboard testing. Ultra-high purity neon was used for the initial stages of purge and refill in the system to remove contaminants. Research grade neon was used for the final purge and refill stages, and for the tests. A commercial cryogenically cooled charcoal bed adsorber was used to remove condensable contaminants from the neon after initial purge and refill cycles. Gas flowing through the cryogenic adsorber is cooled to approximately 77 K (liquid nitrogen temperature). Contaminants that will condense at or above this temperature do so in the adsorption heat exchanger and are removed from the gas stream. The gas also flows through a bed of activated charcoal, where contaminants not condensed in the heat exchanger are adsorbed onto the surfaces of the granular charcoal particles. The gas was circulated through the adsorber for the first few hours of cooldown prior to testing. The adsorber was then isolated from the circuit.

The facility includes a precooler to assist in speeding the rate of cooldown of the system. The precooler consists of a vacuum jacketed counterflow heat exchanger made by brazing two stainless steel tubes together along their length. During operation of the precooler, a fraction of the compressor outlet flow is directed through one of the tubes of the precooler, then returned to the main flow just upstream of the turbine. Liquid nitrogen or helium flows through the other tube in the precooler which is open to atmosphere. The precooler is isolated from the system when the desired system temperature is achieved.

Vacuum System

The portions of the cryocooler and facility that are subject to cryogenic temperatures are contained within a vacuum vessel to reduce convective heat leak from ambient. These components are also wrapped in multilayer insulation to reduce radiation from the surfaces within the vacuum vessel that are at ambient temperatures. The main components involved are

the heat exchanger, the turboexpander and load. Figure 3.9 shows a physical view of the cold end of the cryocooler facility, showing the arrangement of components within the vacuum vessel.

The vacuum vessel is a 30.5 cm (12 inch) diameter × 91 cm (36") long stainless steel cylinder with a flanged top plate that provided structural support for the components mounted within. Tubing passthroughs were sealed with Buna-N O-rings in flanges. Electrical passthroughs rated for 10^{-8} torr or below were used for power and instrumentation leads. Buna-N O-rings were used to seal the other ports on the cold box, such as for the ionization vacuum gage.

Vacuum inside the vessel was maintained at 10^{-5} torr or better during testing. The vacuum system consists of a roughing pump, a diffusion pump, and a high vacuum valve. The roughing pump was an Alcatel direct-drive pump, model 2012A, with a capacity of 11 ft^3/min. The diffusion pump was a Varian model HS-2, with a capacity of 285 liters of air per second from a pressure of $5x10^{-4}$ torr or less. An Airco-Temescal 2 inch sliding gate high vacuum valve was used to isolate the diffusion pump from the cold box when the pressure in the cold box was too high for the diffusion pump to operate effectively. A 2.5 inch (6.35 cm) vacuum port on the collar of the cold box was used to connect the pumps to the cold box.

Cold Load Heater

Load on the cryocooler at the cold end was controlled and simulated with a model PFO-6 Hotwatt heater, rated for 400 watts of heating at an input voltage of 120 volts. The neon passes over a heating element which is enclosed in stainless steel. The enclosure eliminates the potential for contamination of the gas.

Heat Rejection System

Heat is rejected from the cryocooler at the following warm locations of the system:

- Inverter
- Motor/compressor housing,
- Compressor gas, and
- Turboexpander brake.

The inverter was kept at nominal ambient temperature by a muffin fan mounted above the circuit board. The motor/compressor housing was cooled by water flowing through passages in the housing. The gas from the compressor was cooled in a commercial shell and tube heat exchanger using water on the shell side. The heat generated in the brake was removed from the gas using commercial shell and tube heat exchanger constructed of 316 stainless steel. House water, at approximately 290 K, flowed on the shell side, with the neon flow on the tube side.

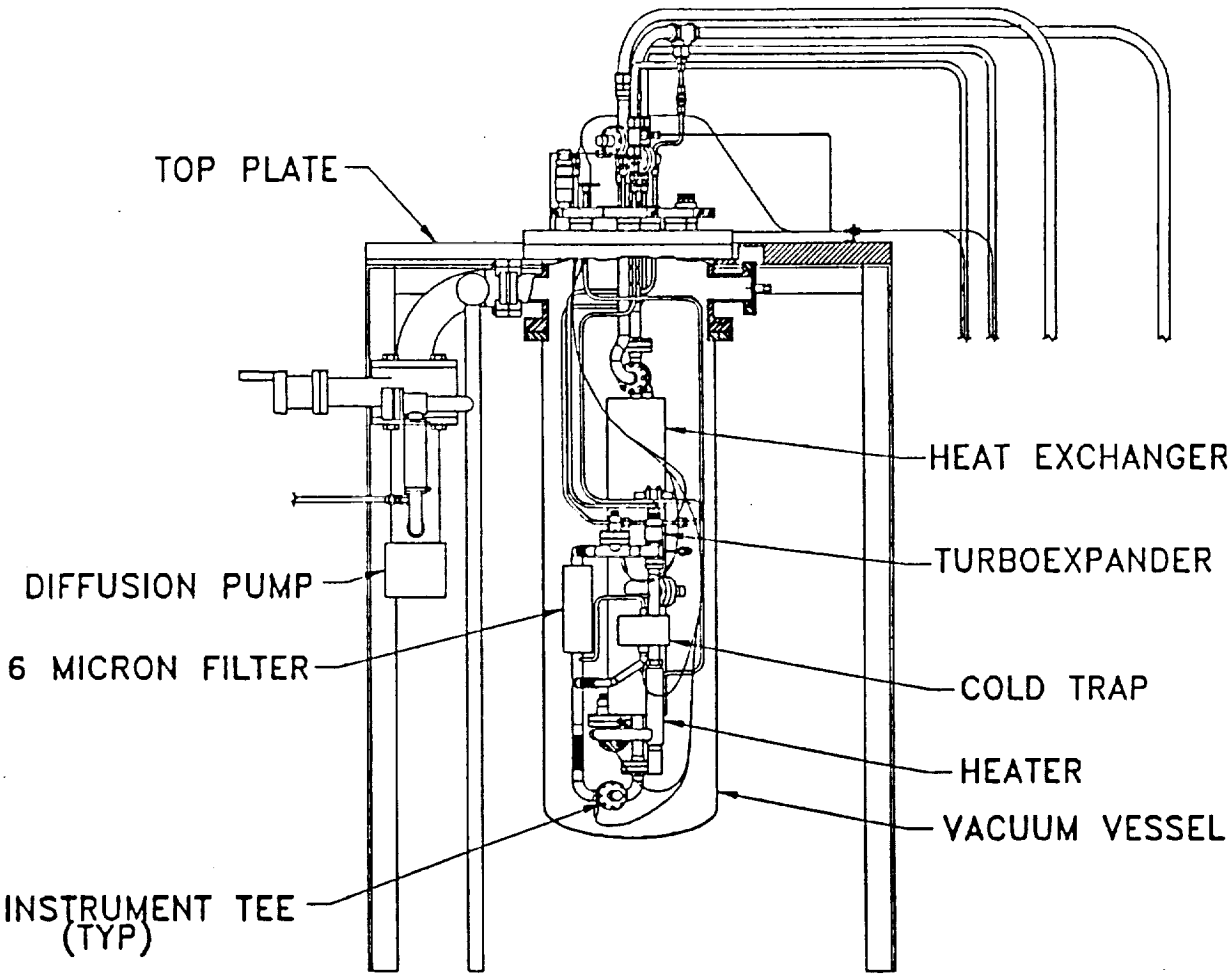

Figure 3.9. Brassboard Test Facility Cold End (Multilayer Insulation has been Omitted)

Tubing, Connections and Valving

The tubing, connections and valving used in the test facility fall into two general categories. Inside the vacuum vessel, primarily 316 stainless steel tubing was used. Connections were made either with a welded joints or with flanged static connections sealed with a Buna-N O-rings or indium seals. All tubing in the vacuum vessel was assembled from new materials for the brassboard tests. The cryocooler components and flow passages within the vacuum vessel were leak tested, and there was no detectable leakage.

Tubing exposed to ambient conditions outside the vacuum vessel consisted primarily of copper tubing. Connections were typically made with metal to metal compression fittings, such as Swagelok®. Ball valves, needle valves, and regulators used for control of the facility outside the vacuum vessel were generally commercial quality, not intended for high vacuum service. The plumbing outside the vacuum vessel contained some small leaks, which were considered to have a negligible impact on the operation of the system.

Filters

Two filters are installed in the test loop to trap particulates that might remain in the system. One is located upstream of the inlet to the turbine and one is upstream of the inlet to the compressor. Each consists of 6 micron stainless steel mesh elements in a welded cylindrical assembly.

Cycle Cold Trap

A small experimental counterflow heat exchanger was installed at the cold end of the system to freeze out contaminants upstream of the turbine inlet. A small portion (about 7 %) of the flow in the high pressure stream to the turbine was diverted through this cold trap. The cooling was provided by the low pressure stream exiting from the turbine. This design was relatively ineffective in removing contaminants. Contamination in the facility was more effectively controlled by bypassing flow through the cryogenic adsorber described above.

Test Procedures

Each test series consisted of several phases: system cleaning, cooldown, thermal stabilization, steady state tests, and shutdown. The system was first flushed with clean neon. Next, the compressor was started to begin gas circulation. The gas in the facility was then cleaned using the cryogenic adsorber. The cooldown began after the cryogenic adsorber was isolated from the flow circuit. During tests performed in June the system was cooled solely by the turboexpander. For tests in September and December the precooler was used to speed the cooldown process. In general, cooldown continued until a target temperature at the cold end was reached. Then the system was allowed to stabilize. During cooldown, the turbine and the external precooler provided refrigeration to cool all components inside the vacuum vessel. Because of the thermal mass of the heat exchanger, this component was the slowest to reach thermal equilibrium. In tests where detailed performance of the heat exchanger was important, the facility was allowed to operate for 6 - 12 hours at a nearly constant cold end temperature until thermal equilibrium was reached. Then the steady state tests were performed. Once the steady state test matrix was completed, the turbine and compressor were stopped, and the system was allowed to warm slowly to room temperature.

3.3 Instruments and Data Acquisition

Two types of instruments were used in the facility: precision instruments to measure detailed performance of the cooler and of the individual components, and instruments to support

the operation of the facility. Figure 3.8 shows the location of the instruments. Table 3.1 is a list of instruments with important characteristics of each. Most performance measurements were recorded automatically with a 386 personal computer. Figure 3.10 shows the basic configuration of the data acquisition system and associated supporting equipment.

Software based on ASYST® was used to coordinate the reading and recording of the data. Each instrument was scanned once a minute and its value was then recorded. A majority of the parameters were recorded by the computer. Turbine and compressor speed, inverter DC input current and voltage, and inverter frequency were manually entered. Data files were recorded for one hour intervals. In addition to the automated recording of data every half hour, a reduced set of screen parameters were printed to provide a hard copy record.

Temperatures

Two types of instruments were used for temperature measurements. Platinum resistance thermometers (PRT's) were used to record all performance measurements inside the cold box. They were also used for the heat exchanger temperatures just outside the cold box. Omega Type T thermocouples were used for the remainder of the temperature measurements.

PRT's were used for measurements at the turbine because they are more sensitive than other sensors in the 65-70 K range. Their high accuracy also accounts for their selection for the heat exchanger warm end temperature measurements. Figure 3.11 shows how the PRT's were installed within tube sections. The PRT elements are attached to a G-10 mounting board with thread and shellac. The electrical leads for each PRT are threaded through holes in the mounting board. The primary path for heat leakage to the sensors is through the center of the mounting board to the end, along the end to the outer sides, and back down to the point where the sensors are attached. The secondary path for heat leakage is along the electrical leads. A very fine gauge wire is used to minimize this effect. The direct path from the base of the mounting board to the sensor has been eliminated by removing the connection along the outer edge of the mounting board.

Pressures

Performance measurements of pressure were made using pressure transducers. In addition, pressure gages were included in the facility, as backup for critical pressure measurements and for operational information. Each transducer and gage was installed with a set of valves. These valves allowed isolation of the pressure instruments during the cleaning of the system before testing, or flow through the piping leading to the pressure instrument, minimizing the volume which did not have clean gas circulated through it prior to testing.

The pressure transducers were calibrated over their desired ranges. A least squares fit was performed on the calibration data in order to generate a linear equation to convert the voltage output to the desired value in engineering units.

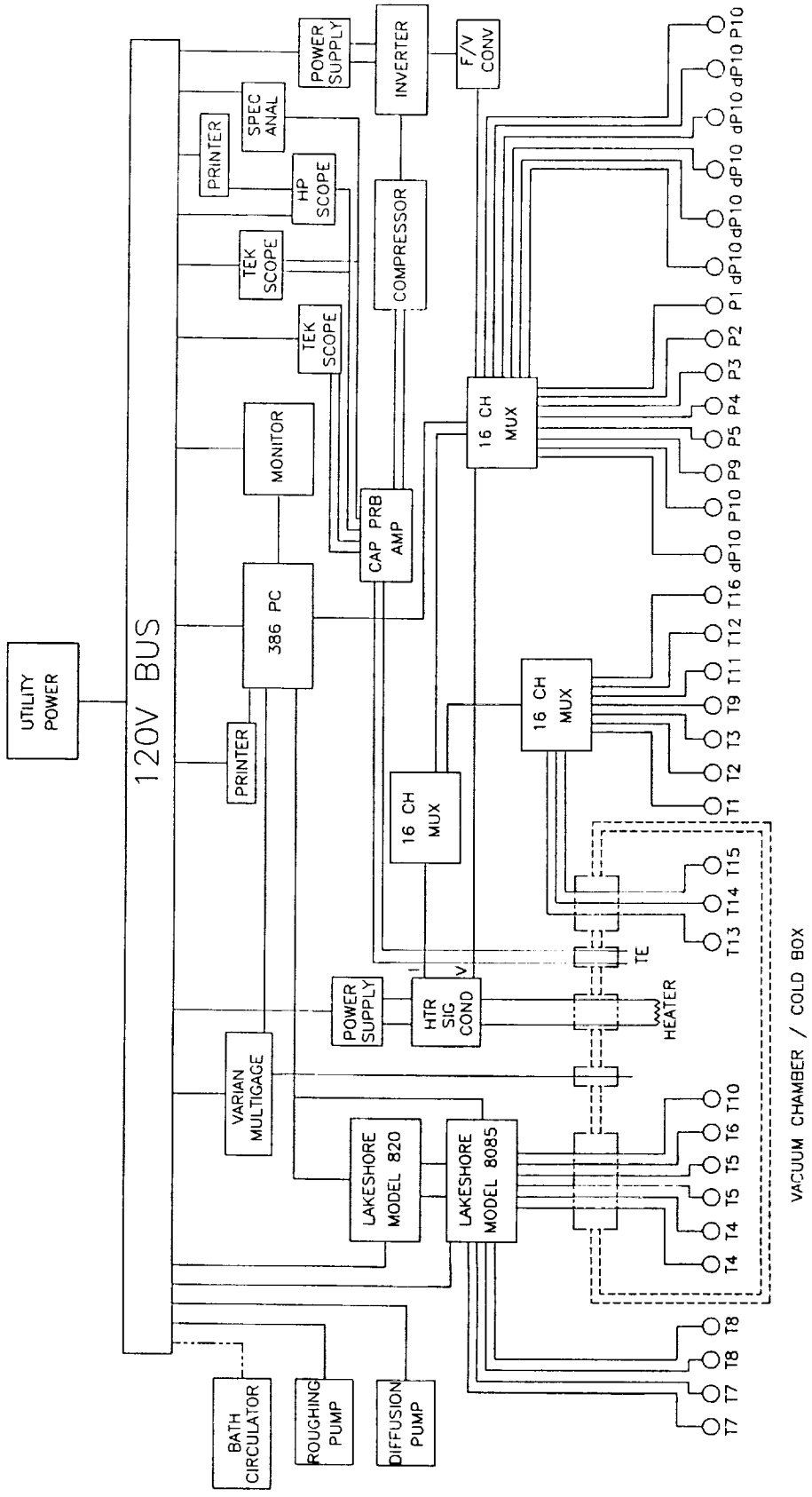

Figure 3.10. Schematic Diagram of Data Acquisition and Support Systems

Table 3.1 Instruments in the Brassboard Test Facility

ID	LOCATION	TYPE	RANGE	ACCURACY
		PRESSURES		
P1	Compressor Inlet	Rosemount	0-15 psig	0.0375 psi
P2	Compressor Exit	Omega	0-25 psig	0.0375 psi
P3	Flowmeter Inlet	Omega	0-25 psig	0.0375 psi
P4	Turbine Inlet	Omega	0-25 psig	0.0375 psi
P5	Turbine Exit	Rosemount	0-15 psig	0.0375 psi
P9	Nozzle Exit	Omega	0-25 psig	0.0375 psi
P10	Bypass Flowmeter Inlet	Omega	0-25 psig	0.0375 psi
P11	Impeller Exit	Omega	0-25 psig	0.0375 psi
Pg6	Brake Exit	Helicoid	0-30 psi	
dP10	Bypass Flowmeter	Gould	0-10 in H_2O	0.025 in H_2O
dP11	HX Low P Side	Gould	0-30 in H_2O	0.075 in H_2O
dP12	HX High P Side	Gould	0-30 in H_2O	0.075 in H_2O
dP13	Turbine Labyrinth Seal	Rosemount	± 30 in H_2O	0.15 in H_2O
dP14	Turbine Brake	Rosemount	0-100 in H_2O	0.25 in H_2O
dP 15	Compressor Flowmeter	Gould	1-10 in H_2O	0.025 in H_2O
		TEMPERATURES		
T1	Compressor Inlet*	Type T TC	30-625 K	1.0°C
T2	Compressor Exit	Type T TC	30-625 K	1.0°C
T3	Compressor Flowmeter Inlet	Type T TC	30-625 K	1.0°C
T4	Turbine Inlet	LS PT-111 (2) **	14-325 K	0.07°C
T5	Turbine Exit	LS PT-111 (2)	14-325 K	0.07°C
T6	HX Lo P Side Inlet	LS PT-111	75-475 K	0.10°C
T7	HX Lo P Side Exit	LS PT-111 (2)	75-475 K	0.11°C
T8	HX Hi P side Inlet	LS PT-111 (2)	75-475 K	0.11°C
T9	Cooling Water	Type T TC	30-625 K	1.0°C
T10	HX Hi P Side Exit	LS PT-111	14-325 K	0.10°C
T11	Turbine Brake Return	Type T TC	30-625 K	1.0°C
T12	Turbine Brake	Type T TC	30-625 K	1.0°C
T13	Cold Trap	Type T TC	30-625 K	3.0°C
T14	Turbine Housing	Type T TC	30-625 K	3.0°C
T15	Turbine Brake Housing	Type T TC	30-625 K	1.0°C
T16	Bypass Flowmeter Inlet	Type T TC	30-625 K	1.0°C
T17	Bootstrap	Type T TC	30-625 K	3.0°C

NOTES:

* Compressor Inlet Temperature located in tube upstream of housing for June tests.
Inlet Temperature measured at the inlet to the impeller during September and December Tests.

** LS PT-111 refers to Lakeshore platinum resistance thermometers, part #111.

Mass Flow Rate

Flow rate in the test loop was measured using Flow-dyne venturi type flow meters at two locations: the compressor outlet and the turbine bypass loop. The pressure and temperature at each meter's inlet and the pressure drop across each meter were used to determine the flow rate.

During parameter testing for the 3.18 mm turbine, no flow through the bypass loop was permitted. During this period, the measured flow rate at the compressor outlet is the same as the flow rate to the turbine. During the cooldown phase of the tests, when the cryogenic adsorber is not in the flow loop, a fraction of the compressor flow is bypassed around the turbine, through a throttling valve and back to the compressor inlet. For this reason, it is necessary to measure both the compressor output flow and the bypass flow, as the flow to the turbine is the difference between the two.

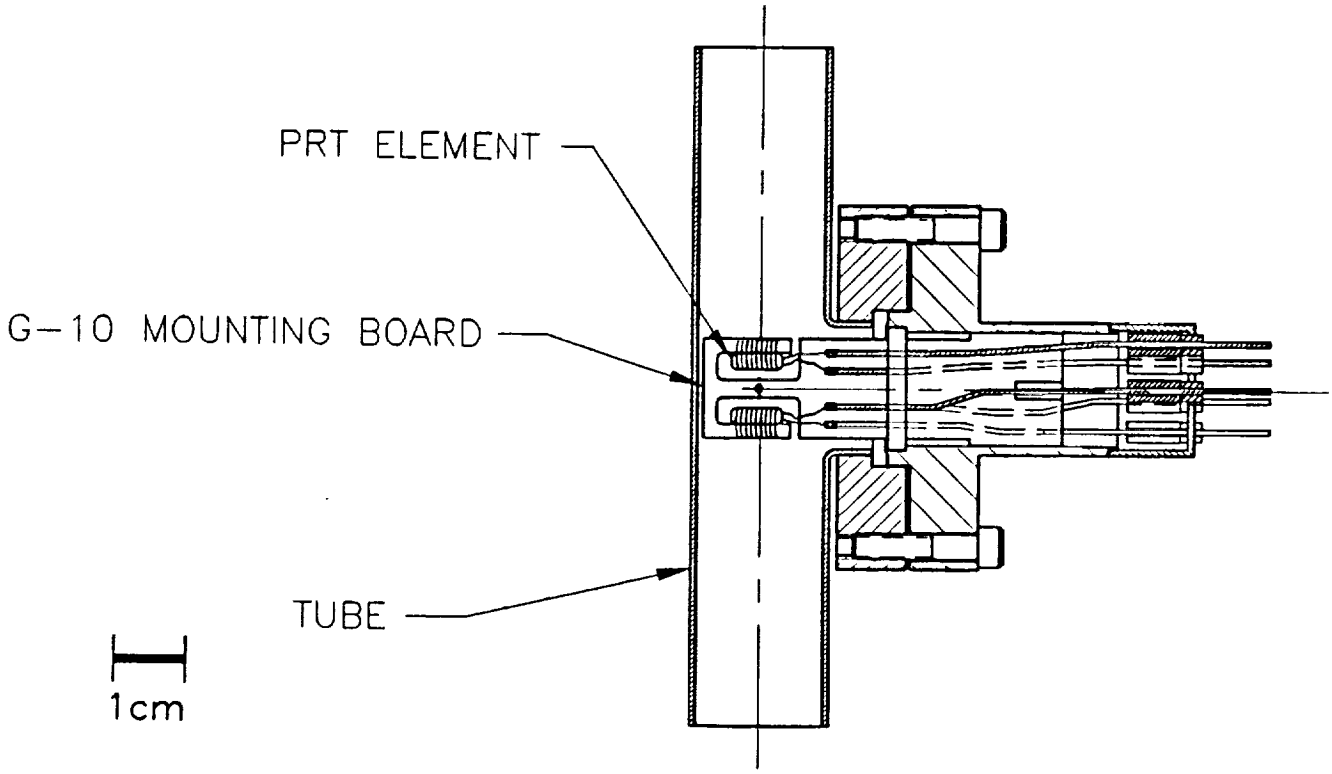

Figure 3.11. Mounting Detail for Platinum Resistance Thermometers

Turbine and Compressor Rotational Speed

The rotational speeds of the turbine and compressor were measured using capacitance probes. On each shaft there is a small flat surface ground on the shaft. A capacitance probe in the wall of the housing is used to measure the capacitance between the probe and the shaft. As the flat on the shaft passes the probe, there is an increase in the measured capacitance. An amplified signal is sent to an oscilloscope, where the speed is determined by the time between "spikes" in the voltage signal.

Inverter Power

The inverter power is determined by measuring the DC power supply's output power, calculated as the product of the measured voltage and current. The voltage was measured with a Hewlett-Packard 3478A Multimeter. The current was determined by measuring the voltage drop across a precision resistor, also using a Hewlett-Packard 3478A Multimeter. The voltage was measured to 0.01 volts, and the current was measured to 0.01 amps.

Cold Load Heater Power

The heater power was calculated as the product of the heater power supply voltage and current. The voltage was reduced using precision resistors and read directly as an analog signal by the computer. The current was determined by measuring the voltage drop across a precision resistor, and then calculating the current.

Vacuum

The pressure level in the vacuum vessel is measured with a Varian Multigauge System. It is equipped with thermocouple gage tubes to measure rough vacuums ($> 1x10^{-3}$ torr) and a Bayard-Alpert Ionization tube for high vacuum measurement. Measurements of the vacuum are recorded manually from the Varian Multigauge Unit's display onto the data sheets.

3.4 Contamination Control

Specific procedures were implemented to control contamination in the brassboard cryocooler prior to assembly and during the testing program [9]. The experience gained from Phase I also provided input to define the requirements for contamination control in the engineering model. The engineering model is intended for long term testing where contamination, if present, would be more troublesome than in the brassboard facility.

Fluid lines and fittings (elbows, tee and cross junctions, flexible tubing and flanges) were cleaned using paper wipes and isopropyl alcohol (IPA) and blown dry using nitrogen gas. The compressor aftercooler, brake heat exchanger and flow meters were cleaned by rinsing with IPA and dried with nitrogen. Valves in the flow loop were disassembled and cleaned to remove grease and other contaminants from internal surfaces. A two-step process was used employing IPA in an ultrasonic bath, followed by deionized water rinse and air drying. In general, parts were cleaned immediately prior to use to minimize the possibility for recontamination during

storage and handling. The heat exchanger was rinsed thoroughly using IPA to dissolve the residual solvent used in the vapor reflow soldering process. This cleaning step was repeated several times until the effluent from the heat exchanger was visibly clean. Heated nitrogen gas was circulated through the heat exchanger to dry it and to remove any loose particulate material. Completed subassemblies such as the turboexpander and compressor were tested previously in separate facilities. They were removed from these test setups and were stored in clean packaging prior to installation in the brassboard facility. Particulate filters (6 micron) were installed in the inlet lines of the compressor and the turboexpander to eliminate particles from the flow.

Prior to the start of testing, the flow loop was filled with high purity neon gas and the gas was run through a cryogenic trap. This involved evacuation to about 50 millitorr to remove most of the air and then backfilling with ultra-high purity (UHP) neon to about 15 psig to dilute the residual air. The system pressure was then reduced to about 1 psig by venting gas to atmosphere through pressure gauges and transducer fittings which purged the air from the system. This fill/vent process was repeated for a total of eight cycles, five times with UHP grade neon and three times with certified research grade neon. Flow was started in the brassboard facility and the gas was cleaned using a liquid nitrogen cooled charcoal adsorber. This additional cleaning procedure was implemented following the first cooldown test. It had been observed that the pressure drop across the turbine rotor increased when the turbine exhaust temperature had reached about 240 K and the differential pressure could be restored following a brief warm-up of only a few degrees. This experience indicated the possible presence of contamination in the gas, which was freezing at low temperature and restricting the flow in the turbine. This anomalous behavior disappeared after the cryogenic cleaning step was introduced.

Gas samples were extracted from the flow loop several times during the course of the testing program in Phase I. Samples were sent to an outside laboratory for analysis of possible contaminants including air, water vapor, IPA, and other solvents. One set of samples was found to contain about 180 ppm by volume of nitrogen. This represented a potential freeze out problem for the turboexpander at temperatures below about 42 K. After further sampling and analysis, it was determined that the gas had been contaminated by the supplier at the time the gas bottles were filled, even though the certifications indicated that the gas met the standards for research grade. The contaminated gas cylinders were returned to the supplier and new gas was obtained with verified certificates of analysis. No affect on turboexpander performance could be directly attributed to this nitrogen contamination.

The experience gained in contamination control for the Phase I brassboard test facility will have a direct benefit in the design and operation of the engineering model cooler. Fabrication methods, particularly for the heat exchanger, have been altered to eliminate braze and solder flux compounds which could outgas into the process gas during long-term testing. Cleaning techniques for lines, fittings and other components were developed and new cleaning processes were defined which eliminate the use of CFC-based and alcohol-based solvents. All tubing used in the cooler will be polished to minimize the potential for surface-absorbed contaminants and fittings will be metal-sealed and vacuum tight so that vacuum bakeout will be feasible. Gas filling and cleaning procedures were also developed that will be implemented on the EM cooler and sampling ports will be installed which will allow access to the process gas to determine contamination levels at any time.

4. TEST RESULTS

This section presents the results of the three series of tests performed with brassboard components at the system level. The first series was performed with a 3.18 mm diameter turboexpander in June 1992 and without supplemental precooling. The objective of this series was to obtain detailed performance measurements on the system and the individual components over a range of temperatures and loads. The second series was performed in September 1992 employing a 2.38 mm diameter turbine. A special precooling heat exchanger was used to speed the rate of cooldown to steady state conditions. These tests provided additional performance data at lower flow rates and cooling capacities. The third test series was carried out in December 1992 with the 3.18 mm diameter turbine. These tests yielded data with the turbine brake at lower temperatures and at higher turbine speeds.

4.1 June 1992 Tests - 3.18 mm Diameter Turbine

The objectives of this first test series were to obtain system performance data at 65 K, and 40 K, and to obtain accurate performance data for the components over a range of pressures, flow rates and temperatures. Each of these objectives was met. Overall system behavior was well characterized for cold end temperatures from 300 K to 37 K. The performance of the individual components was also well documented:

1) relationships between compressor speed, pressures, temperatures, flow rate and input power were established,

2) thermodynamic performance of the heat exchanger at design temperatures was measured, providing corroboration for predictive models, and

3) the thermodynamic performance of the turboexpander was defined for a range of temperatures, speeds and pressures.

Furthermore, the system was operated successfully for about 60 hours without incident.

The following pages present selected data from this test series. Plots of raw data (in engineering units) are first presented in the format of parameter vs. time. Plots of reduced data are then presented in combinations which are meaningful to performance assessment. Finally, a few selected data points are tabulated for detailed discussion and analysis.

The electric input power, cooling load, and turbine exit temperature are shown for the complete 60 hour test in Figure 4.1. The heavy solid line is the temperature of the gas at the exit from the turbine (at the inlet to the load). The initial temperature is about 260 K, reflecting the fact that the data acquisition system did not actively begin recording information until the turbine exit had been lowered to this temperature during initial gas cleaning operations. Input power (the heavy dashed line) is the product of DC voltage and DC current supplied to the inverter. Cooling capacity, or load, is the light solid line. This value is the difference between the enthalpy at the

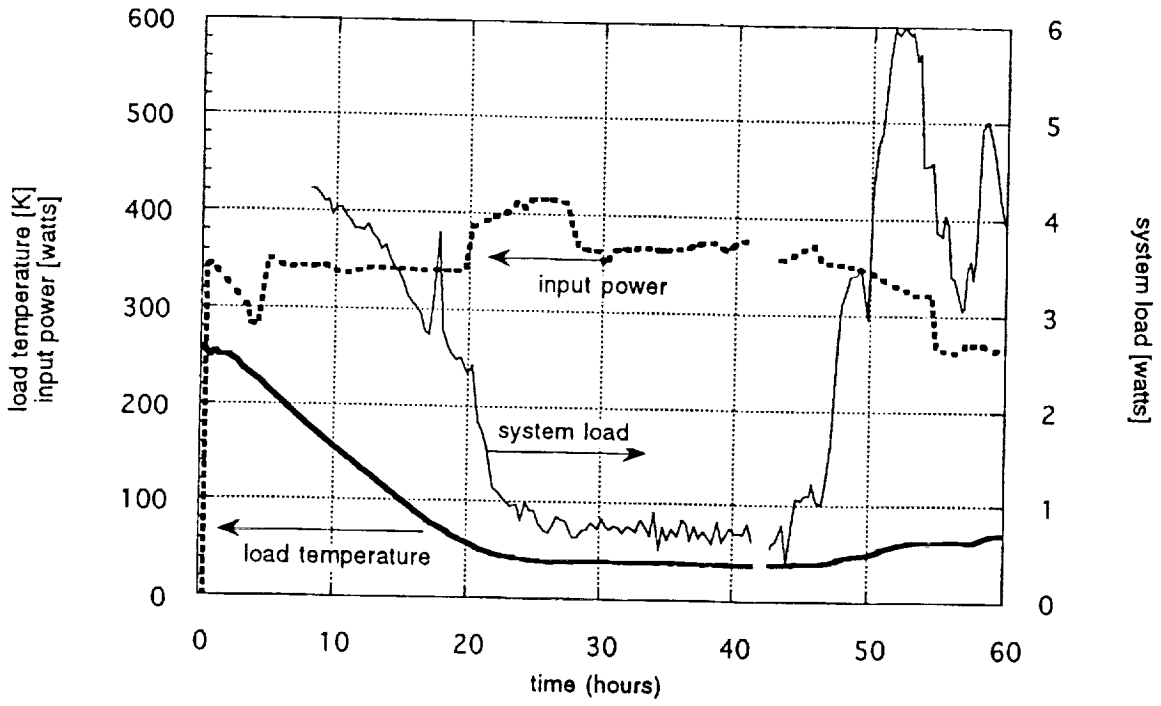

Figure 4.1. Brassboard Cooldown and Steady Test Matrix - 3.18 mm Turbine - June 1992.

turbine exit and at the inlet to the cold end of the recuperator. This load therefore includes parasitic heat loads to the section of tubing between these components as well as the electric heat load to the heater. The parasitic heat load was about 0.6 W for this test series, mostly because of 0.5 W of conductive heat leak through the power leads to the electric heater. The data omissions in the figure reflect periods during which data were not recorded.

The initial cooldown phase took about 24 hours. The turbine exit temperature leveled off at about 37 K. Just prior to the leveling of turbine exit temperature, the compressor speed was increased to 7750, then 8000 revs/second in order to raise the pressure ratio and flow rate through the system. This is reflected as an increase in power to the system for the 8 hour period beginning in the 20th hour. This was felt to be the maximum prudent input power to the system (the rated power for the motor and inverter are approximately half the 400 W that was being supplied). The high power was continued to complete the cooldown of the cold end of the heat exchanger. The intent was to reach thermal equilibrium at the cold end of the heat exchanger in order to obtain an accurate measure of the thermal effectiveness of this component at low temperature.

Figure 4.2 illustrates the thermal stability at the cold end. Two temperature differences are plotted in the figure showing the behavior at the warm end of the recuperator and the cold end as a function of time. The solid curve is the temperature difference between the high and low pressure streams at the warm end, the dashed line is the corresponding difference at the cold end.

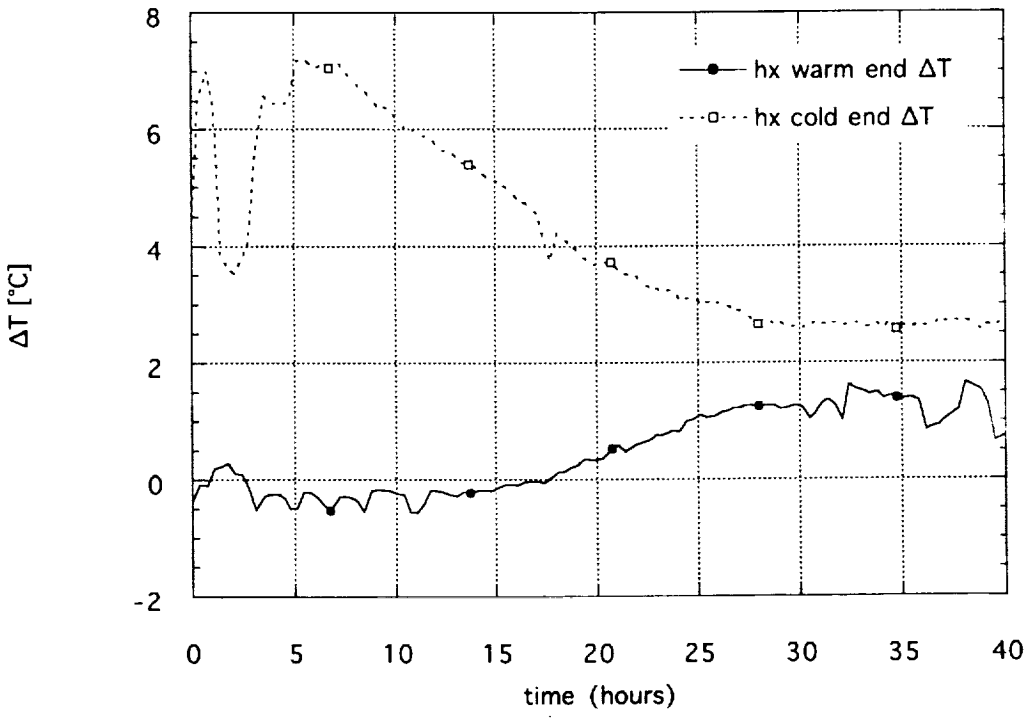

Figure 4.2. Temperature Differences Between the High and Low Pressure Gas Streams at the Warm and Cold Ends of the Recuperator During System Cooldown.

At an approximate time of t = 28 hours, the two temperature differences remain nearly constant, indicating thermal stability in the loop. Prior to that time, the differences between the two "curves" reflect the cooling rate of the heat exchanger. After thermal stability was achieved, the differences reflect parasitic heat leak in the recuperator due to conduction from the warm end and radiation through the multilayer insulation surrounding the cold end components. Figure 4.3 illustrates this approach to stability in terms of the thermal effectiveness of the heat exchanger. Thermal effectiveness was calculated for each set of measurements from real gas properties using the expression given in Appendix I - Definitions of Performance Parameters. The figure shows that the thermal effectiveness of the heat exchanger levels out at just greater than 0.99 at about t = 28 hr. As it became clear that the system was reaching thermal equilibrium, the compressor speed was reduced and the system was allowed to operate without changes in conditions for about 12 hours.

A series of "steady state" tests were then performed. These tests were conducted over a 17 hour period beginning approximately at t = 43 hr. The purpose of the tests was to obtain good performance data primarily for the turboexpander over a range of temperatures, loads and turbine speeds. Eighteen data points were obtained during the 17 hour period. Data were recorded for each test point under relatively steady conditions. That is, a system parameter (such as turbine speed) was changed to a desired condition. Key parameters (such as turbine and heat exchanger temperatures) were then monitored until they reached steady values.

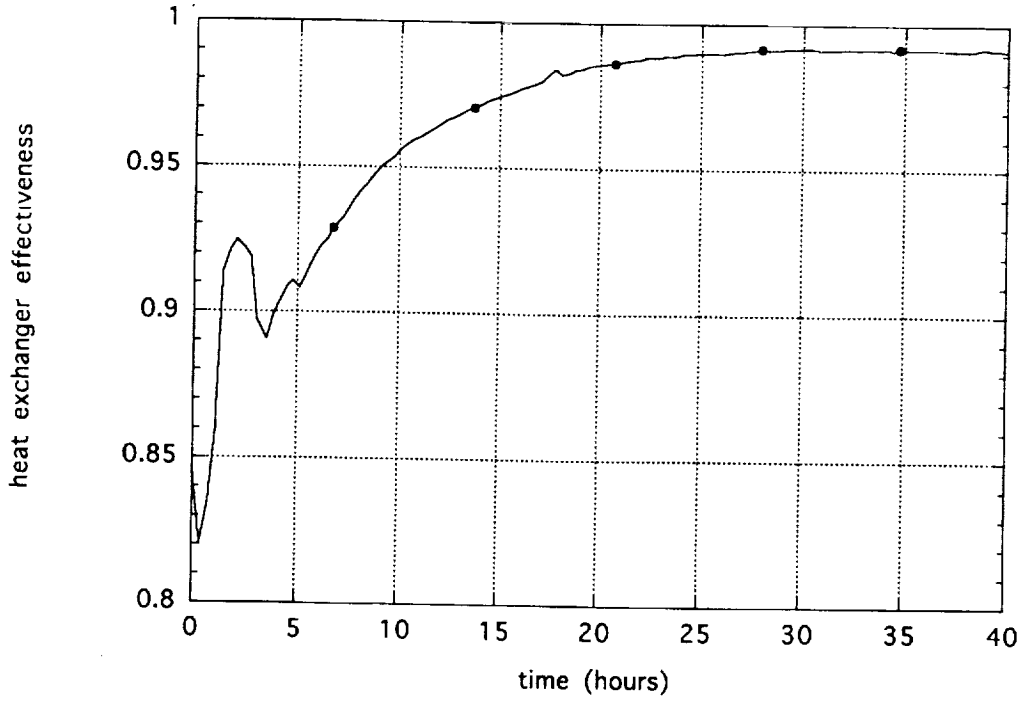

Figure 4.3. Thermal Effectiveness of the Heat Exchanger during Cooldown

In general, temperatures at the inlet and exit of the turbine stabilized relatively quickly. This is because of the low thermal mass of the turboexpander assembly. Steady state test results accurately reflect the performance of this machine. On the other hand, the large thermal mass of the heat exchanger made it too time consuming to wait for equilibrium for the cold end of this component for each test. Many of the "steady state" results yield optimistic characterization of the thermal effectiveness of the heat exchanger. However, two critical tests accurately reflect the steady state performance of the heat exchanger - Test J1 and Test J12. Test J1 data were recorded after approximately 15 hours of steady operation at the same low end temperature. The thermal inertia of the heat exchanger after this period of time had no effect on the measured results. Test 12 data were recorded after the cold end of the cycle had been at approximately 63 K for 3 hours. For this test condition, the effects of thermal mass of the heat exchanger should be negligible. A comparison between the measured performance (listed in Table 5.1) and predicted behavior was excellent. See Section 5. for discussion.

Steady state test results are summarized in Table 4.1, which gives measured parameters at several locations in the cycle. However, because of the thermal mass of the heat exchanger, only a few of these test conditions can be used to accurately characterize system performance. The data are more useful in documenting the performance of the individual components.

The first six columns list the pressures at the compressor, the inlet compressor temperature, the flow rate, and the electric voltage and current to drive the compressor. From these data, overall power train efficiency can be directly calculated (column 7) for each test point.

Overall power train efficiency is the ratio of work for an isentropic compression to the actual electric input power (see Appendix I). Column 8 lists the calculated thermal effectiveness of the heat exchanger for each point. Under steady conditions, for the full range of tests encountered, the value should have varied from 0.991 (at a load temperature near 40 K), to about 0.993 (at a load temperature of 65 K). To the extent that the tabulated effectiveness differs from these values, the corresponding tests will give erroneous relations between system refrigeration and input power. Columns 9 - 14 list turbine inlet temperature, pressure ratio, rotational speed, net efficiency and calculated heat leak. Gas temperature at the exit from the load heater, and system load (including the 0.62 W parasitic) are given in columns 15 and 16.

Data for the performance of the compressor and motor during these tests are limited to the 18 test conditions listed in the table. Overall, the power train efficiency varied from about 0.27 to 0.30 during these tests. Separate tests using other combinations of impellers and diffusers gave power train efficiencies as high as 0.31 for the same motor under comparable test conditions. Later tests on the compressor show that the power train efficiency is improved by modifications to the motor design.

As noted earlier, one of the key objectives for these tests was to establish the performance of the turboexpander over a range of conditions. The purpose was to verify the relationship between efficiency and speed coefficient for the turbine. This information is used to establish the diameter of the brake wheel that will yield best efficiency at the turbine design point. Figure 4.4 summarizes turbine performance during the steady state tests. Net efficiencies and aerodynamic efficiencies (corrected for heat leak as described in Appendix I) for each of the test points are plotted as a function of the speed coefficient u/c_0. The plot shows that once the heat leak to the turbine is properly accounted for, the trend in efficiency with speed coefficient is well defined. The plot also shows that as the maximum efficiency obtained during tests was about 0.77 at $u/c_0 = 0.63$.

The conditions for test point J7, seen in Table 4.1, correspond closely to the system design point. Net refrigeration produced by the system was 5.9 W at a load temperature of 65 K. At this condition, u/c_0 for the turbine was 0.51, with a corresponding aerodynamic efficiency of 0.52. Discussions in Section 5 explain how this information will be used to improve the overall cycle efficiency by modifications to the turbine.

Table 4.1. Steady StateTests - June 1992

	COMPRESSOR				INVERTER		PWR TR	HX	TURBINE					LOAD	
Test #	P_{in}	P_{out}	T_{in}	FLOW	I	V	Effic.	Th.Eff.	T_{in}	PR	Speed	Eff.(N)	Ht.Lk.	Temp.	Load
	atm	atm	K	(g/s)	amp	volt	%	–	K	–	rps	%	W	K	W
J1	1.353	2.133	294.8	1.61	26.35	13.78	26.8	0.992	40.61	1.52	7000	41.8	3.34	38.18	0.62
J2	1.353	2.133	294.4	1.61	24.54	14.54	27.3	0.992	40.72	1.52	6500	42.0	3.25	38.25	0.64
J3	1.363	2.157	294.8	1.6	24.95	14.93	26.3	0.992	42.25	1.52	7200	43.7	3.33	39.85	1.13
J4	1.357	2.143	295	1.6	24.95	14.2	27.5	0.992	42.21	1.52	6500	43.5	3.08	39.79	1.03
J5	1.382	2.235	294.9	1.48	24.97	13.94	28.2	0.993	51.24	1.56	7760	47.6	3.43	49.37	3.35
J6	1.375	2.22	295.1	1.49	24.97	13.91	28.2	0.993	51.67	1.56	6500	45.3	3.05	49.68	2.95
J7	1.345	2.222	296.2	1.36	24.37	13.32	28.4	0.994	66.05	1.6	8000	49.4	3.34	64.88	5.88
J8	1.348	2.221	296.2	1.35	23.97	13.39	28.4	0.994	67.25	1.6	7386	47.7	3.09	66.07	5.68
J9	1.343	2.209	296	1.35	23.97	13.39	28.3	0.993	66.79	1.59	6500	44.0	2.9	65.09	4.51
J10	1.378	2.149	296.6	1.26	21.02	12.56	28.4	0.993	66.6	1.51	7350	45.0	3.14	65.05	3.82
J11	1.371	2.141	296.3	1.25	21.02	12.51	28.3	0.993	66.9	1.51	7670	45.0	3.4	65.38	3.86
J12	1.369	2.134	296.3	1.25	20.86	12.57	28.3	0.993	67.37	1.51	6410	41.7	2.99	65.87	3.49
J13	1.076	1.773	296.3	1.07	22.65	12.03	26.4	0.993	67.6	1.58	6580	39.4	2.93	65.95	3.05
J14	1.089	1.794	296.2	1.08	22.66	11.9	26.9	0.993	67.37	1.59	7300	42.4	3.08	65.74	3.45
J15	1.1	1.813	296.3	1.09	22.66	11.96	27.0	0.993	67.32	1.59	7690	42.9	3.28	65.7	3.52
J16	1.095	1.817	295.8	1.04	22.5	11.8	26.8	0.994	74.62	1.6	7940	43.5	3.4	73.51	4.53
J17	1.088	1.807	295.8	1.04	22.5	11.76	26.8	0.994	74.94	1.6	7300	41.8	3.17	73.7	4.21
J18	1.077	1.79	295.9	1.03	22.51	11.69	26.8	0.994	75.24	1.6	6670	39.7	2.94	73.97	3.90

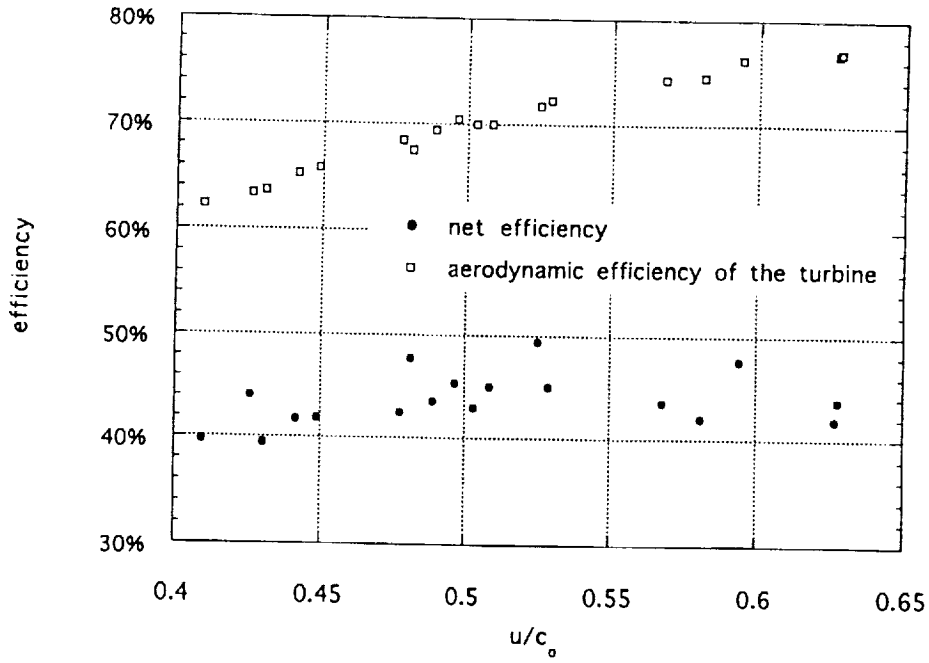

Figure 4.4. Turbine Efficiencies During Steady State Tests (3.18 mm Turbine).

4.2 September 1992 Tests - 2.38 mm Diameter Turbine

Tests were performed during two separate cooldowns with a reduced capacity turbine to provide further information about the performance of the system at lower flow rates. The turboexpander consisted of a 2.38 mm diameter turbine rotor that had been designed for use in helium at about 5 K. Thus it was not optimized for operation at 65 K in neon. However, it gave reasonable performance and was mechanically compatible with the rest of the system. The tests were specifically aimed at acquiring data at lower system flow rates for comparison with the performance of the system with the 3.18 mm turbine. Because of the lower turbine capacity (about 5 W compared with 10+ W from the 3.18 mm turbine), the cooldown was accelerated by using a portion of the compressor flow directly through a precooler using liquid nitrogen and liquid helium.

The flow capacity of the small turbine was less than the design flow rate for the compressor. As a result, a portion of the compressor flow at the warm end of the cycle was bypassed through a throttle valve and returned directly to the compressor inlet. Only about one - half the compressor flow was sent through the heat exchanger and the turboexpander. This mode of operation is equivalent to replacing the compressor with a smaller one specifically designed for lower capacity. Figure 4.5 shows the system refrigeration load, load temperature and equivalent input power for portions of the cooldown and steady state tests (after t = 28 hr.). The equivalent input power is the product of the total electric input power and the ratio of the turbine

flow rate to the total flow rate. This is the power that would result from a smaller compressor with the same power train efficiency.

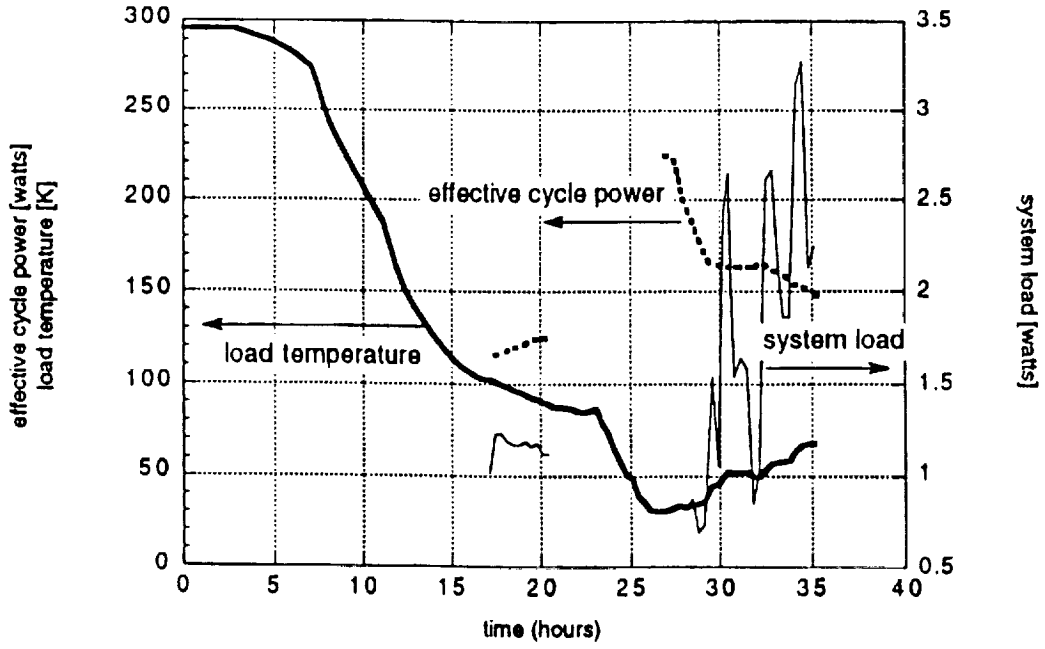

Figure 4.5. Cooldown and Steady State Tests with the 2.38 mm Turbine.

Four steady state test points were recorded - three during the first cooldown on Sept. 22 and one additional point during a second cooldown on Sept. 28. The steady state results are listed in Table 4 2. The columns correspond to those for the June tests except that the flow rate through the turbine has been added. The calculated thermal effectiveness values for the heat exchanger are not meaningful during these tests because of the thermal lag of the heat exchanger.

4.3 December 1992 Tests - 3.18 mm Diameter Turbine

Tests were conducted in December to evaluate the performance of the turboexpander at higher speed, and to obtain data over a broader range of conditions. The brake wheel on the original turboexpander shaft was reduced to 4.83 mm (0.190") diameter to increase the rotational speed. The temperature of the brake circuit was controlled during tests to temperatures as low as 220 K, and system performance was evaluated at loads approaching 10 W at 65 K.

The cooldown of the system was accelerated by means of the liquid nitrogen precooler that had been used during tests with the smaller turbine. Figure 4.6 summarizes important system performance parameters during the cooldown and the steady state tests. The nitrogen precooler was isolated from the system after about 7.5 hours of operation (as the turbine exit temperature approached 80 K). The turbine provided all additional refrigeration to complete the cooldown. The system steadied out at a load temperature of about 36 K at the exit from the load

heater after about 2.5 hours of operation at 36 K. At this time there was about 0.68 W of parasitic heat load at the cold end of the system. The source of this parasitic load has not been determined. The temperature at the exit from the turbine at this condition was 35.6 K with an input power to the inverter of 381 V.

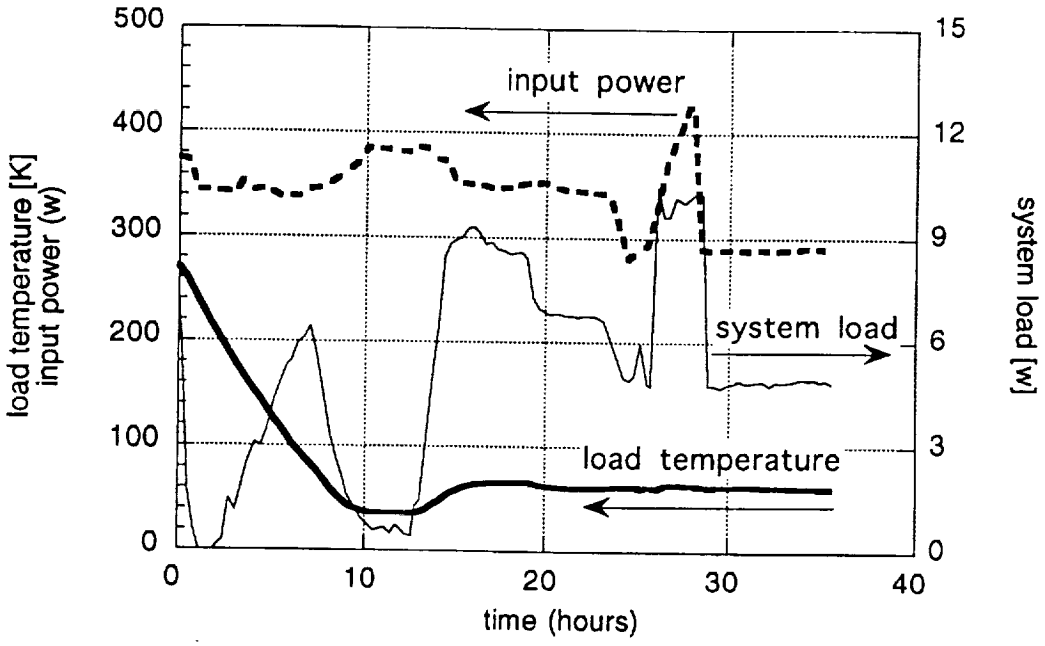

Figure 4.6 Cooldown and Steady State Tests w/ 3.18 mm Turbine (Reduced Brake).

The load heater was turned on to warm the cold end of the system to about 65 K for a series of steady state tests. The tests had three objectives:

- to evaluate the turbine at higher speed,
- to evaluate the system at increased loads, and
- to obtain data with a reduced brake temperature.

A total of 13 steady state test points were selected to demonstrate the flexibility of the system. Results are listed in Table 4.2. The first point was recorded at the end of the cooldown, at a load temperature of 36 K. The next 6 tests were recorded for a range of turbine speeds at two pressure ratios. The load temperature was held to approximately 65 K by varying the heater input power. The following two conditions were recorded at elevated system pressure, with the heater load of about 10 W at 65 K. The final four tests were conducted at reduced system pressure and varying brake temperature.

Several data points show how these tests met the objectives. First, compare test D2.1 with test J7. Conditions for both tests are similar. For both tests, the load temperature is close to 65 K, the pressure ratio at the turbine is about 1.6, and the load is larger than the 5 W design value. The DC input power to the cycle for test J7 is 324.6 W. For test D2.1, the power is 345.4 W. The ratio of the input power to the net cooling is 55 W/W for test J7 and 51 W/W for test

D2.1. Most of this difference is because of the improved turbine efficiency at the higher speed achieved in test D2.1. This resulted from the reduction in the brake wheel diameter. The calculated power train efficiency for the two tests implies that the power train efficiency was significantly higher for the December and September series. In fact this was not the case. The perceived improvement is a result of using different measurement locations for the compressor inlet temperature for these test series. For the June tests, the gas temperature upstream of the compressor housing was used for compressor inlet temperature. For the September and December tests, the gas temperature at the inlet to the impeller was used. This temperature is somewhat higher than the upstream temperature because some heat is transmitted to the gas from the housing.

Tests D3.1 and D3.2 illustrate how the cycle efficiency improves with increased load - basically because the parasitic heat leak through the turbine has a reduced impact on the net efficiency of this component. For these tests, the total cooling available was slightly in excess of 10 W. The DC electric input power was 424 - 425 W for the two tests. This corresponds to a specific power of about 42 W/W at the load temperature of 67 - 68 K. As noted earlier, this test condition was achieved simply by increasing the system pressure. Note also that the speed of the turbine was allowed to increase to 9600 rev/sec. for these two tests, yielding a net turbine efficiency of about 0.61.

The data recorded for tests D4.1 - D4.4 were used to assess the accuracy of estimates of heat leak in the turboexpander. For these tests, the pressure ratio and flow rate was kept nearly constant, resulting in a nearly constant input power to the system. The brake temperature was lowered, reducing the conductive heat leak in the turboexpander assembly. This produced changes in the load and load temperature, generally decreasing the load temperature and increasing the net refrigeration. However, as the brake temperature was reduced to approximately 220 K (test D4.4), the turbine speed decreased because of the increased density in the brake circuit. This produce a decrease in turbine aerodynamic efficiency that offset the improvement from the reduced heat leak. If an increase in overall cycle efficiency is to be realized by operating the brake at lower temperature, the brake wheel diameter must be adjusted accordingly to allow the turbine to operate at optimum (higher) speed.

Table 4.2. September and December, 1992, Steady State Tests

	COMPRESSOR				INVERTER		PWR TR	HX	TURBINE					LOAD	
Test #	P_{in}	P_{out}	T_{in}	FLOW	I	V	Effic.	Th.Eff.	T_{in}	PR	Speed	Eff.(N)	Ht.Lk.	Temp.	Load
	atm	atm	K	(g/s)	amp	volt	%	–	K	–	rps	%	W	K	W
S1	1.501	2.548	312.7	0.675	24.01	13.70	31.40	0.986	52.88	1.68	7150	27.0	1.75	52.15	1.642
S2	1.503	2.564	312.4	0.638	24.00	13.59	31.20	0.990	59.54	1.69	7350	28.3	1.74	58.86	1.794
S3	1.538	2.627	312.5	0.61	24.00	13.69	31.20	0.991	68.53	1.71	7500	29.4	1.73	68.12	2.205
S4	1.532	2.614	311.0	0.83	24.26	13.79	31.10	0.981	36.26	1.69	6900	25.8	1.74	34.90	1.181
D1	1.441	2.238	308.4	1.24	29.36	14.47	27.90	0.992	38.51	1.493	7200	45.6	3.3	35.97	0.606
D2.1	1.461	2.423	307.8	1.49	25.10	13.76	31.00	0.992	66.77	1.606	9200	54.6	3.52	64.97	6.752
D2.2	1.442	2.392	308.1	1.48	25.10	13.70	30.70	0.992	66.67	1.601	8400	54.8	3.09	64.92	6.738
D2.3	1.432	2.375	208.3	1.47	25.10	13.60	30.70	0.992	66.75	1.600	7800	54.2	2.92	64.99	6.563
D2.4	1.458	2.290	305.5	1.37	22.30	12.54	30.50	0.992	66.82	1.520	7800	51.1	3.08	65.07	4.853
D2.5	1.446	2.284	306.0	1.37	22.29	12.72	30.50	0.992	66.82	1.526	7900	51.1	3.11	65.10	4.944
D2.6	1.180	1.960	307.0	1.20	23.73	12.38	29.10	0.993	66.69	1.594	7950	48.9	3.20	65.09	4.759
D3.1	1.832	3.065	310.1	1.88	26.83	15.82	32.30	0.991	70.0	1.625	9600	60.7	3.30	67.90	10.165
D3.2	1.844	3.086	310.3	1.89	26.80	15.86	32.50	0.991	69.54	1.626	9600	60.9	3.32	67.48	10.279
D4.1	1.179	1.953	306.6	1.19	22.94	12.58	29.20	0.993	66.98	1.589	8000	48.9	3.16	65.40	4.715
D4.2	1.183	1.958	306.7	1.2	22.90	12.57	29.40	0.992	67.05	1.59	8000	51.0	2.71	65.26	4.865
D4.3	1.183	1.952	306.4	1.2	22.89	12.57	29.30	0.992	66.5	1.586	7800	53.1	2.21	64.65	4.970
D4.4	1.180	1.948	306.4	1.21	23.14	12.54	29.10	0.992	66.12	1.585	7300	52.3	2.12	64.28	4.880

5. DISCUSSION OF TEST RESULTS

There are several important conclusions derived from the tests:

Inverter - The inverter functioned as designed during all tests. Relationships between inverter efficiency and slip ratio were established. A frequency/voltage relationship can be "hard-wired" into the next generation device. These results are not presented in the prior section dealing with testing, they were a small subset of tests performed during system tests.

Compressor - Operating conditions for the compressor (speed and flow rate) were maintained at relatively fixed values for the system level tests. From time to time, the compressor speed was changed by adjusting the frequency to the inverter. Separate tests conducted in a closed loop were used to evaluate the performance of various combinations of diffuser and impeller. Generally, these tests resulted in incremental improvements in compressor efficiency. Subsequent to the cryogenic system tests, an improved motor stator was installed in the compressor. Comparative tests were performed to judge the change in efficiency resulting from the changed motor. The same diffuser and impeller combination were used with both tests. Figure 5.1 shows the results. Power train efficiency is shown for two machines. The upper curves result from tests with the changed motor stator. The lower curves give performance at comparable conditions with the compressor assembly used during cryogenic system tests. The conclusion to be drawn is that the improved motor design will produce an increase in power train efficiency of roughly 15 %. This corresponds to a decrease in input power to the cycle of the same magnitude.

Heat Exchanger - Test results for the heat exchanger were used to evaluate the predictions from a thermal model of this device. Table 5.1 shows the comparison. The table shows that the experimental results agree closely with the model predictions, for both thermal effectiveness and pressure losses. The test results confirm that the heat exchanger met the desired target. The test points for this comparison were done so because they were preceded by substantial periods of time at nearly steady temperatures at the cold end, ensuring thermal stability in the heat exchanger.

Turboexpander - Test results for the turboexpander showed that the measured net efficiency is below the value needed for the system to meet its expected targets. There are two contributing factors. First, the aerodynamic efficiency of the turbine was initially lower than the target of 0.76 at design pressure ratio and flow rate. This occurred because the brake wheel was too large, causing the turbine to operate at a less than optimum speed. The tests in December with a reduced brake wheel demonstrated that this modification was successful in increasing the turbine speed and efficiency. The second effect results from conductive heat leak. Test data were used to verify the heat leak calculation for the turboexpander. This calculation method was then used to predict the heat penalty for a design in which the conductive path through the turboexpander assembly was modified to reduce heat leak.

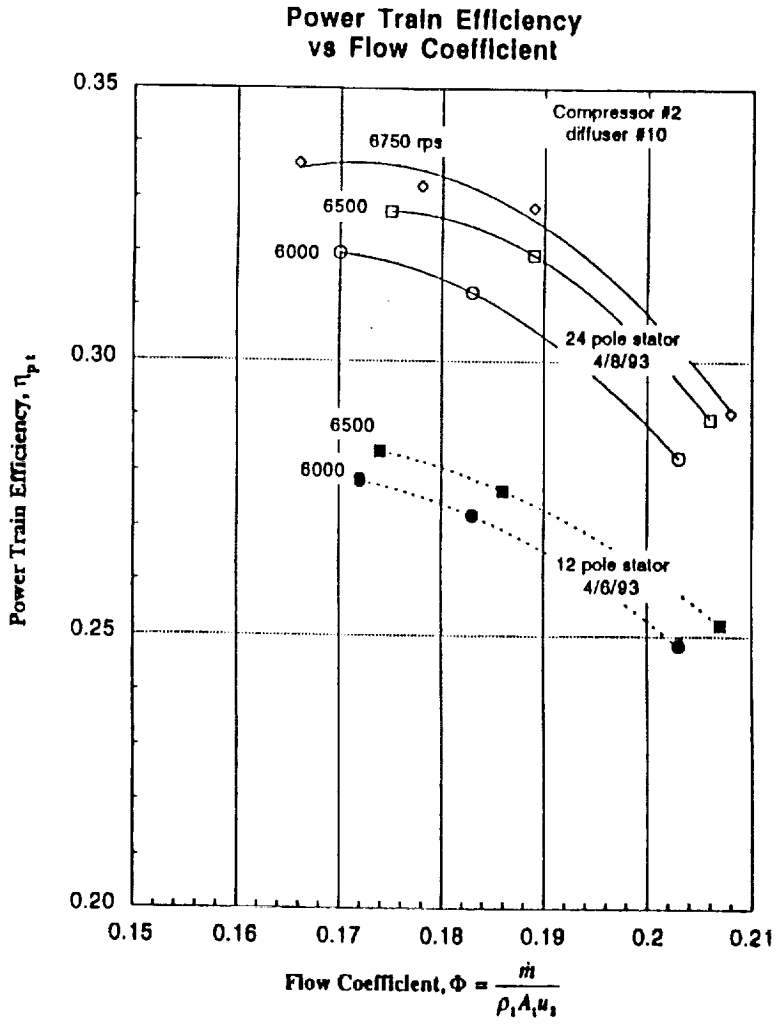

Figure 5.1. Comparison between Brassboard Compressor (12 pole stator) and Modified Compressor (24 pole stator). The 12 pole design was used in Brassboard System Tests.

Figure 5.2 illustrates the effects of heat leak and turbine speed on efficiency. The figure shows test data for the 3.18 mm diameter turbine, before and after the change in brake diameter. The horizontal axis is u/c_0 , the speed coefficient, relating the turbine rotor tip speed to the theoretical "spouting" fluid velocity. The upper series of points are the calculated efficiencies from test data corrected, for heat leak. The corrections were based on the relationships plotted in Figure 2.11. The lower series of points reflects the measured net efficiency, without correction. From the upper series of data, one concludes that the design point for the turbine should be set at a speed coefficient near 0.65. This would correspond roughly to the maximum aerodynamic efficiency that can be achieved for this machine. Since c_0 is related only to the inlet temperature and pressure ratio, it is the tip speed that must be adjusted to achieve the desired value for u/c_0. This was done during testing by reducing the diameter of the brake wheel to allow the turbine to operate at higher speed, one that corresponds to u/c_0 of nearly 0.63 at design conditions.

Table 5.1. Comparisons between Heat Exchanger Tests Results and Model Predictions.		
	Test J1	**Test J12**
Flow Rate	1.61 g/s	1.25 g/s
Temperatures		
Warm Stream Inlet	295.5 K	297.4 K
Cold Steam Inlet	38.2	65.9
Pressures		
Warm Stream Inlet	.209 MPa	.214 MPa
Cold Stream Inlet	136 MPa	.141 MPa
Thermal Effectiveness		
Data	0.9918	0.9934
Model	0.9914	0.9925
Pressure Losses (dP/P)		
Warm Stream (meas.)	0.014	0.012
(model)	0.015	0.012
Cold Stream (meas.)	0.012	0.010
(model)	0.012	0.010

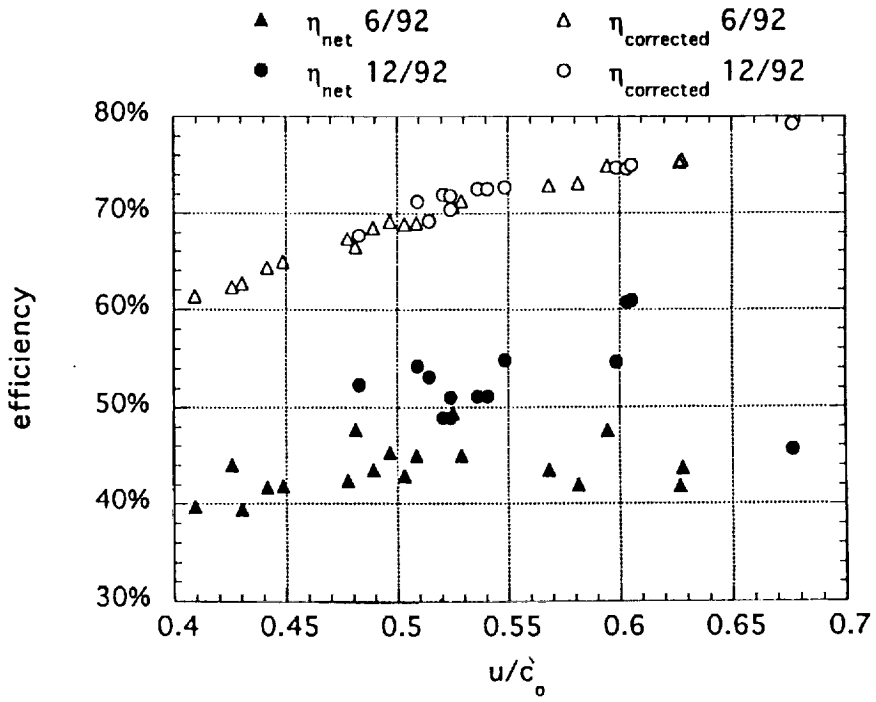

Figure 5.2. Effects of Heat Leak and Turbine Speed on Efficiency

A second important fact can be derived from this figure. All corrections for heat leak were made by calculating the heat leak through the turboexpander using a consistent thermal model incorporating thermal conductivity integrals for the materials of construction. This model is most sensitive to the temperature difference between the brake and the cold end of the turbine. However, the effect of heat leak on efficiency is strongly affected by the turboexpander operating conditions, including inlet temperature, flow rate, and pressure ratio. These parameters varied widely during testing. To the extent that the aerodynamic (corrected) efficiencies show a clear and consistent trend, this is a strong indication that the model used to calculate heat leak is accurate.

System Performance and Implications for the Engineering Model

The test results were used to establish design changes for the components and to assess the expected performance of the Engineering Model. This assessment has been performed using the system model incorporating losses assumed for the prototype system. Table 5.2 summarizes the results of this assessment.

Test J7 was used as a baseline for the assessment. Important parameters from this test are listed in the Table. Electric input power to the inverter was 324 W. Net cooling from the cycle was 5.88 watts including 0.5 watts of parasitic heat leak through heater leads. The power train efficiency was 0.29. The inlet temperature to the compressor (at the impeller) was 305 K. The turboexpander aerodynamic efficiency and net efficiencies were 0.707 and 0.494, respectively, where the lower value reflects the 3.3 W heat leak from the brake (at 310 K). The turbine speed was 8000 rev/s for this test corresponding to a u/c_0 of 0.525. The heat exchanger thermal effectiveness was 0.994 by the definition used in reducing test data (Appendix I). Using the definition applied in the system model, the thermal effectiveness was 0.993. The pressure losses through the tubing between the turboexpander and the compressor (which includes losses in the heat exchanger) were 3.6 kPa on the high pressure side and 2.3 kPa on the low pressure side.

The second column of values in the table show what the system model calculates for the same test conditions. Test values in normal type are input to the model. The values in bold type are predicted. The significance of this column is that the model uses several of the test parameter values, such as aerodynamic efficiency for the turbine, power train efficiency, flow rate, inlet pressure and temperature to the compressor, and compressor speed and fairly accurately predicts other system parameters including the load and input power.

The third column of numbers uses the same system model to calculate the expected cycle performance of the Engineering Model at design conditions. For this calculation, the efficiencies to be expected in the engineering model components have replaced those measured during system tests on the brassboard. Specifically, the power train efficiency has been increased to 0.33 based on the results of the tests shown in Figure 5.2, and the net turbine efficiency has been increased to 0.58 as a result of operating at higher speed and reduced heat leak. No changes are expected in the performance of the heat exchanger. The input values to the model are given in normal type, bold values are predicted by the model.

Table 5.2. Comparison Between Test Results and System Predictions			
	Test J7 (Meas.)	**Model (J7) (Calc.)**	**Eng. Model (Calc.)**
Input Power	324 W	**325 W**	**200 W**
Power Train Efficiency	0.29	0.29	0.33
Compressor Inlet Temp.	305 K	305 K	290 K
Compressor Inlet Press.	35.0 kPa	35.0 kPa	8.1 kPa
Compressor Exit Press.	123.8 kPa	**120.5 kPa**	71.9 kPa
Flow Rate	1.36 g/s	1.36 g/s	1.07 g/s
Heat Exch. Effectiveness	0.993	0.993	0.993
Turbine Inlet Temperature	66.05 K	**66.5 K**	**66.7 K**
Turbine Inlet Pressure	120.2 kPa	**117.5 kPa**	**70.3 kPa**
Turbine Exit Pressure	37.3 kPa	**37.3 kPa**	**8.8 kPa**
Turbine Speed	8000 rps	8000	9600
Turbine Efficiency	0.494	**0.51**	**0.58**
Turbine Aero Efficiency	0.707	0.707	0.76
Net Cooling	5.88 W	**5.83 W**	**5.0 W**
Load Temperature	64.88 K	64.88	65 K

6. ENGINEERING MODEL

The Engineering Model is designed to incorporate all major design features that will be present in the Prototype Cooler. The main differences between the Engineering Model and the Prototype involve construction details and the presence of instrumentation. The Engineering Model hardware will be fabricated using the same materials that would be present in the Prototype, but components are assembled using threaded fasteners to permit disassembly, adjustment, and replacement or repair of internal components if necessary. This requires the use of seals, some of which are located in the cryogenic regions. Secondly, instrumentation is present in the Engineering Model that would be absent in the Prototype. The instrumentation provides additional data used for verification and diagnostics during testing at the component level. The presence of additional instruments also involves additional flanged and sealed connections. As a result, the Engineering Model hardware is somewhat heavier and more complex than an all-welded, hermetic Prototype.

Similarities between the Engineering Model and the Prototype include the geometric details and materials of key components. The following paragraphs describe each of the Engineering Model components, identifying the changes that have been made to the brassboard configurations. A description of the Preliminary Design of the Engineering Model System is also presented.

6.1 The Components

Inverter

The inverter has been modified to upgrade from discrete electronics components and wired circuits to printed circuitboards and integrated components. The components selected for the Engineering Model are designed to be either S-class or have comparable components available as S class. The housing for the inverter is designed so that the heat generated in the inverter is transmitted by conduction to the mounting plate. The inverter housing is 171 mm (6.75") diameter x 102 mm (4.0") long and has a mass of 2.3 kg (5 lb.). Figure 6.1 shows a physical layout of the inverter and housing. There are no changes to the operating or performance characteristics of the inverter. Table 6.1 lists the design point characteristics. Appendix II lists the circuit components for the Engineering Model and their S-class counterparts.

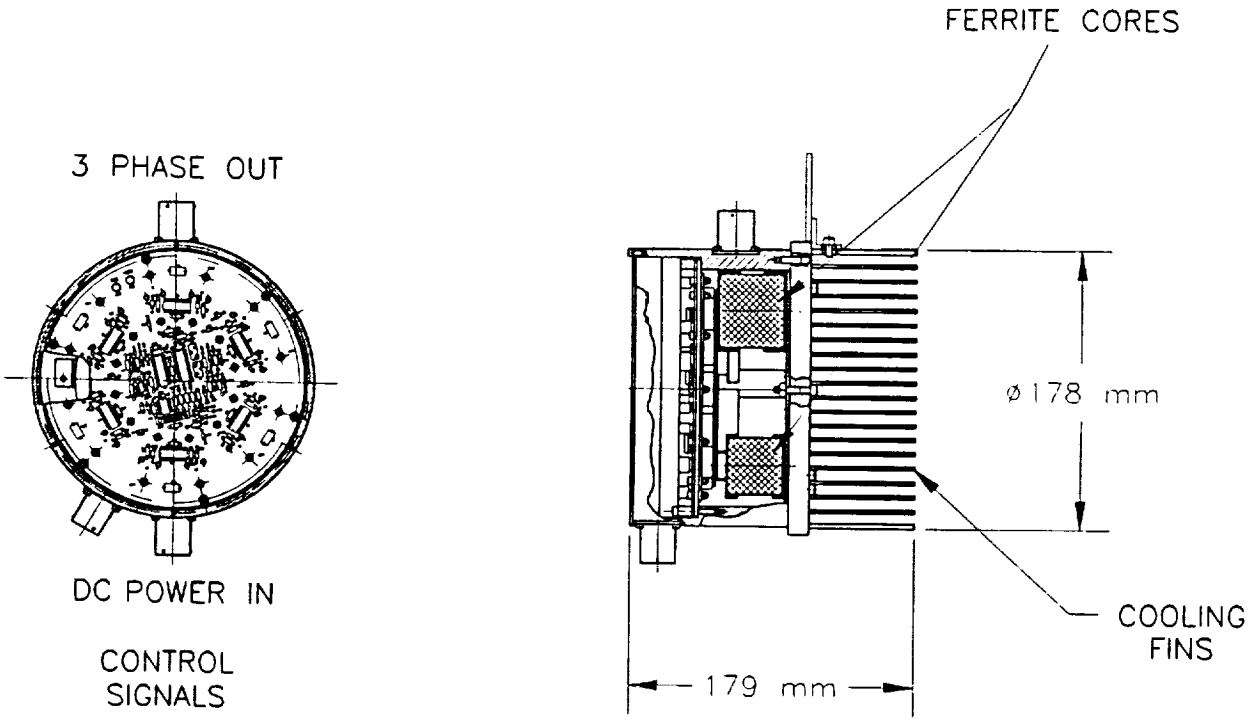

Figure 6.1. Engineering Model Inverter.

Table 6.1. Inverter Characteristics.	
Maximum Input Power	400 W
Rated Input Power	300 W
Input DC Voltage	28 V
Input Current	11 A
Output Voltage (per Phase)	15.4 V - rms
Output Current	6.2 A - rms
Output Frequency (3 Phase)	3 - 10 kHz
Operating Temperature Range	240 K - 350 K
Efficiency (Design Point)	0.95
Size	171 mm dia. x 102 mm (6.75" x 4.0")
Mass	2.3 kg (5 lb)

Compressor

The Engineering Model version of the compressor incorporates minor modifications intended to improve aerodynamic performance and efficiency of the motor, and a major change in the housing design to reduce the overall mass of the assembly. The housing design has also been modified to allow for heat rejection by means of conduction to a cold plate at the end of the compressor. The rotating assembly, gas bearings and basic assembly of internal components has been relatively unchanged from the brassboard design. Metal seals have been incorporated into the design to reduce the possibility of outgassing of contaminants from organic o-rings (such as those used on the brassboard assembly). This has resulted in some weight penalty because the flange bolting forces for metal seals are substantial, requiring additional material near the flanges. In the prototype, additional weight savings would be realized because the bolted flanges would be replaced by braze or weld joints.

Figure 6.2 shows the compressor assembly. The material for the compressor housing is tellurium copper. It is selected because of its high thermal conductivity, necessary to transfer the heat from the motor and bearings to the cold plate interface at the large end of the assembly. The housing was designed to accommodate a temperature difference of 25 C between the motor stator and the cold plate interface with a heat load of 400 W. As noted in the introductory paragraph to this section, flanged connections are provided to allow for assembly and disassembly of internal components. The seals used in the compressor are metal o-rings. Two shaft sensors and connectors are provided to allow for shaft position and speed monitoring during testing. One or both of these sensors would be eliminated in the Prototype assembly. The sensors are capacitance probes of the type used in the brassboard assembly. Table 6.2 summarizes key features for the Engineering Model.

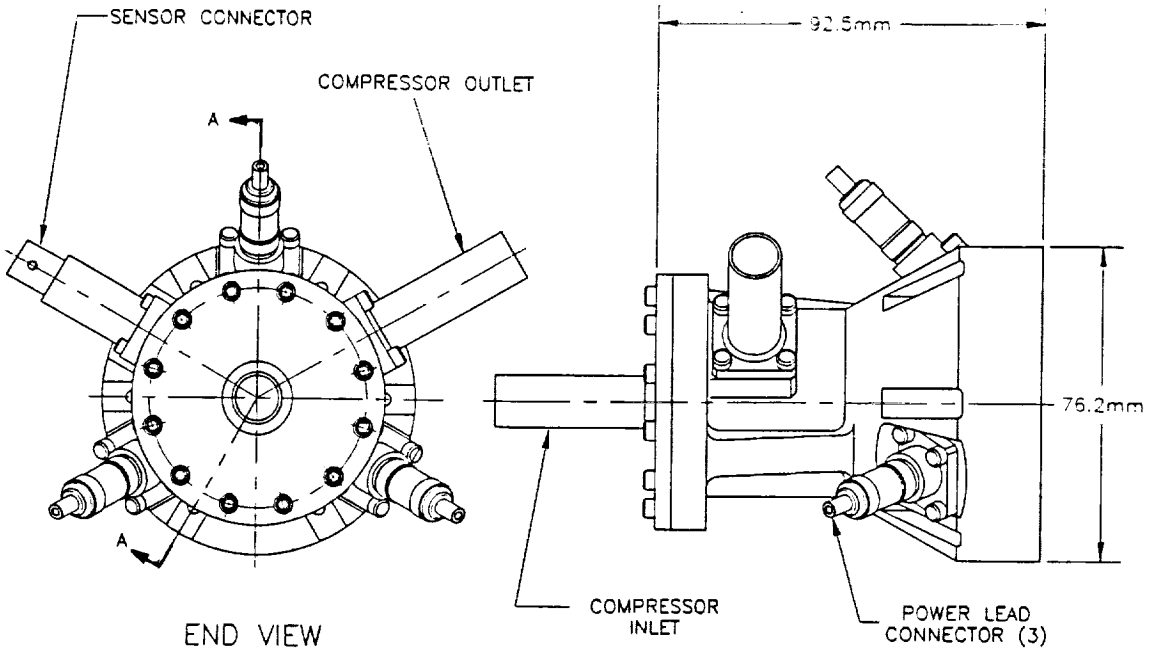

Figure 6.2a. Outline Drawing of Engineering Model Compressor

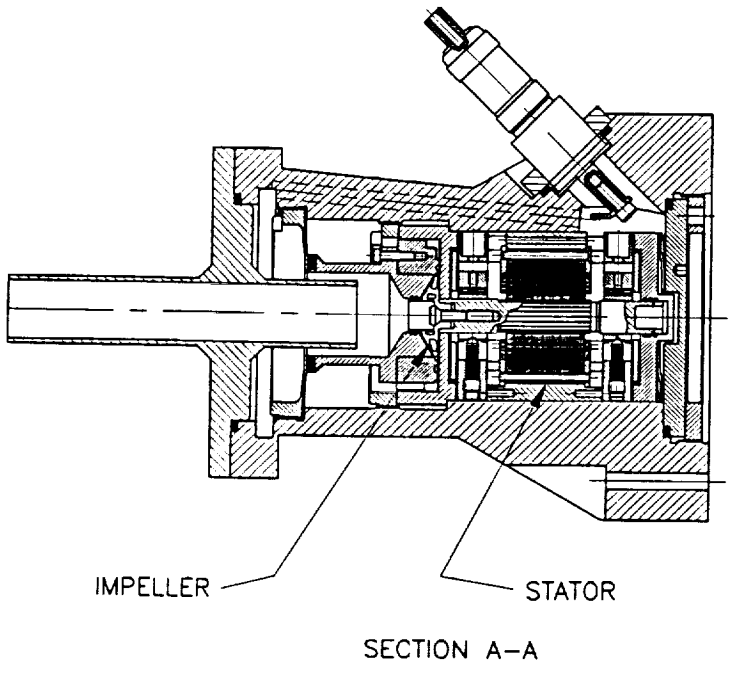

Figure 6.2b. Cross Section Assembly of Engineering Model Compressor

Table 6.2. Engineering Model Compressor	
Rated Conditions	
Inlet Pressure	1.1 atm.
Inlet Temperature	283 K
Pressure Ratio	1.58
Flow Rate	1.05 g/s
Input Power	190 W
Rotational Speed	6550 rev/s
Features	
Impeller Exit Diameter	15.2 mm (0.6")
Impeller Inlet Diameter	5.3 mm (0.21")
Number of Blades	18
Channel Height at Blade Tip	0.5 mm (0.02")
Motor Rotor Diameter	6.35 mm (0.25")
Stator Length	14.5 mm (0.57")

Heat Exchanger

The heat exchanger has been redesigned to increase its strength and improve system cleanliness. This component has the largest internal volume in the system and the largest exposed surface area of material. The brassboard assembly was soldered using a low temperature freon reflow technique requiring flux. Because of the soldered assembly, it was not possible to provide a high temperature vacuum bake of the assembly. The residual contaminants trapped in this volume would be unacceptable for long term testing at cryogenic temperatures. Furthermore, the low temperature solder joints were not adequate to withstand vibration loads ultimately expected in the system. The Engineering Model version is a vacuum brazed assembly providing improved cleanliness and acceptable levels of strength. The internal geometry has been modified slightly to meet these objectives.

Figure 6.3 shows important details of the heat exchanger assembly. Three hundred disks are positioned axially within a single outer tube. The disks are electrolytic tough pitch copper, and each contains four annular series of slots. The disks are separated by formed 300 series stainless steel "c-rings". Braze preforms are used between the disks and the spacers. The disk/spacer assemblies are brazed in a vacuum furnace in subassemblies consisting of up to 50 disks. These subassembly stacks are then brazed together prior to insertion in the outer stainless steel tube . The final fabrication step is the welding of the headers to the ends of the tube. The details of the internal geometry (slots, number of disks, spacer thickness and length, etc.) have been determined using the same thermal performance model that was used in the brassboard heat exchanger. The performance specification for this design is comparable to that of the brassboard assembly. Table 6.4 summarizes the important heat exchanger features.

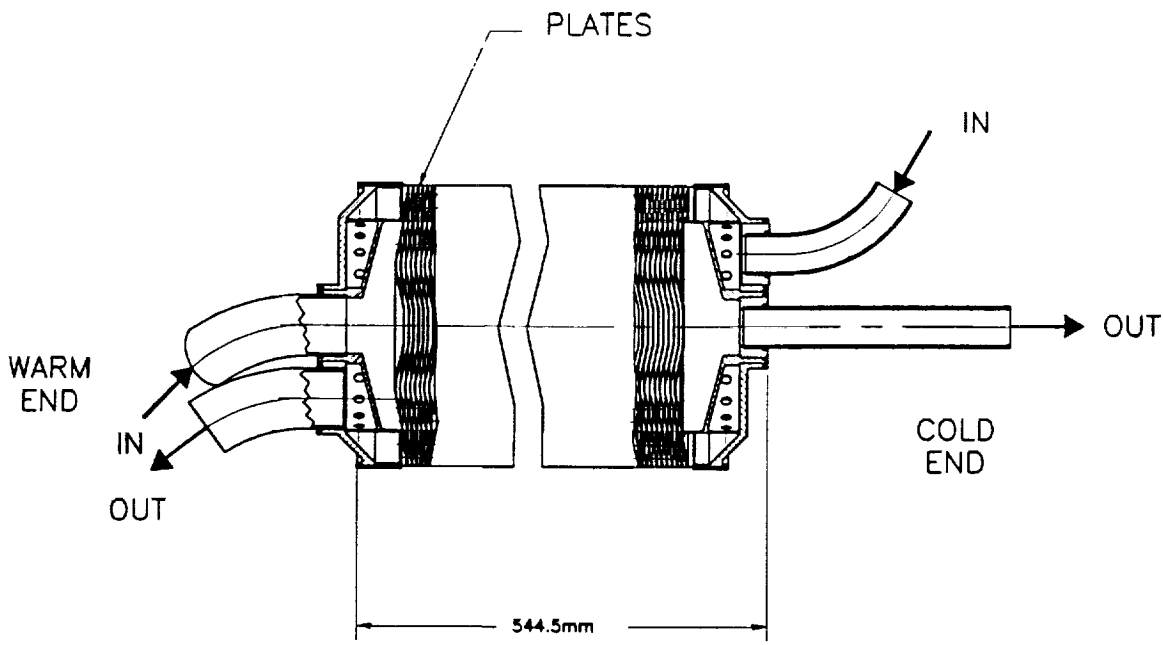

Figure 6.3. Engineering Model Heat Exchanger.

Table 6.3. Heat Exchanger Features	
Rated Conditions	
Flow Rate	1.05 g/s
Inlet Pressure (High Pressure Side)	1.74 atm.
Inlet Temperature (H.P. Side)	284 K
Pressure Loss (H.P. Side)	1.2 kPa
Inlet Pressure (low Pressure Side)	1.4 atm.
Inlet Temperature (L.P. Side)	65 K
Pressure Loss	1.1 kPa
Thermal Effectiveness	0.993
Features	
Core Diameter	8.9 cm (3.5")
Core Length	51 cm (20")
Number of Plates	300
Core Mass	5.3 kg (13.5 lb)
Header Mass	0.5 kg (1.1 lb)
Assembly Mass	5.8 kg (14.6 lb)

Turboexpander

Three minor changes were incorporated into the Engineering Model version of the turboexpander. First, the brake wheel diameter has been reduced to allow the turbine to operate at higher speed at design conditions. This will improve the aerodynamic efficiency of the machine at design point. Secondly, the wall thickness of the cylindrical shell connecting the cold and warm ends of the machine has been reduced from 0.25 mm (0.010") 0.15 mm (0.006"). This change will reduce the heat conducted from the warm end of the machine to the turbine, improving the overall efficiency of the turboexpander. Finally, organic seals have been replaced by metal seals to reduce the potential for contamination resulting from outgassing. The turboexpander assembly is shown in Figure 6.4. Important features of the design are listed in Table 6.4.

6.2 The Engineering Model Cryocooler

The components will be assembled into a cryocooler loop for performance and endurance testing. Figure 6.5 shows an outline drawing of the preliminary design of this assembly. The heat exchanger, turboexpander, a filter and electric heater to simulate the load will be located inside a vacuum vessel, mounted on top of a steel frame. The vacuum pumping system will be located under the mounting surface, with a pressure actuated isolation valve between the vacuum pump and the port in the bottom of the basewell. The tabletop basewell contains all vacuum passthroughs for tubing, power and instrumentation leads. The compressor and inverter will be attached to a vertical mounting plate that provides support for the heat rejection system. Heat is rejected from the inverter through vertical fins to naturally convected air behind the panel. Heat from the compressor conducts to a cold plate on the back of the panel. Refrigerant is circulated through this cold plate and through an aftercooler for the compressor. A computerized data acquisition system and panel gages will be mounted on an adjacent electronics rack (not shown).

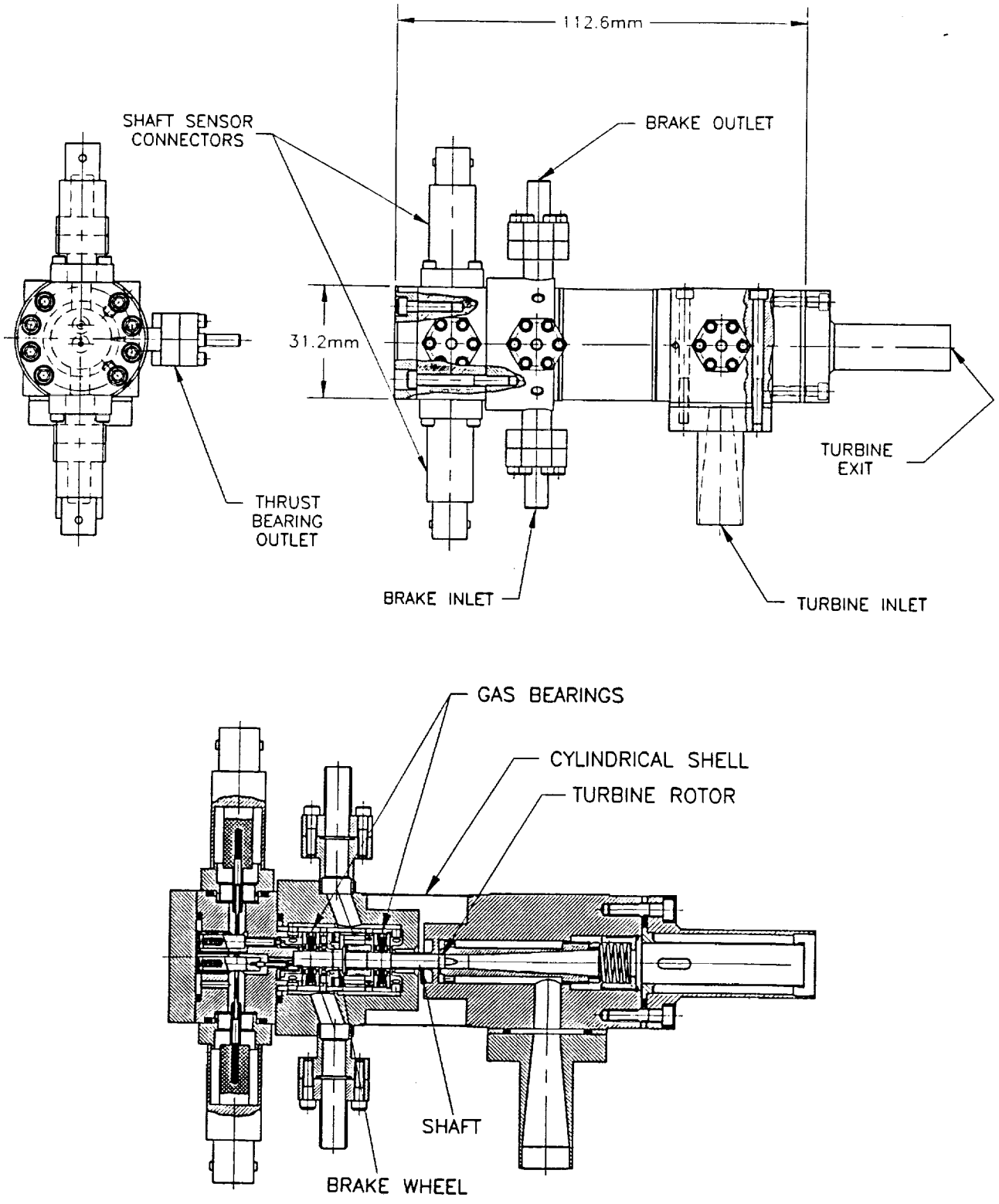

Figure 6.4. Engineering Model Turboexpander

Table 6.4. Engineering Model Turboexpander	
Rated Condition	
Flow Rate	1.05 g/s
Inlet Temperature	66.7 K
Inlet Pressure	1.70 atm.
Brake Temperature	290 K
Expansion Ratio	1.55
Net Efficiency	0.60
Features	
Turbine Rotor Diameter	3.18 mm (0.125")
Nozzle Height	0.61 mm (0.023")
Nozzle Width	0.22 mm (0.009")
Inlet Blade Angle	0^0 (radial)
Exit Blade Angle	30^0
Rotational Speed	9400 rev/s
Brake Diameter	4.8 mm (0.19"

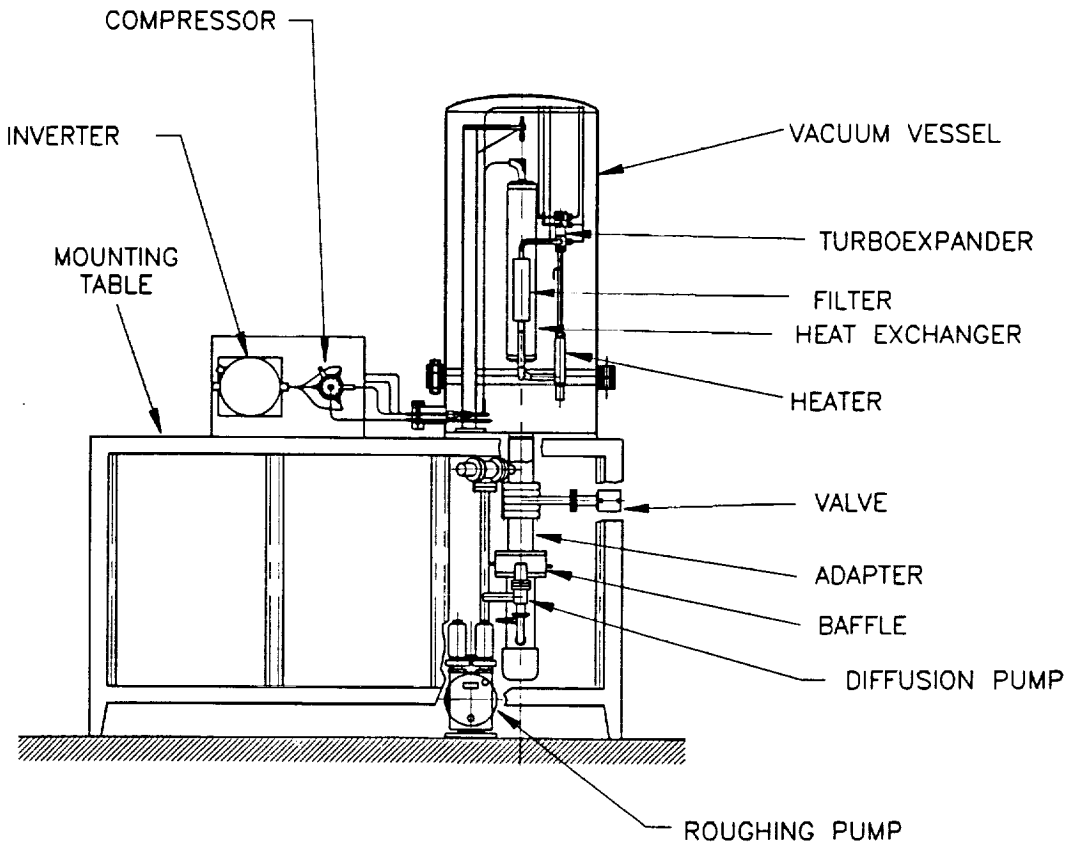

Figure 6.5. Preliminary Design of Engineering Model Cryocooler

7. REFERENCES

1. McCormick, J.A.; Valenzuela, J.A.; *Three-Phase Inverter for Small High Speed Motors*; Creare TM-1499; July 1991.

2. Swift, W.L.; *A Reliable Long-Life Closed-Cycle Cryocooler for Space*; Creare TN-453; Sept., 1988.

3. Swift, W.L.; Valenzuela, J.A.; Sixsmith, H.; *All-Metal, Compact Heat Exchanger for Space Cryocoolers*; Creare TM-1450; Nov., 1990.

4. *Specifications For Long-Life Single Stage Reverse Brayton Cycle Cooler For Space Applications.* Attachment B, Contract # NAS5-31281. September 11, 1989.

5. Dolan, F. X.; *Preliminary Thermal Performance For The Single Stage Reverse-Brayton Cycle Cryogenic Cooler Model Description and Sample Calculations*; Creare TM-1465; Feb. 1991

6. Ent, R.S.; *Cycle Performance Code for SSRB*; Creare TM-1590; Feb., 1990.

7. Arp, V. and McCarty, R.D.; Gas Pak (Ver. 3.1); Cryodata Inc., 1992.

8. Swift, W.L.; *Performance of a Single Stage Reverse Brayton Cooler at 35 K*; Creare TM 1569; Aug., 1992.

9. Goeking, K.W.; *Contamination Control for SSRB* I; Creare TM 1494; Apr., 1991.

APPENDIX I

DEFINITIONS OF PERFORMANCE PARAMETERS

Compressor

$$\psi = \frac{\Delta H_S}{U^2}$$

$$\Delta H_s = C_P T_{CI}\left(PR_C^{\frac{k-1}{k}} - 1\right)$$

$$U = \pi N_C D_C$$

$$\phi = \frac{C_I}{U}$$

$$C_I = 4\dot{m}_c / \rho\pi D_{eye}^2$$

$$P_I = V_I I_I$$

$$\eta_{PT} = \frac{\dot{m}_C Cp T_{CI}(PR_C^{\frac{k-1}{k}} - 1)}{P_I}$$

Ψ	Compressor head coefficient
Φ	Compressor flow coefficient
ΔH_S	Isentropic enthalpy change (J/kg)
U	Tip speed (m/s)
Cp	Specific heat (J/kg-K)
T_{CI}	Compressor inlet temperature (K)
PR_C	Compressor pressure ratio
k	Ratio of specific heats
N_C	Compressor rotational speed (rev/sec)
D_C	Compressor diameter (m)
C_I	Compressor inlet velocity (m/s)
$\dot{m}_C$	Compressor mass flow rate (kg/s)
ρ	Compressor fluid density (kg/m^3)
D_{EYE}	Compressor impeller inlet diameter (m)
P_I	Inverter power (W)
V_I	Inverter voltage (V)
I_I	Invert current (amps)
η_{PT}	Power train efficiency

Heat Exchanger

$$\varepsilon_{HX} = \frac{MIN[(H1 - H2),(H4 - H3)]}{MIN[(H1 - H2_{MIN}),(H4_{MAX} - H3)]} \quad \text{(Data Reduction)}$$

$$\varepsilon_{HX} = \frac{H4 - H3}{H1 - H3} \quad \text{(Cycle Analysis)}$$

ε_{HX} Heat exchanger effectiveness

H1 HX high pressure inlet enthalpy (J/kg)

H2 HX high pressure exit enthalpy (J/kg)

H3 HX low pressure inlet enthalpy (J/kg)

H4 HX low pressure exit enthalpy (J/kg)

$H2_{MIN}$ Minimum H2 (=f(P1,T3)) (J/kg)

$H4_{MAX}$ Maximum H4 (=f(P3,T1)) (J/kg)

Turbine

$$u = \pi N_T D_T$$

$$c_0 = \sqrt{2(H_{TI} - H_{TO,S})}$$

$$P_{NET} = \dot{m}_T (H_{TI} - H_{TO})$$

$$P_{SHAFT} = P_{NET}\eta_{T,NET}$$

$$\eta_{T,NET} = \frac{H_{TI} - H_{TO}}{H_{TI} - H_{TO,S}}$$

where $H_{TO,S} = f(P_{TO}, T_{TI})$ (Ignores heat leak)

$$\eta_{T,A} = \frac{H_{TI} - H_{TO} + \frac{Q_{LK}}{\dot{m}_T}}{H_{TI} - H_{TO,S}}$$

where Q_{LK} is the combined conduction and radiation heat leak from the warm end of the turboexpander to the cold end gas stream (calculated in SSRB Calculation 92-07-01).

u	Tip speed (m/s)
N_T	Turbine rotational speed (rev/sec)
D_T	Turbine diameter (m)
C_0	Ideal velocity (m/s)
Q_{LK}	Heat leak (W)
P_{NET}	Net turbine power (W)
P_{SHAFT}	Turbine shaft power (W)
$\dot{m}_T$	Turbine mass flow rate (kg/s)
H_{TI}	Turbine inlet enthalpy (J/kg)
H_{TO}	Turbine exit enthalpy (J/kg)
$H_{TO,S}$	Isentropic turbine exit enthalpy (J/kg)
$\eta_{T,NET}$	Turbine net efficiency
$\eta_{T,A}$	Turbine aerodynamic efficiency (corrected for heat leak)
P_{TO}	Turbine exit pressure (Pa)
T_{TI}	Turbine inlet temperature (K)
T2	HX high pressure exit temperature (K)

APPENDIX II
INVERTER PARTS LIST

PRELIMINARY PARTS LIST FOR INVERTER							
Component Ref.	Commercial Part No.	Military Part No.	GSFC PPL-18	MIL-STD-975	Grade	Class/Failure Rate	Description
U1	LM555CN	M38510/10901 SPA	Yes	Yes	1	S	Microcircuit, Timer
U2	CD40174BE	M38510/17505 BEA	No	No			Microcircuit, Hex Flip Flop
U3	CD4049UBE	M38510/H05553 SEA	Yes	Yes	1	S	Microcircuit, Hex Inverter
U4 - U9	IR2110	To Be Qualified	No	No			Microcircuit, Floating FET Driver
Q1 - Q12	2N6764	JANTXV2N6764	No	No	2	JANTXV	Transistor, N-Channel MOSFET
CR1 - CR23	1N4148	JANS1N4148-1	Yes	Yes	1	JANS	Semiconductor, Diode
VR1 - VR12	1N966B	JANS1N966B-1	Yes	Yes	1	JANS	Semiconductor, Zener
R7 - R19	RLR07C1002FS	RLR07C1002FS	Yes	Yes	1	S	Resistor, Fixed Film, 10k, 1%
R2	RLR07C1213FS	RLR07C1213FS	Yes	Yes	1	S	Resistor, Fixed Film, 121k, 1%
R4	RNC55J1002FS	RNC55J1002FS	Yes	Yes	1	S	Resistor, Fixed Film, 10k, 1%
R5	RNC55J1581FS	RNC55J1581FS	Yes	Yes	1	S	Resistor, Fixed Film, 1.58k 1%
R6	RLR07C2001FS	RLR07C2001FS	Yes	Yes	1	S	Resistor, Fixed Film, 2.0k, 1%
R20	RNC55J5111FS	RNC55J5111FS	Yes	Yes	1	S	Resistor, Fixed Film, 5.11k, 1%
R1	73JA-100K	TBD					Resistor, Potentiometer, 100k
R3	73JA-10K	TBD					Resistor, Potentiometer, 10k
C2 - C4	CKR06BX104KR	M123A02-BXB104KC	Yes	Yes	1	N/A	Capacitor, Ceramic, 0.1mF, 50V
C7 - C8	CKR06BX104KR	M123A02-BXB104KC	Yes	Yes	1	N/A	Capacitor, Ceramic, 0.1mF, 50V
C11 - C12	CKR06BX104KR	M123A02-BXB104KC	Yes	Yes	1	N/A	Capacitor, Ceramic, 0.1mF, 50V
C15 - C16	CKR06BX104KR	M123A02-BXB104KC	Yes	Yes	1	N/A	Capacitor, Ceramic, 0.1mF, 50V
C19 - C20	CKR06BX104KR	M123A02-BXB104KC	Yes	Yes	1	N/A	Capacitor, Ceramic, 0.1mF, 50V
C23 - C24	CKR06BX104KR	M123A02-BXB104KC	Yes	Yes	1	N/A	Capacitor, Ceramic, 0.1mF, 50V
C28 - C31	CKR06BX104KR	M123A02-BXB104KC	Yes	Yes	1	N/A	Capacitor, Ceramic, 0.1mF, 50V
C1	CKR05BX102KR	M123A02-BXC102KC	Yes	Yes	1	N/A	Capacitor, Ceramic, .001 mF, 100V
C27	CKR05BX471KR	M123A02-BPC471-C	Yes	Yes	1	N/A	Capacitor, Ceramic, 470pf, 100V
C5	CKR06BX105KR	M123A03-BXB105KC	No	No		N/A	Capacitor, Ceramic, 1.0mF, 50V
C9	CKR06BX105KR	M123A03-BXB105KC	No	No		N/A	Capacitor, Ceramic, 1.0mF, 50V
C13	CKR06BX105KR	M123A03-BXB105KC	No	No		N/A	Capacitor, Ceramic, 1.0mF, 50V
C17	CKR06BX105KR	M123A03-BXB105KC	No	No		N/A	Capacitor, Ceramic, 1.0mF, 50V
C21	CKR06BX105KR	M123A03-BXB105KC	No	No		N/A	Capacitor, Ceramic, 1.0mF, 50V
C25	CKR06BX105KR	M123A03-BXB105KC	No	No		N/A	Capacitor, Ceramic, 1.0mF, 50V
C6	RPE11425U225M050V	M83421/01-3282S	No	No			Capacitor, Ceramic, 2.2mF, 100V

C10	RPE114Z5U225M050V	M83421/01-3282S	No	No			Capacitor, Ceramic, 2.2mF, 100V
C14	RPE114Z5U225M050V	M83421/01-3282S	No	No			Capacitor, Ceramic, 2.2mF, 100V
C18	RPE114Z5U225M050V	M83421/01-3282S	No	No			Capacitor, Ceramic, 2.2mF, 100V
C22	RPE114Z5U225M050V	M83421/01-3282S	No	No			Capacitor, Ceramic, 2.2mF, 100V
C26	RPE114Z5U225M050V	M83421/01-3282S	No	No			Capacitor, Ceramic, 2.2mF, 100V
T1	B-6837-2014	Procured Per MIL-STD-981					Transformer Core, Ferrite
T3	B-6837-2014	Procured Per MIL-STD-981					Transformer Core, Ferrite
T5	B-6837-2014	Procured Per MIL-STD-981					Transformer Core, Ferrite
T2	B-6837-2015	Procured Per MIL-STD-981					Transformer Core, Ferrite
T4	B-6837-2015	Procured Per MIL-STD-981					Transformer Core, Ferrite
T6	B-6837-2015	Procured Per MIL-STD-981					Transformer Core, Ferrite
J1	NB0E14-4PNT2	NB0E14-4PNT2	Yes	Yes	1	N/A	Connector, Electrical
J2	NB0E12-10SNT2	NB0E12-10SNT2	Yes	Yes	1	N/A	Connector, Electrical
J3	NB0E14-4SNT2	NB0E14-4SNT2	Yes	Yes	1	N/A	Connector, Electrical
P1	NB6E14-4SNS2	NB6E14-4SNS2	Yes	Yes	1	N/A	Connector, Electrical
P2	NB6E12-10PNS2	NB6E12-10PNS2	Yes	Yes	1	N/A	Connector, Electrical
P3	NB6E14-4PNS2	NB6E14-4PNS2	Yes	Yes	1	N/A	Connector, Electrical
J200	MMD1P22-PSLL	TBD	No	No		N/A	Connector, PC Board
P200	MMS22-9SK030	TBD	No	No		N/A	Connector, PC Board